



Forschungszentrum Karlsruhe
in der Helmholtz-Gemeinschaft

Wissenschaftliche Berichte
FZKA 7379

Separate Effects Tests on Hydrogen Combustion during Direct Containment Heating Events

**L. Meyer, G. Albrecht, M. Kirstahler,
M. Schwall, E. Wachter**

**Institut für Kern- und Energietechnik
Programm Nukleare Sicherheitsforschung**

Januar 2008

Forschungszentrum Karlsruhe

in der Helmholtz-Gemeinschaft

Wissenschaftliche Berichte

FZKA 7379

**Separate Effects Tests
on Hydrogen Combustion during
Direct Containment Heating Events**

L. Meyer, G. Albrecht, M. Kirstahler, M. Schwall, E. Wachter

Institut für Kern- und Energietechnik
Programm Nukleare Sicherheitsforschung

Forschungszentrum Karlsruhe GmbH, Karlsruhe

2008

Für diesen Bericht behalten wir uns alle Rechte vor

Forschungszentrum Karlsruhe GmbH
Postfach 3640, 76021 Karlsruhe

Mitglied der Hermann von Helmholtz-Gemeinschaft
Deutscher Forschungszentren (HGF)

ISSN 0947-8620

urn:nbn:de:0005-073797

ABSTRACT

In the frame of severe accident research for light water reactors Forschungszentrum Karlsruhe (FZK/IKET) operates the facilities DISCO-C and DISCO-H since 1998, conceived to investigate the direct containment heating (DCH) issue. Previous DCH experiments have investigated the corium dispersion and containment pressurization during DCH in different European reactor geometries using an iron-alumina melt and steam as model fluids. The analysis of these experiments showed that the containment was pressurized by the debris-to-gas heat transfer but also to a large part by hydrogen combustion.

The need was identified to better characterize the hydrogen combustion during DCH. To address this issue separate effect tests in the DISCO-H facility were conducted. These tests reproduced phenomena occurring during DCH (injection of a hot steam-hydrogen mixture jet into the containment and ignition of the air-steam-hydrogen mixture) with the exception of corium dispersion. The effect of corium particles as igniters was simulated using sparkler systems. The data will be used to validate models in combustion codes and to extrapolate to prototypic scale.

Tests have been conducted in the DISCO-H facility in two steps. First a small series of six tests was done in a simplified geometry to study fundamental parameters. Then, two tests were done with a containment geometry subdivided into a subcompartment and the containment dome. The test conditions were as follows:

- As initial condition in the containment an atmosphere was used either with air or with a homogeneous air-steam mixture containing hydrogen concentrations between 0 and 7 mol%, temperatures around 100°C and pressure at 2 bar (representative of the containment atmosphere conditions at vessel failure).
- Injection of a hot steam-hydrogen jet mixture into the reactor cavity pit at 20 bar, representative of the primary circuit blow down through the vessel and hydrogen produced during this phase.

The most important variables measured were (1) the increase in pressure in the containment vessel, (2) gas temperatures, and (3) the number of moles of hydrogen burnt.

These tests characterize the time scale of the hydrogen combustion, its completeness and the combustion mode for different initial conditions in the containment. The fraction of burnt hydrogen was between 55% and 100% of total available hydrogen in the basic geometry, and 46% and 67%, respectively in the more prototypic geometry. The efficiency of the hydrogen combustion in respect to pressure rise in the containment was between 46% and 67%.

Dedicated combustion codes must be applied to verify, if these results prove true for reactor scale.

Experimente zur Wasserstoffverbrennung bei DCH-Prozessen

ZUSAMMENFASSUNG

Im Rahmen der Forschung zu schweren Unfällen in Leichtwasserreaktoren werden im Institut für Energie- und Kerntechnik des Forschungszentrums Karlsruhe seit 1998 die Versuchsanlagen DISCO und DISCO-H betrieben, konzipiert zur Untersuchung der Druckbelastung des Sicherheitsbehälters durch Schmelzedispersion (Direct Containment Heating, DCH) bei Versagen des Reaktordruckbehälters (RDB). Vorangegangene Experimente haben die Schmelzeverteilung und Druckerhöhung im Sicherheitsbehälter bei verschiedenen europäischen Reaktorgeometrien untersucht, unter Anwendung von Eisen-Aluminium-Schmelzen und Dampf als Modellfluide.

Die Analyse dieser Experimente hat gezeigt, dass der Druckanstieg sowohl durch den Wärmeübergang von der Schmelze an das Gas, aber auch zum nicht unerheblichen Teil durch Wasserstoffverbrennung verursacht wurde. So hat sich die Notwendigkeit ergeben, die charakteristischen Eigenschaften der Wasserstoffverbrennung während des DCH-Prozesses besser beschreiben zu können. Um diese Fragen zu klären, wurden Einzeleffektexperimente in der DISCO-H Versuchsanlage durchgeführt. Mit Ausnahme der Schmelzedispersion laufen in diesen Experimenten die gleichen Prozesse ab, wie sie während des DCH-Vorganges auftreten, das sind das Abblasen einer heißen Wasserstoff-Dampf Mischung in den Sicherheitsbehälter und die Zündung dieses Gasgemisches in einer Luft-Dampf-Wasserstoff Atmosphäre. Der Effekt der Schmelzepartikel als Zünder wurde mit Thermitkerzen simuliert. Die experimentellen Daten werden benutzt, um Modelle in Verbrennungscodes zu kalibrieren und um auf Reaktormaßstab zu extrapolieren.

Die Experimente wurden in zwei Schritten durchgeführt. Für eine Serie von 6 Tests wurde eine vereinfachte Geometrie benutzt, um die Hauptparameter der Verbrennung zu studieren. Dann wurden zwei Tests in einer prototypischeren Geometrie durchgeführt, bei der das Gas aus der Grube zuerst in einen separaten Reaktorraum und von dort in den Sicherheitsbehälter strömt. Die Versuchsbedingungen waren wie folgt:

- Als Anfangsbedingung im Sicherheitsbehälter wurde eine Luft- bzw. ein Luft-Dampf-Atmosphäre bei 100°C und 2 bar eingestellt, mit Wasserstoffkonzentrationen zwischen 0 und 7 mol%, repräsentativ für die Atmosphäre im Containment bei Versagen des RDB.
- Einblasen eines heißen Dampf-Wasserstoffgemisches in die Reaktorgrube bei 20 bar, repräsentativ für ein Kühlmittelabblasen durch ein Leck im RDB und der Wasserstoffherzeugung während dieser Phase.

Die wichtigsten gemessenen Größen waren (1) der Druckanstieg im Sicherheitsbehälter, (2) die Gastemperaturen und (3) die Anzahl der verbrannten Wasserstoffmole. Diese Experimente kennzeichnen die Rate der Wasserstoffverbrennung, die Vollständigkeit und die Art der Verbrennung bei verschiedenen Anfangsbedingungen. Der Anteil des verbrannten Wasserstoffs betrug zwischen 55% und 100% der Gesamtmenge in der einfachen Geometrie und 46% bzw. 67% in der mehr prototypischen Geometrie. Der Wirkungsgrad hinsichtlich Druckerhöhung im Sicherheitsbehälter lag zwischen 46% und 67%.

Spezielle Verbrennungscodes müssen angewendet werden um zu prüfen, ob diese Ergebnisse auch für den Reaktormaßstab gelten.

TABLE OF CONTENTS

1	Introduction.....	1
2	Geometry and Dimensions.....	1
3	Instrumentation.....	3
3.1	Temperature	3
3.2	Pressure	3
3.3	Gas composition.....	3
3.4	Video observation	4
4	Test parameters	4
5	Experimental procedure	5
5.1	<i>Test G01 with rupture disk.....</i>	5
5.2	<i>Test G02 with valve</i>	5
5.3	<i>Test G03.....</i>	6
5.4	<i>Test G04.....</i>	6
5.5	<i>Test G05.....</i>	7
5.6	<i>Test G06 and G07</i>	7
5.7	<i>Test G08.....</i>	7
6	Results	7
6.1	<i>Test G01 and G02</i>	7
6.2	<i>Test G03 and G04.....</i>	8
6.3	<i>Test G05 and G06.....</i>	8
6.4	<i>Test G07 and G08.....</i>	9
6.5	<i>Gas Temperatures.....</i>	9
6.6	<i>Gas Analysis.....</i>	10
7	Analysis of Results and Energy Balance.....	11
7.1	<i>Present tests without melt.....</i>	11
7.2	<i>Tests with melt from H-series</i>	11
8	Conclusions.....	14
	References	15
	TABLES.....	16
	FIGURES: Geometry.....	25
	FIGURES: Results	37
	Video Pictures	60
	Annex A Gas analysis	71

LIST OF TABLES

Table 1: Geometric parameters of the test facility 16

Table 2. Thermocouple Summary 17

Table 3. Pressure transducer summary 19

Table 4. Initial Gas Composition in the Containment vessel 20

Table 5. Compilation of main initial conditions in RPV/RCS 21

Table 6. Measured gas concentrations in G01..... 21

Table 7. Measured gas concentrations in G02..... 21

Table 8. Measured gas concentrations in G03..... 22

Table 9. Measured gas concentrations in G04..... 22

Table 10. Measured gas concentrations in G05..... 22

Table 11. Measured gas concentrations in G06..... 23

Table 12. Measured gas concentrations in G07..... 23

Table 13. Measured gas concentrations in G08..... 23

Table 14. Initial Conditions, Results and Analysis of G-series..... 24

Table 15. Initial Conditions, Results and Analysis in H-series 24

LIST OF FIGURES

Fig. 1. The containment pressure vessel with internal structures.....	25
Fig. 2. Dimensions of the cavity.....	26
Fig. 3. Dimensions of the RPV vessel.....	27
Fig. 4. Positions of gas filling and gas sample lines.....	28
Fig. 5. RPV exit formed by a pipe.....	29
Fig. 6. Thermite igniters and electrical starter.....	29
Fig. 7. Positions of thermocouples for G02-G05	30
Fig. 8. Positions of thermocouples for G06.....	31
Fig. 9. Configuration of test facility in tests G07 and G08	32
Fig. 10. Positions of pressure transducers and thermocouples in the cavity	33
Fig. 11. Data of the ball valve	34
Fig. 12. View into containment vessel and cavity during assembly, G01-G06.....	35
Fig. 13. View into containment vessel, actual test configuration, G01-G06.....	35
Fig. 14. View into containment vessel, actual test configuration, G07-G08.....	36
Fig. 15. Flow path from subcompartment with igniter, G07 – G08.....	36
Fig. 16. Pressures in the RPV	37
Fig. 17. Pressures in the RPV, rupture disk versus ball valve.....	37
Fig. 18. Pressures in the RPV	38
Fig. 19. Pressures in the RPV	38
Fig. 20. Pressures in the RPV	39
Fig. 21. Pressures in the RPV	39
Fig. 22. Pressure gradient dp/dt in the RPV	40
Fig. 23. Containment pressure.....	41
Fig. 24. Containment pressure.....	42
Fig. 25. Containment pressure (zoom)	43
Fig. 26. Gas temperature in RPV vessel, G01	44
Fig. 27. Gas temperature in RPV vessel, G02.....	44
Fig. 28. Gas temperature in RPV vessel, G03.....	45
Fig. 29. Gas temperature in RPV vessel, G04.....	45
Fig. 30. Gas temperature in RPV vessel, G05.....	46
Fig. 31. Gas temperature in RPV vessel, G06.....	46
Fig. 32. Gas temperature in RPV vessel, G07.....	47
Fig. 33. Gas temperature in RPV vessel, G08.....	47
Fig. 34. G01: Temperatures in the reactor pit	48
Fig. 35. G01: Temperatures in the containment vessel and subcompartment.....	48
Fig. 36. G02: Temperatures in the reactor pit	49
Fig. 37. G02: Temperatures in the containment vessel and subcompartment.....	49
Fig. 38. G03: Temperatures in the reactor pit	50
Fig. 39. G03: Temperatures in the containment vessel and subcompartment.....	50
Fig. 40. G04: Temperatures in the reactor pit	51
Fig. 41. G04: Temperatures in the containment vessel and subcompartment.....	51
Fig. 42. G05: Temperatures in the reactor pit	52
Fig. 43. G05: Temperatures in the containment vessel and subcompartment.....	52
Fig. 44. G06: Temperatures in the reactor pit	53
Fig. 45. G06: Temperatures in the containment vessel and subcompartment.....	53

Fig. 46. G07: Temperatures in the reactor pit	54
Fig. 47. G07: Temperatures in the containment vessel and subcompartment	54
Fig. 48. G08: Temperatures in the reactor pit	55
Fig. 49. G08: Temperatures in the containment vessel and subcompartment	55
Fig. 50. Pressure increase versus blow down hydrogen	56
Fig. 51. Pressure increase versus total available hydrogen	56
Fig. 52. Pressure increase versus burned hydrogen.....	57
Fig. 53. Comparison of possible maximum pressure increase with measured data	57
Fig. 54. Experimental pressure increase vs. energy release by oxidation and hydrogen combustion...	58
Fig. 55. Experimental pressure increase versus thermal energy release	58
Fig. 56. Experimental pressure increase versus estimated total energy release	59
Fig. 57. G01: Video frames from top view into the containment.....	60
Fig. 58. G01: Video frames from the endoscope inside the subcompartment.....	61
Fig. 59. G02: Video frames, top view into the containment	62
Fig. 60. G02: Video frames from the endoscope inside the subcompartment.....	63
Fig. 61 G03: Video frames, top view into the containment	66
Fig. 62. G03: Video frames, view from the side, inside containment	67
Fig. 63. G05: Video frames, top view into the containment	68
Fig. 64. G06: Video frames, top view into the containment	69
Fig. 65. G07: Video frames, top view into the containment	70

1 Introduction

In case of a core melt accident in European light water nuclear reactors the pressure vessel may fail at elevated pressure of 1 to 2 MPa after the forming of a molten pool. Then, the molten core debris will be ejected forcefully into the reactor cavity and beyond, depending on the specific reactor design. This may pressurize the reactor containment building beyond its failure pressure.

In the frame of the program for the investigation of melt dispersion and direct containment heating (DCH) phenomena during a severe accident in European reactor geometries experiments were performed in the DISCO-H facility using an iron-alumina melt as model fluid [1,2]. The analysis of these experiments showed that the containment was pressurized not only by the debris-to-gas heat transfer but also to a large part by hydrogen combustion [2,3]. Whether these two sources of energy transfer to the containment atmosphere are fully additive, depends on the concurrence of the two processes. The critical question is how much hydrogen burns during the period of debris dispersal [4]. A time shift could arise if the flow paths for debris and hydrogen reaching an oxygen rich atmosphere are different. Furthermore, the rate of combustion determines the time scale of heat transfer to the atmosphere and thereby the peak containment load. Hydrogen combustion cannot contribute to peak containment pressure unless the energy release rate is greater than the heat transfer rate to structures. The experimental data base for hydrogen burns during DCH events is, however, not sufficient for model development particularly for scaling effects. The need for separate effects experiments was evident.

This report presents results from experiments performed in the same facility without melt but otherwise similar conditions. The objective of this series of experiments is to study the effect of hydrogen combustion separately from the debris-to-gas heat transfer. The data will be used to validate models in combustion codes and to extrapolate to prototypic scale.

In these experiments, the fraction of hydrogen, that is produced during steam blow down by oxidation of the metal part with steam in DCH experiments or in real case, is filled into the vessel modelling the volumes of the reactor cooling system (RCS) and the reactor pressure vessel (RPV) pre-test and is blown out together with the other gases used, i.e. nitrogen or steam. Since generally most of the oxidation takes place within the cavity, this simulation of hydrogen production should not have a major impact on the outcome of the experiment. The atmosphere in the containment was varied in these tests, containing either air or a mixture of air and steam with different amounts of pre-existing hydrogen.

2 Geometry and Dimensions

The geometry of the DISCO-H facility represents the EPR reactor pit as in former tests described in the FZK report [1]. No direct flow path from the cavity into the containment exists. Fig. 1 shows the scheme of the containment vessel, the subcompartment, the cavity and the RPV- and RCS-pressure vessel. All relevant dimensions are given in Table 1. The linear scale of the experiment relative to the EPR-reactor is 1:18.

Some parts of the test facility have been changed to simplify the geometry for base case investigations. The subcompartment cover was removed and four of the eight exits from the cavity to the subcompartment (along the main cooling lines) were connected to a pipe each. The other four exits were closed. Thereby the total flow cross section was kept similar as before. This configuration provides simple initial conditions for code calculations, and parameter studies were performed with this set up. In a second step the original, more prototypic configuration has been tested to study the effect of this simplification (see Fig. 9 and description of tests G07 and G08, below).

Because of the absence of melt droplets no natural igniters for the hydrogen are available. Therefore, it was decided to place thermite igniters, so-called sparklers, at the end of each pipe exit. The igniters must sustain a steam atmosphere and should have an ignition capability within a certain volume. Conventional thermite sparklers have been made steam-tight by coating with a water-resistant lacquer. They are started by electric resistance heating 1.2 seconds before initiating the blow down (Fig. 6). They can ignite a hydrogen-air mixture in a radius of approximately 5 cm. They furnish sparks for a period of approximately 10 seconds, which is sufficient to guarantee ignition when the conditions are right.

The characteristic time of hydrogen release should be similar as in tests with melt. In those experiments three stages of flow at the vessel breach existed, single-phase melt flow, two-phase flow and single-phase gas flow [1]. Consequently, the blow down was slow at the start and became faster with decreasing liquid fraction. A shake down test with hydrogen had shown, that the blow down was too fast, compared to the tests with melt, because of the absence of the melt and the high velocity of sound in hydrogen. Therefore, the hole size in the RPV was reduced from 50 mm to 25 mm diameter in the first test. Additionally, starting with test G02 a ball valve instead of a rupture disk was being applied to model the break of the lower head including the slow beginning of the outflow due to the existence of melt. The opening time of the rupture disk is only in the order of 2 ms, while the valve opens the flow cross section gradually.

The ball valve has a through boring of 38.1 mm and a sphere diameter of 64.5 mm (Fig. 11). Valve tests showed that it takes approximately 450 ms to turn it by 90 degrees. After a turn of 18 degrees the flow cross section starts to open and after about another 40 degree a flow cross section equivalent to the cross section of the 25-mm-diameter pipe is open. Thus, the opening process takes 200 ms. However, in the real tests the opening times of the valve varied because the axis of the valve was not exactly in line with the driver mechanism. The 90-degree turn was not smooth. Therefore, opening times were deduced from the gradient of the pressure curves (Fig. 22). The maximum pressure gradient was reached at $t = 49$ ms in the test with a rupture disk (G01), although the rupture disk opens in less than 5 ms. To reach the maximum flow rate the gas has to accelerate which took the a certain time. For the tests with ball valve the times of maximum flow rate probably coincide with the instant when the maximum flow cross section is reached. These times varied between 192 ms and 68 ms in the seven tests with valve. It should be noted that the installation of the valve reduced the volume of the RPV (s. Table 1 and Fig. 2) and changed the outflow conditions. The RPV exit is now formed by a pipe with an inner diameter of 25 mm and a length of 65 mm (Fig. 3 and Fig. 5).

3 Instrumentation

3.1 Temperature

Gas temperatures were measured with 0.36-mm-diameter K-type thermocouples.

Three thermocouples are located inside the steam accumulator (T1, T2 and T5), which was used in test G04, G05 and G08 with steam and in test G03 with nitrogen.

Two thermocouples are installed within the RPV-RCS pressure vessel, one in each compartment (T3, RCS (top) and T4, RPV (bottom)). A total of 11 thermocouples are located at different levels in the containment pressure vessel (CPV, level A through D). Three of them are within the subcompartment (A1-A3). Eight are distributed in the upper dome, five of them are positioned above the openings in the subcompartment cover at different heights (B1, B3, C1, C3, D3). The exact positions are given in Table 2 and are shown in Fig. 7, Fig. 8 and Fig. 9. Three thermocouples are installed in the cavity (Fig. 10).

Additional thermocouples are installed at the outside of the steam accumulator tank and the RCS-RPV pressure vessel. These temperatures are monitored at the heater control board to control the electric heaters.

3.2 Pressure

A total of 16 strain gauge-type pressure transducers (14 Kulite® and 2 Kistler®) with ranges of 0-0.7 MPa, 0-1.7 MPa, 0-3.4 MPa and 0-5.0 MPa were used to measure steam and gas pressure (Table 3). The compensated operating temperature range is 27°C – 232°C, with a thermal drift of +/- 5% of full scale output for the Kulite transducers. The Kistler transducers were mounted outside the facility in cold environment connected with a pipe to the measurement position. They were used as reference for the Kulite transducers during stationary periods of the experiment. During the transient period their response is slow due to the long connecting line. The Kulite transducers were adjusted at operating temperature before the start of the experiment. All gages are mounted in tapped holes that are connected gas tight with the outside atmosphere at their backsides. In case of the transducers in the RCS-RPV pressure vessel, the compartment, and the cavity this connection was achieved by flexible steel hoses. The gages in the containment pressure vessel were mounted in the blind flanges of the ports at different levels.

The data acquisition system records data at a rate of 2000 data points per second per channel.

3.3 Gas composition

Nine pre-evacuated 500-cm³ gas grab sample bottles are used to collect dry-basis gas samples at three times and three positions, in the subcompartment and at two positions of the containment (see Fig. 4). The sample lines and the sample bottles are at room temperature, thus the bottles are being filled with non-condensable gases and steam, that condenses. The ventilator inside the containment is running before and after the test to ensure a well mixed atmosphere. One pre-test sample collects background information just prior to the start of the

test. One sample at all three stations each is taken 10 seconds and one 5 minutes after the blow down. The gas samples are analyzed at the Engler-Bunte-Institut at the University Karlsruhe.

3.4 Video observation

Four video cameras with 50 frames/second and one high speed video camera with 125 frames/second were used to record the strength and timing of hydrogen combustion. Two cameras were looking down from the top cover, one had a horizontal view from a level B port, and one used an endoscope introduced in a level A port (Fig. 1). The high speed camera also used an endoscope through a level B port, but yielded underexposed pictures due to the small aperture of the endoscope, so no information could be used from them.

4 Test parameters

The table below lists the nominal parameter matrix.

		G01	G02	G03	G04	G05	G06	G07	G08
RPV: Hole size	mm	25	25	25	25	25	25	25	25
RPV: opening mechanism		rupture disk	valve	valve	valve	valve	valve	<i>valve</i>	<i>valve</i>
RPV: Pressure	MPa	2	2	2	2	2	2	2	2
RPV: Temperature	°C	100	100	100	230	230	180	<i>200</i>	<i>200</i>
RPV: H ₂ + N ₂ or steam		N₂	-	N₂	steam	steam	-	-	<i>steam</i>
RPV: Hydrogen mass	g	100	100	50	50	50	100	<i>100</i>	<i>50</i>
CON: Hydrogen mass	g	-	-	50	50	100	100	<i>100</i>	<i>50</i>
CON: Pressure	MPa	0.2	0.2	0.2	0.2	0.2	0.2	<i>0.2</i>	<i>0.2</i>
CON: Temperature	°C	20	20	20	100	100	100	<i>100</i>	<i>100</i>
CON: Atmosphere: Air + ...		-	-	-	steam	steam	steam	<i>steam</i>	<i>steam</i>

Table 4 and Table 5 give the measured pretest data and all initial conditions. Tests G01 to G06 were performed with the simplified geometry having four pipes and four igniters (Fig. 1). Test G07 and G08 were performed with more prototypic geometry, the same as in the tests with melt (Fig. 9). Here igniters were positioned at each exit from subcompartment to containment and four igniters inside the subcompartment near the main cooling lines.

5 Experimental procedure

5.1 Test G01 with rupture disk

In test G01 a pure air atmosphere in the containment vessel was foreseen. For better comparison with the experiments with an air-steam mixture at 0.2 MPa in the containment, the air pressure was increased to 0.2 MPa in this test also. The gas temperature inside the vessel was slightly above outside temperature because of the preheating of the RCS-vessel.

The pressure vessel modeling the RCS and the upper RPV volume, which is inside the containment vessel, was electrically heated for 20 hours, while continually being flushed with nitrogen. The gas temperature in the upper part was higher ($T_3=120^\circ\text{C}$) than below the separation plate ($T_4=95^\circ\text{C}$). The RPV vessel inside the pit is not electrically heated, it will be close to the containment temperature of 24°C at the lowest point. The flushing was stopped 8 minutes before blow down ($t = - 8 \text{ min}$) and the valves were closed. This condition at atmospheric pressure (1000 mbar) determines the initial nitrogen mass inside the RPV/RCS vessel. Then hydrogen was filled into the vessel through the lower gas fill pipe (Fig. 4) over a period of 6 minutes. The exact mass of added hydrogen was determined by weighing the hydrogen gas bottle before and after the filling process with 0,1 g resolution. The filling was stopped at a pressure of 1.7 MPa, which resulted in a hydrogen mass of 0.088 kg. The accumulator vessel outside of the containment was filled before with nitrogen at a pressure of 2.9 MPa.

The experiment is started computer controlled with the ignition of the thermitic sparklers. After two seconds the valve is opened in the pipe connecting the accumulator vessel with the RPV/RSC-vessel. Now nitrogen is flowing into the RPV/RCS-vessel, and the pressure rises until the rupture disk breaks at $p = 2.16 \text{ MPa}$ and blow down starts. This signals the valve to close again, but it takes approximately 200 ms to fully close the valve, meanwhile nitrogen continues to flow into the RPV/RCS-vessel. This leads to the relatively high amount of blow-down nitrogen in this test. The initial conditions inside the RPV/RCS vessel are listed in Table 5.

5.2 Test G02 with valve

Test G02 was intended to have the same initial conditions as G01, except that the start of the blow down was by opening the valve in the RPV bottom instead of by a rupture disk. As in test G01 the containment vessel was filled with air at 0.2 MPa at ambient temperature.

The RPV/RCS pressure vessel was electrically heated for a period of 20 hours, while continually being flushed with nitrogen. The flushing was stopped at $t = - 10 \text{ min}$ and the valves were closed. This condition at atmospheric pressure (1002 mbar) determines the initial nitrogen mass inside the RPV/RCS vessel. Then the planned amount of hydrogen (0.098 kg) was filled into the vessel through the lower gas fill pipe (Fig. 4, Nitrogen fill in) over a period of 8 minutes. The filling was stopped at a pressure of 1.96 MPa.

The experiment is started computer controlled with the ignition of the thermitic sparklers. After two seconds the valve in the RPV is opened and the blowdown starts. All following tests were conducted with the valve, hence the same starting procedure was applied.

5.3 Test G03

Different to test G02 the amount of hydrogen should be divided evenly to the RPV/RCS and the containment vessels. After filling the containment vessel with air at 0.2 MPa the metered amount of hydrogen was filled in (0.050 kg).

The initial procedure for the RPV/RCS vessel was the same as for G02, but half the amount of hydrogen (0.048 kg) raised the pressure only to 1.03 MPa. Nitrogen was added until the pressure reached 1.99 MPa.

5.4 Test G04

Test G04 was the first test with steam. It was intended to have an air-steam-hydrogen atmosphere in the containment and a mixture of hydrogen and steam as blowdown gas.

The containment vessel was closed, when the air temperature was 28°C and the atmospheric pressure was at 1011 mbar. This determines the mass of air in the containment vessel. One day before the test, the electric heaters at the RPV/RCS vessel were turned on. At the day of the test it was heated for 7 hours by filling with steam additional to the atmospheric air. The condensate water was drained at the bottom of the vessel periodically. A metered amount of hydrogen (0.047 kg) was added to the vessel 10 minutes before the blow down ($t = -10$ min) while fans were running inside the vessel. A gas sample was taken and the fans were stopped just before the start of the experiment. The absolute pressure in the containment vessel was 0.204 MPa and the gas temperature was 100°C at that time.

The same amount of hydrogen was planned to be in the blow down gas, so a mixture of nitrogen, hydrogen and steam had to be filled into the RPV/RCS vessel. For that purpose the steam accumulator (volume 0.082 m³) placed outside the containment vessel was connected to the RPV/RCS vessel by a pipe equipped with a electro-pneumatic valve. It was flushed with nitrogen at ambient pressure. The amount of 1000 g water was filled in, and then the vessel was closed ($p = 0.101$ MPa, $T = 25^\circ\text{C}$). The accumulator vessel is heated electrically. Before start of the test the pressure in the accumulator was $p = 2.57$ MPa and the temperature was 270°C.

The RPV/RCS vessel was electrically heated for a period of 20 hours, while continually being flushed with nitrogen. The gas temperature in the upper part was $T_3 = 220$ °C and below the separation plate it was $T_4 = 180$ °C. The RPV vessel inside the pit was probably close to the containment temperature of 100 °C at the lowest point. The flushing was stopped at $t = -10$ min and the valves were closed. This condition at atmospheric pressure (1011 mbar) determines the nitrogen mass inside the RPV/RCS vessel. Then the planned amount of hydrogen (0.050 kg) was filled into the vessel through the lower gas fill pipe over a period of 5 minutes. This changed the gas temperature in the upper part to $T_3 = 216$ °C and to $T_4 = 199$ °C below the separation plate. The pressure was 1.29 MPa.

The experiment was started computer controlled by igniting the sparklers. 0.3 s later the valve between steam accumulator and RPV/RCS vessel opened and stayed open for 2.0 s. The pressure balance between steam accumulator and RPV/RCS vessel occurred 0.40 s after opening of the valve, at a pressure of 1.88 MPa. The blow down valve opened 0,77 s after closing of the steam valve and the blow down commenced.

5.5 Test G05

The only difference to test G04 is the higher amount of hydrogen in the containment vessel, therefore the experimental procedure was the same as for G04. However, because of the high hydrogen fraction in the containment (7 %), which was above the flammability limit, the hydrogen started to burn when the igniters were started at $t = -2.8$ s.

5.6 Test G06 and G07

The procedure for the containment vessel was the same as for tests G04 and G05 (air-steam-hydrogen mixture), while for the RPV/RCS vessel the procedure was identical as for G02 (pure hydrogen blow down), except that the temperature was higher, comparable to the tests with steam. The difference between test G06 and test G07 was the geometry, simplified in G06 versus more prototypical in G07.

5.7 Test G08

Also in test G08 the more prototypical geometry was applied. Since the initial conditions were intended to be identical to those of test G04, the experimental procedure was the same too.

The initial conditions at start of the blowdown for all tests are listed in Table 4 for the containment vessel and in Table 5 for the RPV/RCS vessel.

6 Results

Fig. 16 shows the pressure drop in the RPV/RCS vessel for all tests. The following figures show the pressures grouped for a better identification of specific features.

6.1 Test G01 and G02

Fig. 17 shows the blow down pressures for test G01 with the rupture disk and G02 with the ball valve. While the pressure drop is abrupt in the test with the rupture disk, with the valve it is more similar to the gradual pressure drop of a test with melt. The pressure gradient (Fig. 22) has its maximum near $t = 200$ ms in G02, corresponding to the time when the cross section in the valve has reached the value of the cross section of the 25-mm-diameter pipe. The total blow down time in test G02 is shorter than in test G01, because the RPV/RCS vessel contained much less nitrogen (2.6 mol in G02 versus 20 mol in G01).

Fig. 23 and Fig. 24 show the pressures in the containment, which increase by 0.13 MPa within 1 second in G02, 0.01 MPa less than in G01. Because of the slow start of the blow-down, the G02-pressure raises later than in test G01. While both pressures decrease after

they have reached a peak at 1, respectively 2 seconds, the pressure in test G02 rises a second time at $t = 3.4$ s and reaches the pressure curve of G01 at $t = 4.5$ s (Fig. 24). We can only speculate about this peculiar behaviour. The very bright flame lasted up to 960 ms in G01 (Fig. 59, looking from the top) and up to 600 ms in test G02 dying out slowly (Fig. 60, looking from below at one flame). However, in G02 a second burst could be observed around 3500 ms, which was not the case in test G01, and which could have been the reason for the pressure step at this time.

All early pressures in the reactor pit show short peaks, which are compression peaks due to the fast gas blow down and the restricted flow path out of the pit. Later the pressure follows that in the containment (Fig. 25).

6.2 Test G03 and G04

Fig. 18 shows the blow down pressure curves for the tests G03 and G04 in comparison with that of test G02. While in test G02 the blow down gas was mainly hydrogen (48 mol), in these two tests a mixture of hydrogen and nitrogen (G03), respectively hydrogen and steam (G04) was used. The blow down times vary corresponding to the sound velocity in the gas mixtures, shortest for pure hydrogen and longest for the mixture of hydrogen and nitrogen.

The atmosphere in the containment was air in G03 and air plus steam in G04, in both cases the total pressure was 0.2 MPa. The hydrogen content in the containment was the same with 24 mol, corresponding to 2.2 and 2.6 mol%, respectively. (Total gas moles are not the same in the two tests).

The pressure increase in these two tests was identical with 0.11 MPa (Fig. 23), but less than in G02 (0.13 MPa). The total amount of hydrogen in all three tests was the same (48 mol), but in tests G02 all hydrogen was blown into an air atmosphere, while in the other two tests one half was blown out of the RPV and the other half was existing in the containment. The higher pressure increase in G02 is due to the higher fraction of burned hydrogen, with 0.73 versus 0.55 and 0.58 in G03 and G04 (Table 14).

In tests G03 and G04 the same amount of hydrogen was blown out of the RPV, in one case together with nitrogen, in the other with steam. In G03 it was blown into an air atmosphere, in G04 into an air-steam atmosphere. The pressure peaks are identical, but the pressure drop after the peak is different. In G04 it decreases faster than in G03 and more hydrogen burnt in total, which means that either the hydrogen burning rate was not the same or the heat losses were bigger. Note, that in an atmosphere with steam there is generally some fog, which may absorb more heat.

6.3 Test G05 and G06

Fig. 19 shows the blowdown pressure curves for tests G05 and G06. The curve of G05 is similar to that of G04 (see Fig. 20), since it has similar conditions in the RPV/RCS-vessel. Because of pure hydrogen the blow down in G06 is faster than in G05.

With 64 mol hydrogen in the containment the hydrogen concentration was 7 % in test G05, with 33 % steam. This composition lead to hydrogen burning when the igniters were started 2 seconds before blow down (Fig. 23 and Fig. 24). The pressure increased by 0.11 MPa until blow down started and increased to a total rise of 0.27 MPa when 26 mol of hydrogen were added from the blow down (90 mol total). In test G06 the hydrogen concentration in the containment was only 5 % (48 mol), too small for ignition. The additional 51 mol blow down hydrogen lead to a pressure rise of 0.23 MPa when ignited, less than in G05 although the total available hydrogen was higher (99 mol). In both tests the fraction burned was much higher than in the preceding tests, with 0.86 in G05 and 0.78 in G06. A higher preexisting hydrogen concentration led to a higher burnt fraction. The strongest combustion occurred between $t = 600$ and 800 ms in test G05 and between $t = 600$ and 1100 ms in G06, as can be seen in the video pictures (Fig. 63 and Fig. 64).

6.4 Test G07 and G08

For tests G07 and G08 the geometry was changed, back to the original configuration with eight exits from the cavity along the main cooling lines into the subcompartment (Fig. 9). Four igniters were placed near these exits. The subcompartment was closed with the cover having four exits (0.13 m diameter) to the containment dome. One igniter was placed near each exit. The initial conditions of test G07 were similar to those of G06, and of test G08 to those of G04. The corresponding pressure blow down curves are similar (Fig. 20 and 21)

Comparing the tests with different geometry but similar initial conditions (G04/G08 and G06/G07) we see the following trend: The amount of burned hydrogen is smaller in the more compartmentalized geometry of tests G07 and G08, although the available amount was somewhat greater in both cases. Thus a higher post test hydrogen concentration remains in the vessel.

In the cases of higher initial hydrogen concentrations together with higher blow down masses (G06 and G07) the pressure in the containment reached the same value (0.45 MPa), but at different times. In G07, with the subcompartment, the peak was reached at $t = 1$ s, while in G06 it was reached only a $t = 2$ s. Note also, that the pressure increase was less in G06, since the initial pressure was already higher (0,22 MPa), maybe because less hydrogen was available than in G07 and the burning rate was smaller.

For the two tests with smaller hydrogen masses involved (G04/G08) the trend in pressure increase is different. Here, in G08, with subcompartment, the pressure increases less, but again, faster than in G04, similar to G07.

6.5 Gas Temperatures

The gas temperatures in the RPV/RCS vessel are shown in Fig. 26 through Fig. 33 for two positions, T3 near the top in the upper part (RCS) and T4 in the lower part (RPV). In tests without blow down steam (G01, G02, G03, G06 and G07), the temperature is higher near the top, because of the non-uniform heating of the vessel. When steam is used, it enters the RPV/RCS vessel just before blow down starts at the top of the vessel. Although the steam temperature in the accumulator is much higher, it cools down during the inflow and probably

because of the expansion, and thereby lowers the total gas temperature near the top of the vessel. During the blow down the gas temperatures decrease by up to 140°C, generally more in the upper part than in the lower, again due to the expansion process.

Fig. 34 through Fig. 49 show the gas temperatures measured in the reactor pit and the containment at the positions defined in tables 2a-2c and Fig. 7, Fig. 8 and Fig. 9. The general development of the temperatures *in the reactor pit* is an increase up to 200 to 300°C during blow down and a drop thereafter for 1 or 2 seconds (G02, G03, G05 and G06). Later, several temperature fluctuations are registered with peak temperatures between 400 and 600°C, and even up to 1000°C in test G02. In test G04 the temperature in the reactor pit is practically constant for 11 seconds and rises to a short peak of 400°C. All late temperature fluctuations may hint to some hydrogen burning, which consume hydrogen and oxygen, but do not contribute to the early pressure peak in the containment. In tests G07 and G08, which had the original configuration of cavity exits and subcompartment, the temperature traces are similar to those in the subcompartment and the containment. The temperature rises within the first 2 seconds and decreases slowly again.

The positions of some thermocouples *in the containment* were changed for test G06, and again for tests G07 and G08. In all tests the temperature rises fast within the first second at positions near and above the cavity exits, respectively the subcompartment outlets in tests G07 and G08. Peak temperatures of 1200°C could be observed, most peak temperatures lie between 600 and 1000°C. A detailed analysis should be done case by case, observing thermocouple positions, peak pressures and flame histories.

6.6 Gas Analysis

The individual results of the gas sampling are listed in Table 6 through Table 13, each for the pretest sample and the samples after 10 seconds and after 5 minutes. These data are dry gas values, i.e. without steam fraction. For the gas analysis by the nitrogen ratio method (see appendix A) only the pretest and 5 minutes posttest data were used. In this test series, average values between the three measuring positions were taken. The results of the gas analysis are given in Table 14.

In tests G01 and G02 no hydrogen could be detected in the post test gas samples. The uncertainty in the gas analysis is demonstrated by the pretest data. Since pure air is in the vessel, all data should show identical values. Unfortunately there was a leak in one of the gas lines, so only two measurements are available. They show a difference of 0.37% in both gases, N₂ and O₂. The average is close to the expected value of 21% for oxygen and 79% for nitrogen plus argon and rest gases.

The given uncertainty in the determination of the volume percent of nitrogen and oxygen was relatively large with 0.9 and 0.7, respectively. For hydrogen it is 0.9 vol%. It turns out that only 36 mol of hydrogen was burned out of the existing 49 mol. Since the threshold of measurement for hydrogen is about 10 mol (0.1 vol% of 1000 mol) and no hydrogen was measured post test, we can assume that in fact more than 39 mol was burned in these tests. Starting with test G03 the precision of the determination of the gas species was improved, and was than 0.1% for hydrogen, 0.3% for oxygen and 0.4% for nitrogen.

7 Analysis of Results and Energy Balance

For comparison with tests of the main series, H01-H06 [1], which were tests with iron-alumina melt, an energy balance is presented in the following for both series.

Main initial conditions and results are listed in Table 14 for the G-experiments and for comparison with experiments from the H-series corresponding data are given in Table 15.

7.1 Present tests without melt

In the G-series the fraction of burned hydrogen is higher when more preexisting hydrogen is available (G05-G07 versus G03, G04 and G08), except for the cases of pure hydrogen blow down into an air atmosphere (G01 and G02).

The measured pressure increase does not correlate with the amount of blow down hydrogen (Fig. 50). Plotted over the total amount of available hydrogen (Fig. 51), that is preexisting plus blow down hydrogen, shows two cluster of data, one for high amount and one for low amount of hydrogen. Within the cluster there is no correlation between pressure increase and hydrogen mass.

The measured pressure increase is, with small scatter, a function of burnt hydrogen (Fig. 52). A small part (order of 0.01 MPa) of the pressure increase is due to the additional gas added by the blow down.

The theoretical possible pressure rise resulting from the energy release by hydrogen burning can be obtained by combining the caloric equation of state with the ideal gas law,

$$\Delta p = \frac{\kappa - 1}{V} \Delta Q_H . \quad (1)$$

with κ the ratio of gas specific heats and V the containment volume ($V = 13.75 \text{ m}^3$). When we have a mixture of air and steam in the containment, in our case we take $\kappa = 1.35$ as a rough estimate, with air $\kappa = 1.4$. The steam in the containment is at saturation and does not quite obey the ideal gas law. Furthermore, there is always some fog, that is some liquid water in the air, which consumes energy for vaporization. Nevertheless, we calculate the pressure increase with $\Delta Q_H = \Delta q_H N_H$ and $\Delta q_H = 242 \text{ kJ/mol}$ burnt H_2 (with N_H number of burnt hydrogen moles) and obtain the data shown in Table 14. The ratio of measured peak pressure increase to theoretical pressure increase according to Eq.1 is the efficiency of the process, a measure for all heat losses involved. The efficiency lies between 50 % and 67 % for the tests with steam, the average is 58 %. The data are shown in Fig. 53. The added gas mass from the blow down is neglected in this analysis (adds approximately 0.01 MPa).

7.2 Tests with melt from H-series

The analysis of tests with melt from the H-test series [1] must take into account the contribution of (1) energy release by oxidation of the metallic part, (2) energy release by burning of hydrogen, and (3) the latent and sensible heat of the melt particles.

Assuming an ideal thermite reaction, the used 10.6 kg of thermite melt consists of 101 moles of Fe, 4 moles of Al and 48 moles of Al₂O₃, a total of 153 moles of melt. For a complete oxidation of the metallic part (Fe+Al) 107 moles of H₂O or 54 moles of O₂ are needed. In all tests less than 107 moles of steam were available in the RPV/RCS blow down gas (between 7 and 35 moles), so the reaction is steam limited.

The iron-steam reaction is at equilibrium when the ratio H₂/H₂O has reached a value of 2.1, consequently not all blow down steam can react. Therefore, the oxidation in the cavity was severely limited by the available steam, more oxidation could only take place outside of the cavity by air or steam. The results of the gas sampling indicated a higher hydrogen production than moles of blow down steam were available. This means, that oxidation in the containment continued either with steam or with air. The evaluation method (see Appendix 1) cannot distinguish between a direct reaction of metal with oxygen and the two-tier reaction of metal with steam and a subsequent burning of hydrogen with air. In the first case less hydrogen would be produced and burned than in the second case, but energetically both cases are identical. In any case, according to the measured decrease of oxygen in the containment and the hydrogen balance, less than half of the initially available metal (101 moles of Fe, 4 moles of Al) was oxidized during the test. If the number of produced hydrogen moles is proportional to the number of moles of reacted metal (iron and aluminum), we can assess the maximum droplet size, that took part in the metal-steam reaction, based on the dispersed fraction and the droplet size distribution. This analysis yields a droplet size of 4 mm in tests H02, H03 and H06.

	H02	H03	H05	H06
Oxidized metal (all Al and part Fe) [mol]	52	31	30	37
Oxidized fraction of total metal	0.49	0.29	0.28	0.35
Oxidized fraction of dispersed metal	0.81	0.60	0.74	0.71
Fraction of dispersed debris with diam.< 0.4 mm	0.83	0.62	0.44	0.75

Assuming that all 4 moles of aluminum reacted with steam, according to



we obtain 6 moles of hydrogen and an energy release of 1590 kJ (265 kJ/mol steam). The reaction with iron is



The iron steam reaction adds only little to the energy release (2 kJ/mol steam). The total energy release by oxidation reactions with steam is given in Table 15, line 12 for all experiments.

If no steam is present, as in test H04 (no gas analysis available), we assume that all 4 moles of aluminum are oxidized by air, with an energy release of 3.34 MJ (1670 kJ/mol oxide). Certainly, part of the iron will have been oxidized by air also, but we do not have any data on

that. If we assume that only the fraction of iron was oxidized, which was dispersed into the subcompartment and containment dome with droplet diameters smaller than 1 mm (that is 40% of the dispersed mass), we obtain 30 moles. Oxidized by air, this releases an energy of 7.32 MJ (244 kJ/mol FeO). The total oxidation energy of 10.7 MJ is given Table 15, line 12.

The combustion of the hydrogen releases 242 kJ/mol, the energy release for each test is given in line 13 in Table 15. The theoretical maximum peak pressure increase due to oxidation and hydrogen combustion is calculated by Eq.1 and is listed in next line 14, Table 15.

For the assessment of the energy transfer from the melt to the atmosphere we can assume that only the fraction of melt dispersed into the subcompartment and containment take part. Of course, this is an upper bound, since not all of it is finely dispersed and does not release its energy within the DCH time scale. Based on the above analysis, as a better estimate than the total dispersed fraction, we take the fraction that has a diameter smaller 4 mm.

The specific thermal energy of the melt used in the experiment is given by [6] with

$$\Delta e_{\text{therm}} = 0.182 \text{ MJ/mol.} \quad (4)$$

Only a fraction of thermal energy can be transferred from melt debris to the atmosphere before debris-gas thermal equilibrium is achieved. This fraction is given by the expression $1/(1+\Psi)$ according to Pilch [5], with the heat capacity ratio Ψ , of the debris mass to that of the containment atmosphere. Locally this ratio can be quite large, but referred to the whole of the containment it is small. In this rough estimate of maximum pressure increase we will use the total amount of the containment atmosphere, which is approximately $N_{\text{atmo}}=1000$ moles and the mass fraction of melt that was dispersed:

$$\Delta p = \frac{\kappa - 1}{V} \frac{\Delta e_{\text{therm}} N_m f_d}{1 + \Psi} \quad (5)$$

$$\text{with } \Psi = N_m f_d C_{\text{pm}} / N_{\text{atmo}} C_v.$$

N_m is the number of moles of melt, f_d is the dispersed fraction with debris diameter smaller than 4 mm, C_{pm} is the specific heat of the melt with $C_{\text{pm}} \sim 82.8 \text{ J/mol/K}$, and C_d is the specific heat of the atmosphere with $C_v \sim 28 \text{ J/mol/K}$ ($C_{v \text{ air}} = 20.8 \text{ J/molK}$) ([1],[6]). The heat capacity ratio Ψ lies between 0,15 and 0,25 for the experiments with a steam atmosphere and is 0,50 for test H04, which had a high dispersed melt fraction and an air atmosphere in the containment.

The maximum pressure increase due to heat transfer from the dispersed melt is determined by Eq.5 and is shown in Table 15, line 18.

The theoretical total pressure increase is the sum of the pressure increase due to oxidation/combustion energy release and that due to debris heat transfer, and is given in line 19.

The efficiency (line 20), that is the ratio of the measured pressure increase to the theoretical one, lies between 0,23 and 0,35 for the tests with steam and is 0,24 for the test without steam. Compared to the average of 0,58 for the tests of the G-series without melt, this is rather low.

Fig. 54 through Fig. 56 visualize the relationship between measured pressure increase and energy release either derived from gas analysis as for the oxidation and combustion energy, or by estimation as for the thermal energy transferred from debris to gas. The data from tests H02, H04 and H06 are in line with the data from the G-series (Fig. 54). Since in the H-series there is additional thermal energy release, the combustion energy release must have been less efficient, probably more extended in time. In the two tests with a closed reactor pit H03 and H05 (no direct path to the containment) the efficiency is even lower. Fig. 55 shows the relation between measured pressure increase and estimated thermal release from the debris together with the reference line from the G-series. Finally, Fig. 56 shows the measured pressure increase over the total released energy (lines 12+13+17 in Table 15), which visualizes the low efficiency of the DCH process in the test configuration, about 25% for a 'closed' cavity, and 35% for an 'open' cavity (H02 and H06).

This short analysis was done following the approach of the Single Cell Equilibrium model (SCE) by Pilch [5]. A refined analysis can be done by the Two-Cell Equilibrium model (TCE), also developed by Pilch [5].

8 Conclusions

Separate effects tests, injecting of a hot steam-hydrogen mixture into the reactor cavity, have been conducted in the DISCO-H facility in two steps. First a small series of six tests was done in a simplified geometry to study fundamental parameters. Then, two tests were done with a containment geometry subdivided into a subcompartment and the containment dome. These tests characterized the time scale of the hydrogen combustion, its completeness and the combustion mode for different initial conditions in the containment. The fraction of burnt hydrogen was between 55 % and 100 % of total available hydrogen in the basic geometry, and 46% and 67%, respectively in the more prototypic geometry. The efficiency of the hydrogen combustion in respect to pressure rise in the containment was between 46 % and 67 %.

Specific results are:

- The peak pressures Δp correlate with total hydrogen burned.
- The measured pressure increase is only around 50 % of the theoretical possible one, i.e. the remainder of the hydrogen burnt in a longer time scale and could not contribute to the pressure increase, because heat losses were larger.
- The amount of remaining hydrogen is similar to the amount of preexisting hydrogen, if preexisting $H_2 < 3 \%$, that means, basically, only the produced (blow down) hydrogen was burned.
- For cases with preexisting $H_2 > 5 \%$ the burned fraction is larger $> 70 \%$, and the remaining hydrogen fraction in the containment is between 1 % and 3 %.

Dedicated combustion codes must be applied to verify, if these results prove true for reactor scale.

References

1. L.Meyer, G.Albrecht, M.Kirstahler, M.Schwall, E.Wachter, G.Wörner, 2004, Melt Dispersion and Direct Containment Heating (DCH) Experiments in the DISCO-H Test Facility, FZKA 6988, Forschungszentrum Karlsruhe.
<http://bibliothek.fzk.de/zb/berichte/FZKA6988.pdf>
2. Meyer, L., Albrecht, G., Wilhelm, D., 2004, Direct containment heating investigations for European pressurized water reactors. NUTHOS-6, 2004, Nara, Japan, Proc. on CD-ROM Paper ID. N6P007
3. Wilhelm, D., 2003, Recalculation of corium dispersion experiments at low system pressure, NURETH-10, 2003, Seoul, Korea.
4. M.M. Pilch, Hydrogen combustion during direct containment heating events, Nuclear Engineering and Design, 136, pp. 117-136, 1996
5. M.M. Pilch, A two-cell equilibrium model for predicting direct containment heating, Nuclear Engineering and Design, 136, pp. 61-94, 1996
6. T. K. Blanchat, M.M. Pilch, R.Y. Lee, L. Meyer, and M. Petit, "Direct Containment Heating Experiments at Low Reactor Coolant System Pressure in the Surtsey Test Facility," NUREG/CR-5746, SAND99-1634, Sandia National Laboratories, Albuquerque, N.M., (1999).

TABLES

Table 1: Geometric parameters of the test facility

Containment Pressure Vessel		
Diameter (inner)	m	2.170
Total empty volume of containment	m ³	14.180
Volume of internal structures (RPV, cavity, etc)	m ³	0.300
Total freeboard volume (incl. subcompartment)	m ³	13.880
Subcompartment		
Outer diameter (inside)	m	1.810
Inner diameter	m	0.600
Height	m	1.070
Volume	m ³	2.451
Pressure vessel modeling the Reactor Cooling System (RCS) and Reactor Pressure Vessel (RPV)		
Inner diameter of RCS	m	0.200
Height of RCS	m	1.593
Volume of RCS	m ³	0.0500
Volume of the line connecting to accumulator valve	m ³	0.0011
Total volume of RCS	m ³	0.0511
Height of upper RPV (same diameter as RCS)	m	0.430
Volume of upper RPV	m ³	0.0135
<i>Inner diameter of lower RPV (crucible at flange)</i>	<i>m</i>	<i>0.232</i>
<i>Height of lower RPV (crucible at flange)</i>	<i>m</i>	<i>0.071</i>
<i>Volume of lower RPV (crucible at flange)</i>	<i>m³</i>	<i>0.003</i>
<i>Inner diameter of lower RPV (crucible above valve)</i>	<i>m</i>	<i>0.2685</i>
<i>Height of lower RPV (crucible above valve)</i>	<i>m</i>	<i>0.220</i>
<i>Volume of lower RPV (crucible above valve)</i>	<i>m³</i>	<i>0.0125</i>
Total empty volume of RPV with rupture disk	m ³	0.0290
Total empty volume of RPV with valve	m ³	0.0259
Total volume of RCS and RPV with rupture disk	m ³	0.0801
Total volume of RCS and RPV with valve	m ³	0.0770
Volume of the steam accumulator	m ³	0.0820
Cavity		
Height of cavity	m	0.612
Diameter of cavity (lower part, concrete wall)	m	0.342
Height of lower part (concrete wall)	m	0.462
Diameter of cavity (upper part, steel wall)	m	0.540
Height of upper part (steel wall)	m	0.150
Length from RPV bottom (lower head) to cavity floor	m	0.066
Length of annular cross section	m	0.316
Gap width between RPV and cavity wall	m	0.021
Cut out diameter at nozzles (around main cooling lines)	m	0.086
Diameter of connecting pipe attached to cut out	m	0.107

RPV- exit hole / tube diameter	m	0.025
Empty volume of cavity (without RPV)	m ³	0.0748
Free volume of cavity	m ³	0.0365
Cross sections for flow into containment (G01-G08)		
RPV- exit hole area	m ²	0.0005
Minimum flow area of annulus (between RPV and cavity wall)	m ²	0.0212
Flow area in upper part of cavity	m ²	0.1583
Cross sections for flow into containment (G01-G06)		
Flow area at nozzles (4×cut out area)	m ²	0.0232
Flow cross section of 4 connecting pipes (total)	m ²	0.0360
Cross sections for flow into containment (G07-G08)		
Flow area at nozzles (8 x cut out area – 8 x cold/hot leg area)	m ²	0.0308
Flow area between subcomp. and containment (4 x Ø 0.13 m)	m ²	0.0531

Table 2. a Thermocouple Summary for G02 – G05

No. T	Location	Position		
		height from con- tainment floor cm	distance from con- tainment wall cm	angular degree
1	accumulator low			
2	accumulator high			
3	RCS high (4.4 cm)			
4	RCS low (164 cm)			
5	accumulator (bottom)			
6	CPV A1	46	48.5	45
7	CPV-A2 (subcomp.)	47	53	135
8	CPV-A3 (subcomp.)	45	49	225
9	CPV-B1	120	40	45
10	CPV-B2	119	42	135
11	CPV-B3	114	45	225
12	CPV-C1	205	40	45
13	CPV-C2	206	52	135
14	CPV-D2	293	17	135
15	CPV-D3	272	39	225
16	CPV-D3	274	9.5	225
18	cavity (Fig. 10)			
19	cavity			
20	cavity			

*CPV = Containment Pressure Vessel

Table 2.b Thermocouple Summary for G06

No. T	Location	Position		
		height from con- tainment floor cm	distance from con- tainment wall cm	angular degree
1	accumulator low			
2	accumulator high			
3	RCS high (4.4 cm)			
4	RCS low (164 cm)			
5	accumulator (bottom)			
6	CPV A1	46	48.5	45
7	CPV-A2 (subcomp.)	47	53	135
8	CPV-A3 (subcomp.)	45	49	225
9	CPV-B1	133	50	45
10	CPV-B2	120	40	135
11	CPV-B3	116	38	225
12	CPV-C1	222	41	45
13	CPV-C2	208	40	135
14	CPV-D2	278	43	135
15	CPV-C3	223	37	225
16	CPV-D3	278	38	225

Table 2.c Thermocouple Summary for G07 and G08

No. T	Location	Position		
		height from con- tainment floor cm	distance from con- tainment wall cm	angular degree
1	accumulator low			
2	accumulator high			
3	RCS high (4.4 cm)			
4	RCS low (164 cm)			
5	accumulator (bottom)			
6	CPV A1	46	48.5	45
7	CPV-A2 (subcomp.)	47	53	135
8	CPV-A3 (subcomp.)	45	49	225
9	CPV-B1	118	52	45
10	CPV-B2	123	37	135
11	CPV-B3	118	34	225
12	CPV-C1	216	46	45
13	CPV-C2	218	29	135
14	CPV-D2	263	31	135
15	CPV-C3	228	40	225
16	CPV-D3	253	33	225

Table 3. Pressure transducer summary

No. P	Range [bar]	Position	Position	
			Height* cm	Angular degree
1	50 (Kistler)	RCS, transducer connected with pipe to outside containment		
2	50 (Kistler)	Accumulator top flange		
3A	35	RCS top flange		
3B	35	RCS top flange		
4	35	RCS top flange		
5	17	CPV A1		
6	17	CPV A2		
7	17	CPV B1		
8	17	CPV C2		
9	17	CPV B3		
10	17	cavity – 1 high	408	-35
11	17	cavity – 2 low	158	145
12	17	cavity – 3 high	408	145
13	35	cavity – 4 low	158	-35
14**	7	compartment - 1		
15**	17	compartment - 2		

* from concrete pit floor

** only in tests G07 and G08

Table 4. Initial Gas Composition in the Containment vessel

			G01	G02	G03	G04	G05	G06	G07	G08
Containment volume	V	m ³	13.75	13.75	13.75	13.75	13.75	13.75	13.75	13.75
Initial air temperature	T ₁	K	297	307	304	306	303	300	310	294
Atmospheric pressure	p ₁	MPa	0.200	0.200	0.200	0.100	0.100	0.100	0.100	0.100
Temperature at start	T₂	K	297	307	304	373	370	374	368	363
Pressure at start	p₂	MPa	0.200	0.200	0.205	0.204	0.205	0.221	0.202	0.202
Added hydrogen	m_{H2}	kg	0	0	0.050	0.047	0.130	0.098	0.110	0.050
Air mass	m _{air}	kg	32.250	31.199	31.507	15.651	15.806	15.964	15.449	15.289
Steam mass	m_{steam}	kg	0.0	0.0	0.0	6.138	5.515	6.800	5.762	5.999
Partial pressure of air	P _{2air}	MPa	0.200	0.200	0.200	0.122	0.122	0.125	0.119	0.123
Partial pressure H ₂	p _{2H2}	MPa	0.0	0.0	0.0046	0.0053	0.0144	0.0110	0.0121	0.0054
Partial pressure steam	P _{steam}	MPa	0.0	0.0	0.0	0.0768	0.0685	0.0854	0.0712	0.0731
Added hydrogen	M_{H2}	mol	0	0	24.8	23.3	64.4	48.5	54.5	24.8
Steam moles	M_{H2O}	mol	0	0	0	341	306	377	320	333
Air moles	M _{air}	mol	1114	1077	1088	540	546	551	533	562
Total gas moles	M_{total}	mol	1114	1077	1113	904	916	977	908	920
Nitrogen moles	M _{N2}	mol	869	841	849	422	426	430	416	439
Oxygen moles	M _{O2}	mol	234	226	228	113	115	116	112	118
Argon etc. moles	M _{Ar etc.}	mol	11	10	10	5	5	5	5	5
Mol% of hydrogen	M_{H2}/M_{tot}	%	0	0	2.22	2.58	7.02	4.96	6.00	2.69
Mol% of steam	M_{H2O}/M_{tot}	%	0	0	0	37.67	33.41	38.62	35.23	36.19
Mol% of air	M _{air} /M _{tot}	%	100.00	100.00	97.78	59.75	59.57	56.41	58.77	61.12
Mol% of nitrogen	M _{N2} /M _{tot}	%	78.03	78.03	76.29	46.63	46.48	44.02	45.86	47.69
Mol% of oxygen	M _{O2} /M _{tot}	%	20.99	20.99	20.52	12.54	12.50	11.84	12.34	12.83
Mol% of argon	M _{Ar} /M _{tot}	%	0.96	0.96	0.94	0.58	0.57	0.54	0.57	0.59

Table 5. Compilation of main initial conditions in RPV/RCS

		G01	G02	G03	G04	G05	G06	G07	G08
RPV/RCS pressure	MPa	2.135	1.958	1.990	1.870	2.018	2.175	2.670	1.950
RPV/RCS temperature	K	370	369	365	471	470	400	471	472
RPV/RCS steam	kg	0	0	0	0.208	0.242	0	0	0.210
RPV/RCS nitrogen	kg	0.560	0.073	0.812	0.057	0.057	0.067	0.057	0.057
RPV/RCS hydrogen	kg	0.088	0.098	0.048	0.050	0.052	0.103	0.107	0.053
RPV/RCS steam	mol	0	0	0	12	13	0	0	12
RPV/RCS nitrogen	mol	20	3	29	2	2	2	2	2
RPV/RCS hydrogen	mol	43.6	48.5	23.8	24.8	25.7	51	53	26.2

Table 6. Measured gas concentrations in G01

Time	Location	Species (mole %)		
		N ₂	O ₂	H ₂
-60 s	Subcompartment	78.70	21.30	0
	Containment	78.95	21.05	0
10 s	Subcompartment	78.65	21.35	0
	Containment	79.54	20.46	0
5 min	Subcompartment	79.46	20.54	0
	Containment	80.48	19.52	0

Table 7. Measured gas concentrations in G02

Time	Location	Species (mole %)		
		N ₂	O ₂	H ₂
-60 s	Subcompartment	78.73	21.27	< 0.1
	Containment-low	79.10	20.90	< 0.1
	Containment-high	no data	no data	-
10 s	Subcompartment	79.33	20.67	< 0.1
	Containment-low	80.65	19.35	< 0.1
	Containment-high	80.75	19.25	< 0.1
5 min	Subcompartment	79.99	20.01	< 0.1
	Containment-low	80.65	19.35	< 0.1
	Containment-high	79.97	20.03	< 0.1

Table 8. Measured gas concentrations in G03

Time	Location	Species (mole %)		
		N ₂	O ₂	H ₂
-60 s	Subcompartment	76.97	20.73	2.30
	Containment-low	77.01	20.85	2.14
	Containment-high	no data	-	-
10 s	Subcompartment	77.31	20.42	2.27
	Containment-low	80.37	18.36	1.27
	Containment-high	79.01	19.42	1.57
5 min	Subcompartment	77.84	20.16	2.00
	Containment-low	78.70	19.43	1.87
	Containment-high	78.76	19.30	1.94

Table 9. Measured gas concentrations in G04

Time	Location	Species (mole %)			
		N ₂	O ₂	H ₂	He
-60 s	Subcompartment	74.99	19.79	4.61	0.61
	Containment-low	74.99	19.56	4.60	0.85
	Containment-high	77.45	17.99	3.99	0.66
10 s	Subcompartment	73.92	19.67	5.86	0.55
	Containment-low	77.40	18.08	3.80	0.72
	Containment-high	79.82	16.42	3.04	0.72
5 min	Subcompartment	77.45	17.90	3.99	0.66
	Containment-low	77.98	17.46	3.87	0.69
	Containment-high	77.93	17.55	3.85	0.67

Table 10. Measured gas concentrations in G05

Time	Location	Species (mole %)		
		N ₂	O ₂	H ₂
-60 s	Subcompartment	70.68	17.91	11.41
	Containment-low	71.15	17.32	11.53
	Containment-high	70.82	17.70	11.48
10 s	Subcompartment	77.89	16.90	5.21
	Containment-low	81.53	14.80	3.67
	Containment-high	84.80	13.29	1.91
5 min	Subcompartment	83.39	13.83	2.78
	Containment-low	83.54	13.91	2.55
	Containment-high	84.35	13.13	2.52

Table 11. Measured gas concentrations in G06

Time	Location	Species (mole %)		
		N ₂	O ₂	H ₂
-60 s	Subcompartment	72.46	18.03	9.51
	Containment-low	72.60	17.91	9.49
	Containment-high	72.24	18.08	9.68
10 s	Subcompartment	75.10	17.07	7.83
	Containment-low	79.90	15.15	4.95
	Containment-high	87.40	11.32	1.28
5 min	Subcompartment	82.09	13.56	4.35
	Containment-low	82.56	13.46	3.98
	Containment-high	82.67	13.43	3.90

Table 12. Measured gas concentrations in G07

Time	Location	Species (mole %)		
		N ₂	O ₂	H ₂
-60 s	Subcompartment	71.28	18.26	10.46
	Containment-low	71.49	18.21	10.30
	Containment-high	71.52	18.16	10.32
10 s	Subcompartment	76.44	5.33 ?	18.23 ?
	Containment-low	80.71	15.22	4.07
	Containment-high	80.30	15.85	3.85
5 min	Subcompartment	79.47	13.28	7.25
	Containment-low	79.62	13.78	6.60
	Containment-high	80.01	13.42	6.57

Table 13. Measured gas concentrations in G08

Time	Location	Species (mole %)		
		N ₂	O ₂	H ₂
-60 s	Subcompartment	76.69	18.25	4.46
	Containment-low	75.66	19.96	4.38
	Containment-high	76.27	19.28	4.45
10 s	Subcompartment	81.06	12.15	6.79
	Containment-low	77.92	18.50	3.58
	Containment-high	77.54	18.41	4.04
5 min	Subcompartment	77.48	17.60	4.92
	Containment-low	77.68	17.54	4.78
	Containment-high	77.55	17.75	4.70

Table 14. Initial Conditions, Results and Analysis of G-series

			G01	G02	G03	G04	G05	G06	G07	G08
1	RPV pressure	MPa	2.16	1.96	1.99	1.87	2.02	2.18	2.67	1.95
2	Steam concentration in cont.	mol %	0	0	0	37.67	33.41	38.62	35.23	36.19
3	H ₂ concentration in cont.	mol %	0	0	2.22*	2.58*	7.02	4.96	6.00	2.69
4	Initial H ₂ in containment	mol	0	0	24.8	23.3	64.4	48.5	54.5	24.8
5	RPV-blow down H ₂	mol	43.6	48.5	23.8	24.8	25.7	51.0	53.0	26.2
6	Total available H ₂	mol	43.6	48.5	48.6	48.2	90.1	99.5	107.5	51
7	Burned H ₂ (N _H)	mol	43	36	27	30	81	74	72	24
8	Fraction burned	-	1.0	0.73	0.55	0.58	0.86	0.78	0.67	0.46
9	H ₂ post test concentration	mol %	0	1.2	1.9*	2.2*	1.1	1.7	3.6	2.9
10	Measured peak pressure increase	MPa	0.14	0.13	0.11	0.11	0.27	0.23	0.25	0.09
11	Theor. maximum Δp total	MPa	0,30	0,25	0,16	0,18	0,50	0,46	0,44	0,15
12	Efficiency	-	0,46	0,52	0,67	0,60	0,54	0,50	0,56	0,61

* The smaller number of total gas moles in G04 with steam atmosphere is the reason for the higher H₂-concentration

Table 15. Initial Conditions, Results and Analysis in H-series

			H01	H02	H03	H04	H05	H06
1	RPV pressure	MPa	0.77	1.22	1.25	0.89	1.21	2.16
2	Steam concentration in cont.	mol %	36.6	36.6	34.2	0	33.4	35.8
3	H ₂ concentration in cont.	mol %	2.6	2.6	2.7	0	2.9	3.1
4	Initial H ₂ in containment	mol	24	26	27	0	29	35
5	Blow down steam	mol	7	15	16	0	21	35
6	Produced H ₂	mol	n.a.	54	33	0	32	39
7	Total available H ₂	mol	n.a.	80	60	0	61	74
8	Burned H ₂ (N _H)	mol	n.a.	66	35	0	26	49
9	Fraction burned	-	n.a.	0.82	0.58	-	0.43	0.66
10	H ₂ post test concentration	mol %	n.a.	1.5	2.9	-	3.8	2.8
11	Measured peak pressure increase	MPa	0.170	0.236	0.114	0.156	0.090	0.194
12	Energy release by oxidation	MJ	n.a.	1,70	1,66	10,7	1,65	1,67
13	Energy by H ₂ combustion	MJ	n.a.	15,92	8,37	0	6,33	11,75
14	Max. Δp by oxid. and H ₂ comb.	MPa	n.a.	0,45	0,26	0,31	0,20	0,34
15	$\Delta p_{\text{measured}} / \Delta p_{\text{theor oxy+ combustion}}$	-	n.a.	0,52	0,44	0,50	0,45	0,57
16	Fraction of dispersed melt in SC and containment with diam. < 4 mm	-	0,30	0,50	0,30	0,63	0,30	0,36
17	Thermal energy of dispersed melt	MJ	8.35	13.9	8.35	17.5	8.35	10.0
18	Max. Δp by dispersed melt HT	MPa	0,19	0,28	0,18	0,34	0,18	0,22
19	Theor. maximum Δp total	MPa	n.a.	0,73	0,44	0,65	0,39	0,56
20	DCH efficiency	-	n.a.	0,32	0,26	0,24	0,23	0,35

FIGURES: Geometry

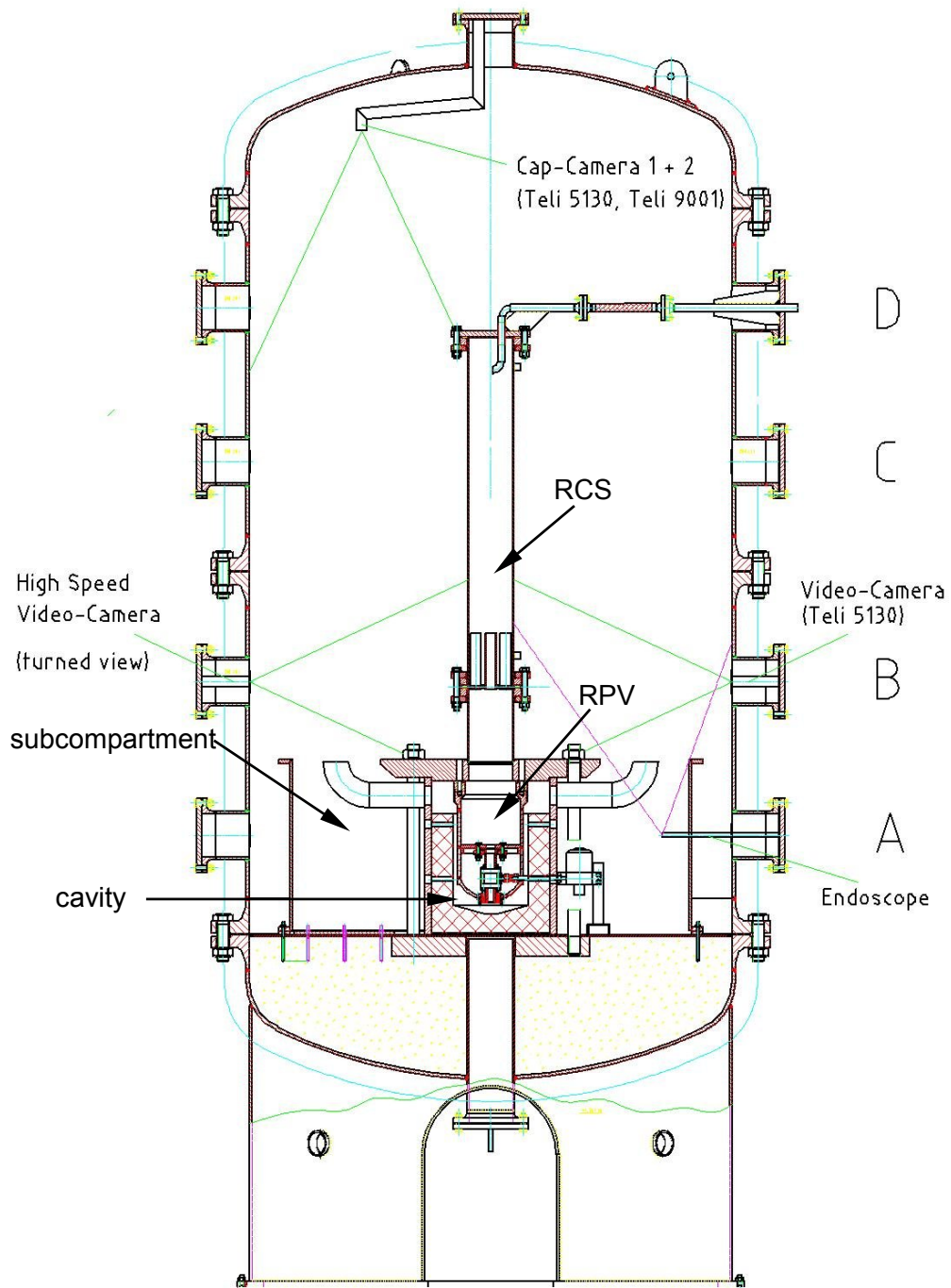


Fig. 1. The containment pressure vessel with internal structures

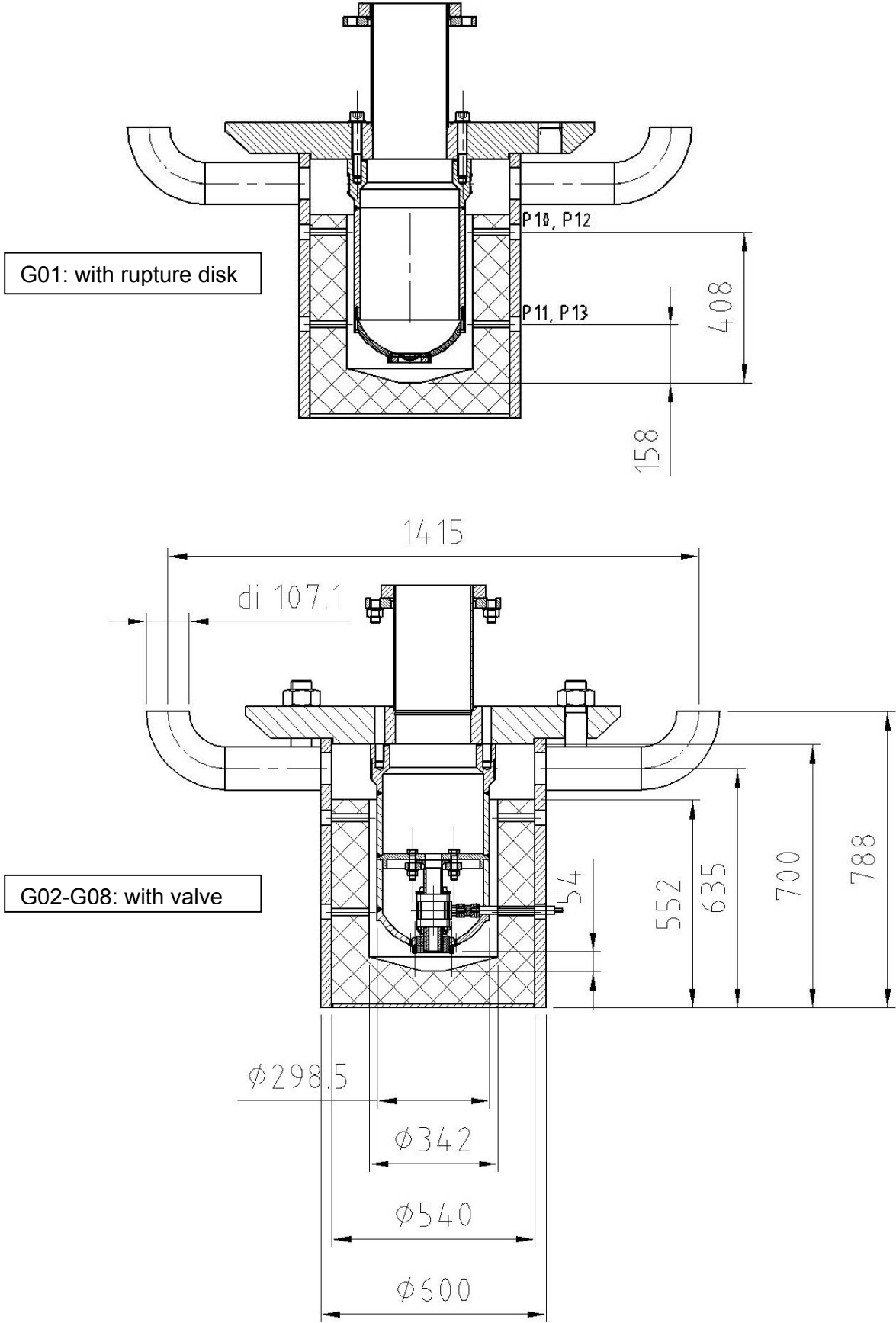


Fig. 2. Dimensions of the cavity

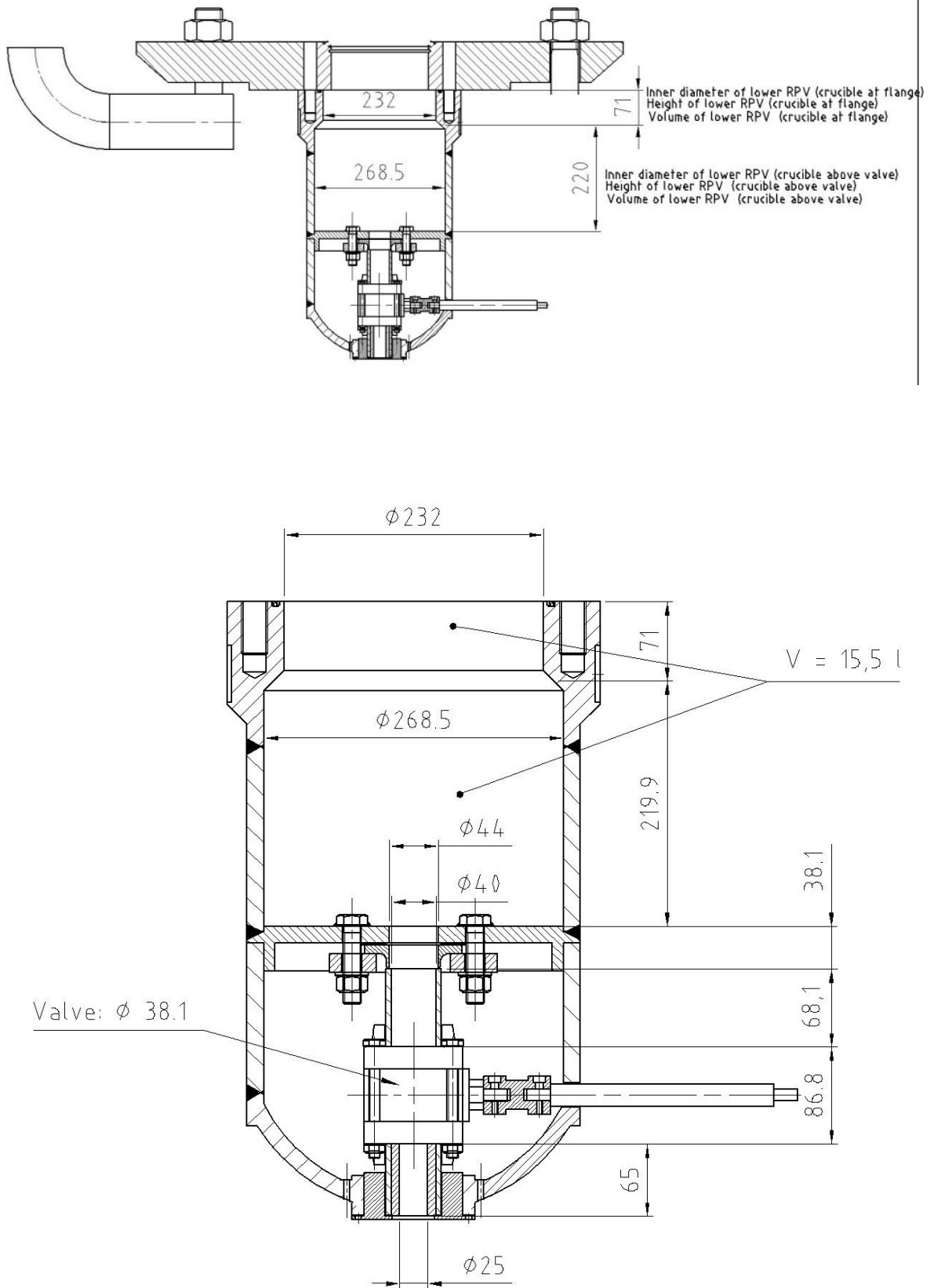


Fig. 3. Dimensions of the RPV vessel

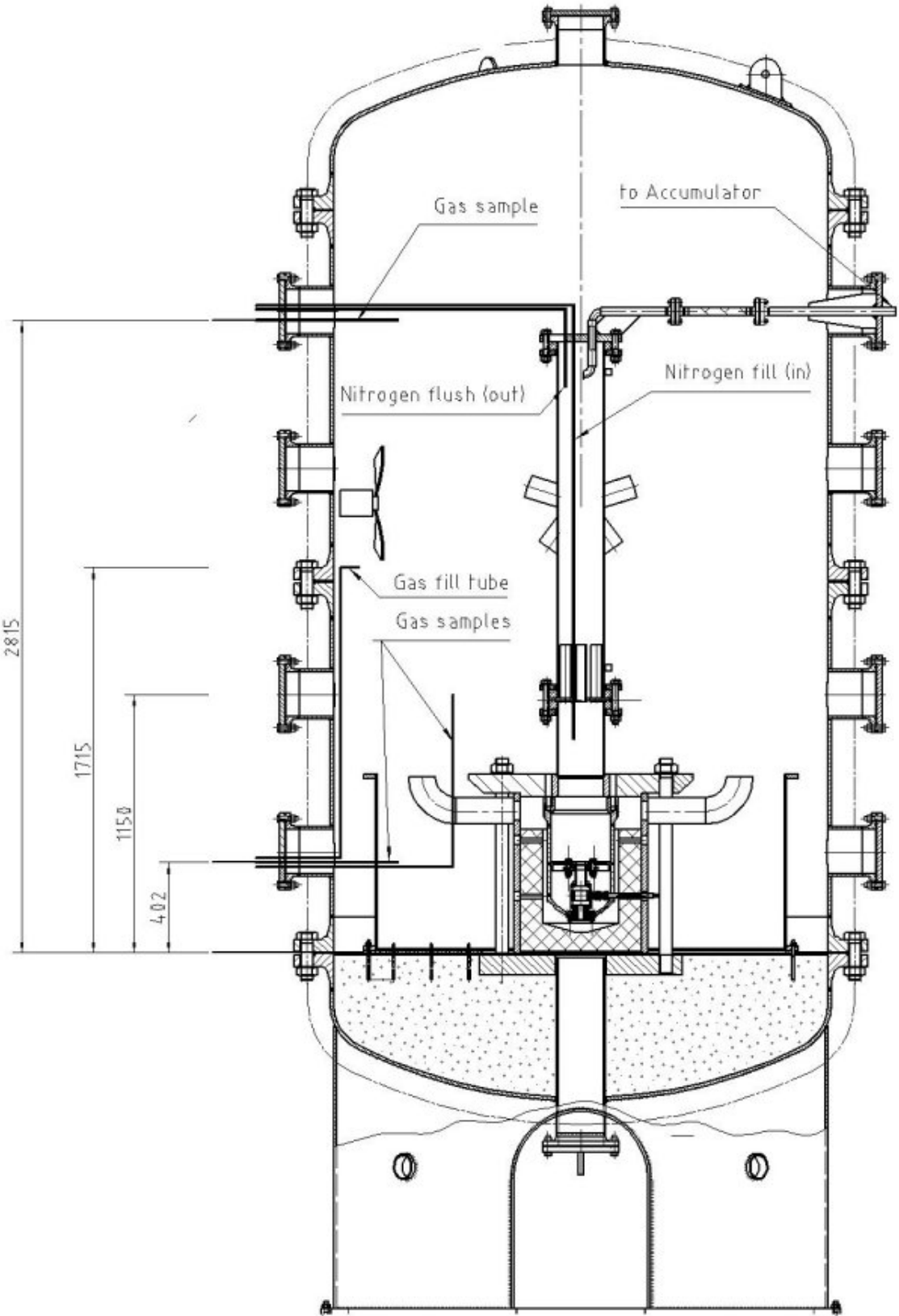


Fig. 4. Positions of gas filling and gas sample lines



Fig. 5. RPV exit formed by a pipe

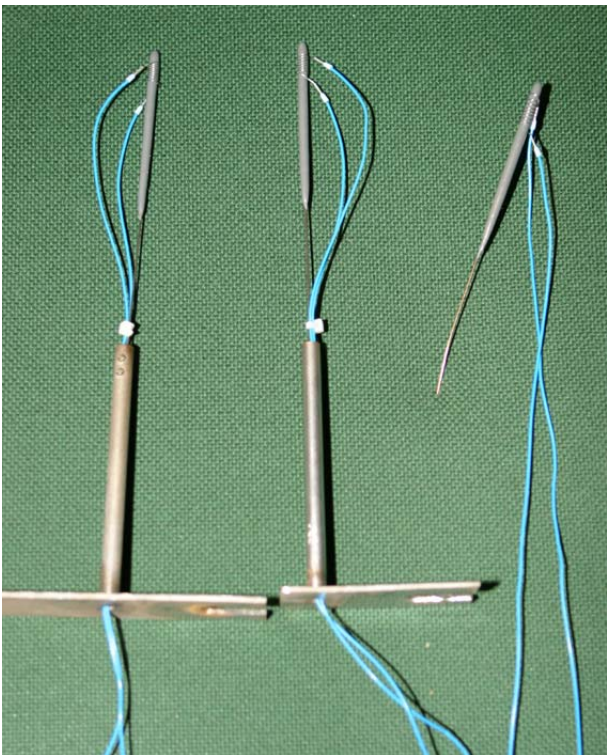


Fig. 6. Thermite igniters and electrical starter

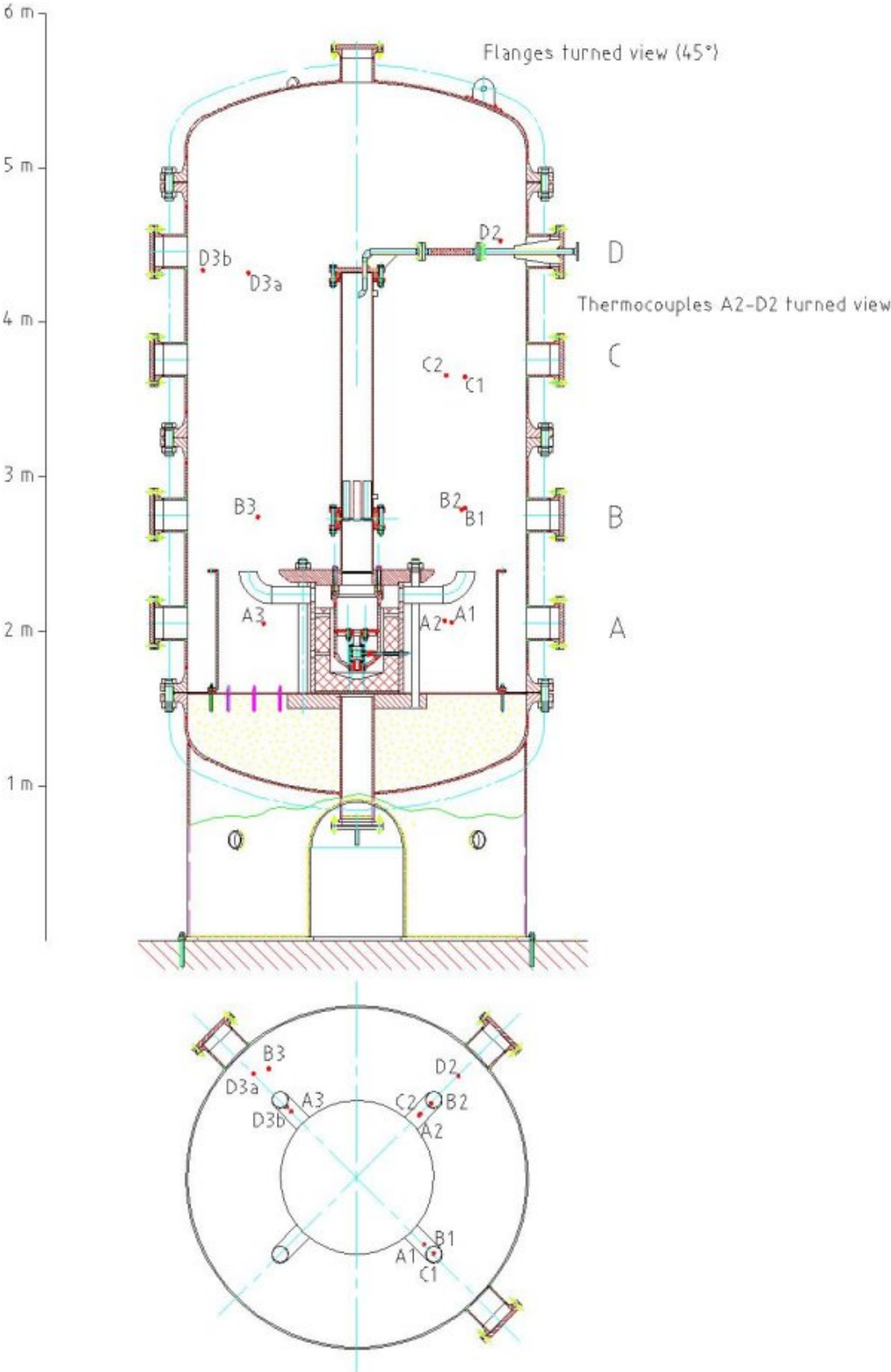


Fig. 7. Positions of thermocouples for G02-G05
(exact positions see Table 2 and 3)

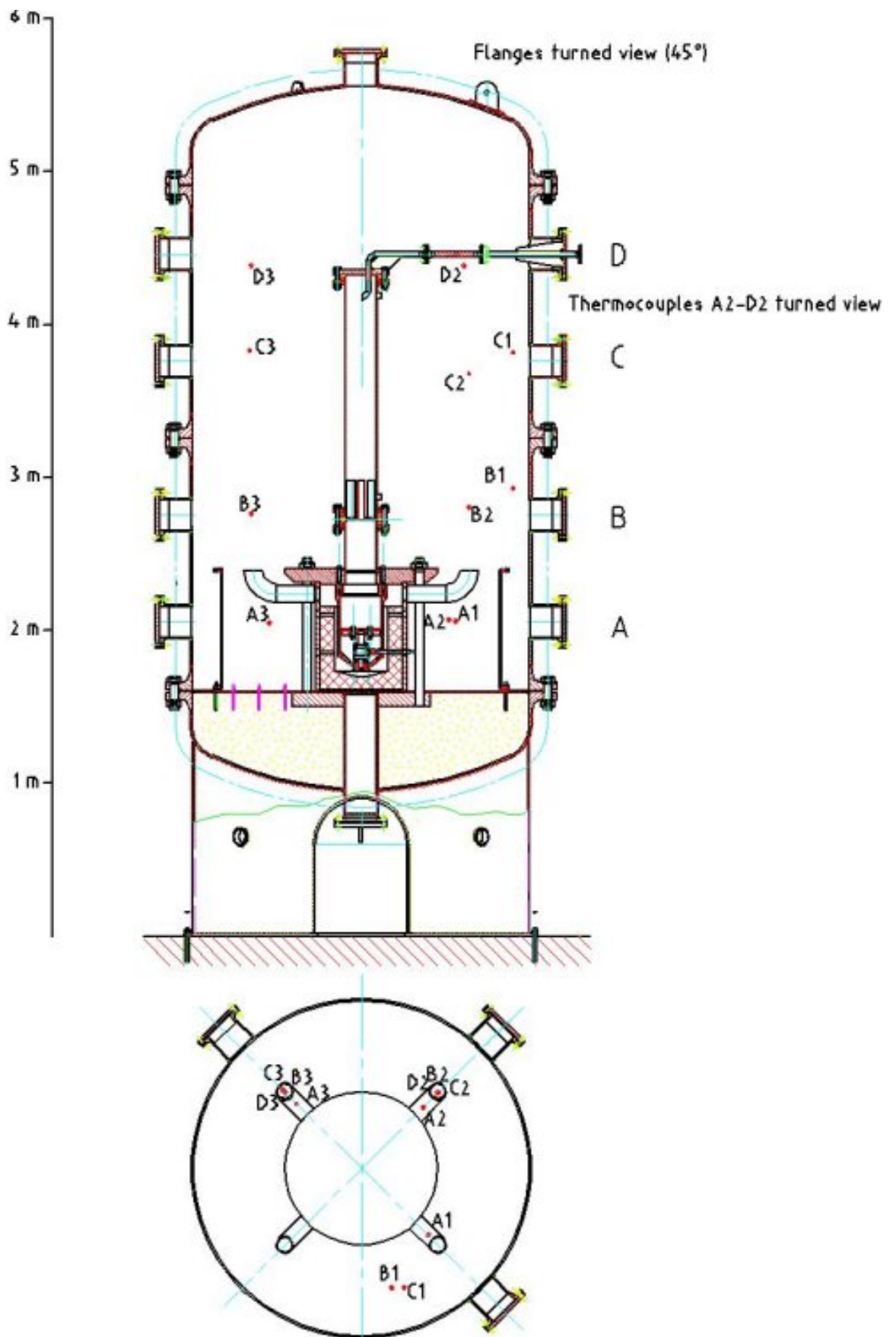


Fig. 8. Positions of thermocouples for G06
(exact positions see Table 2 and 3)

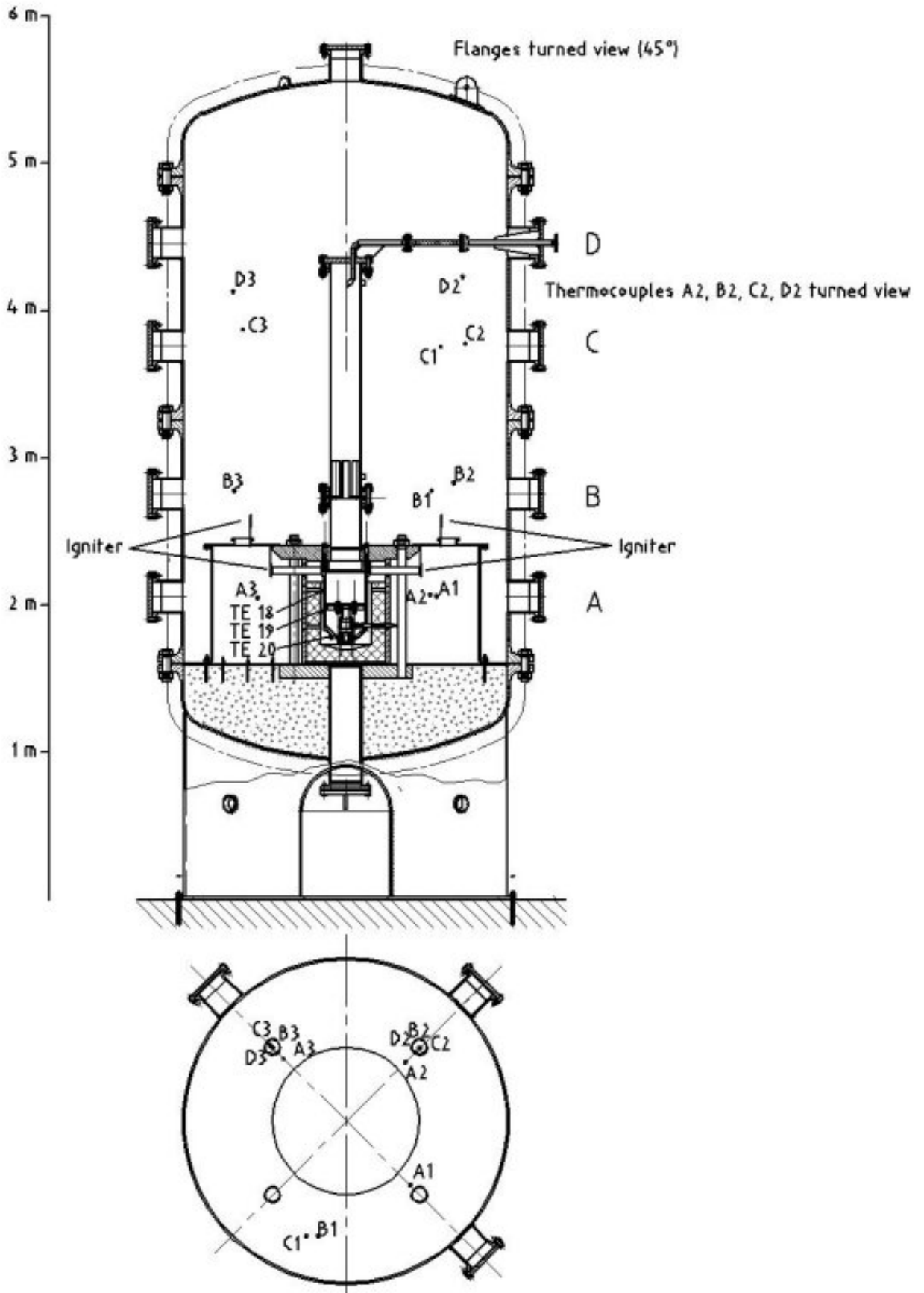


Fig. 9. Configuration of test facility in tests G07 and G08

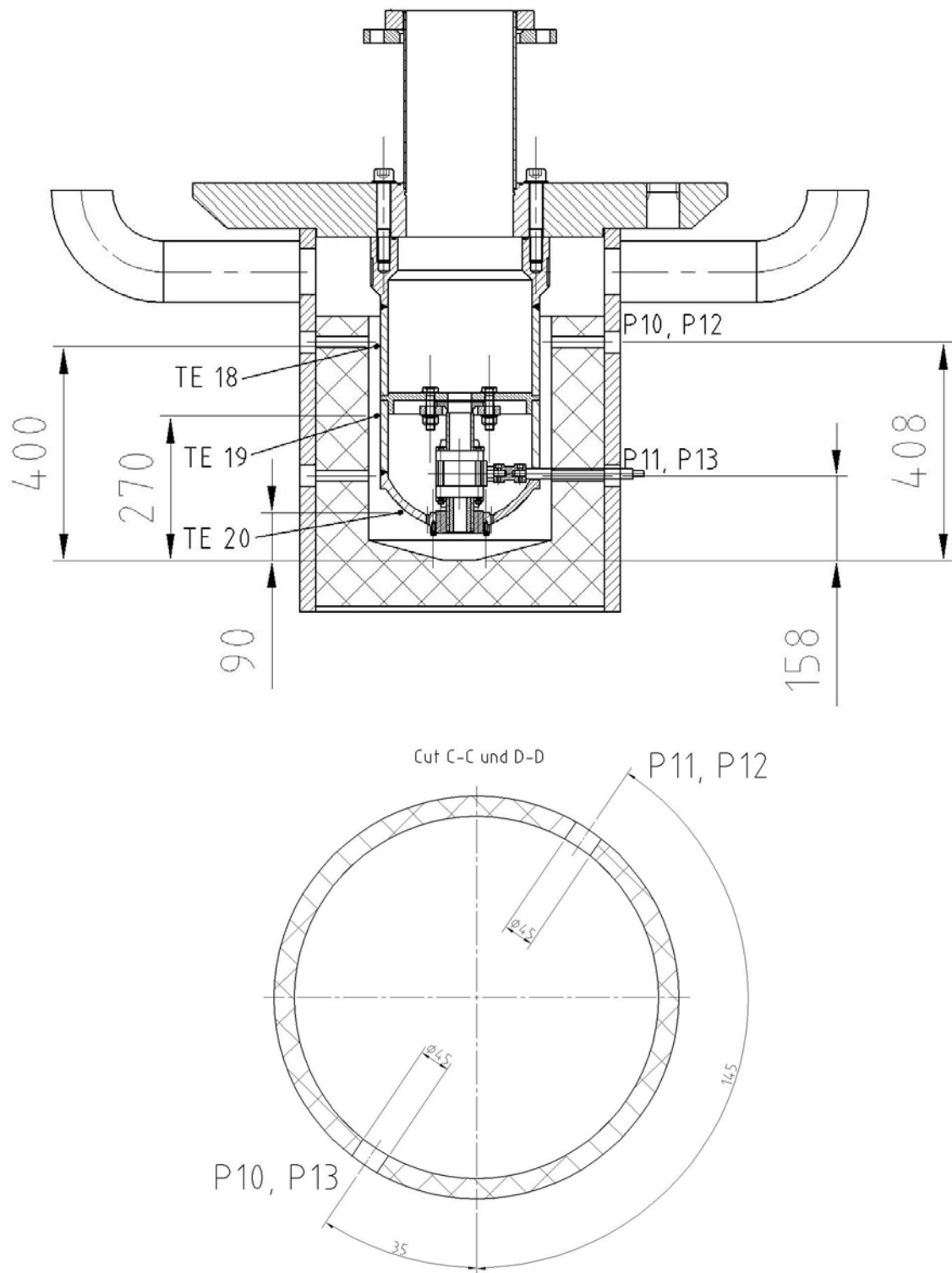


Fig. 10. Positions of pressure transducers and thermocouples in the cavity

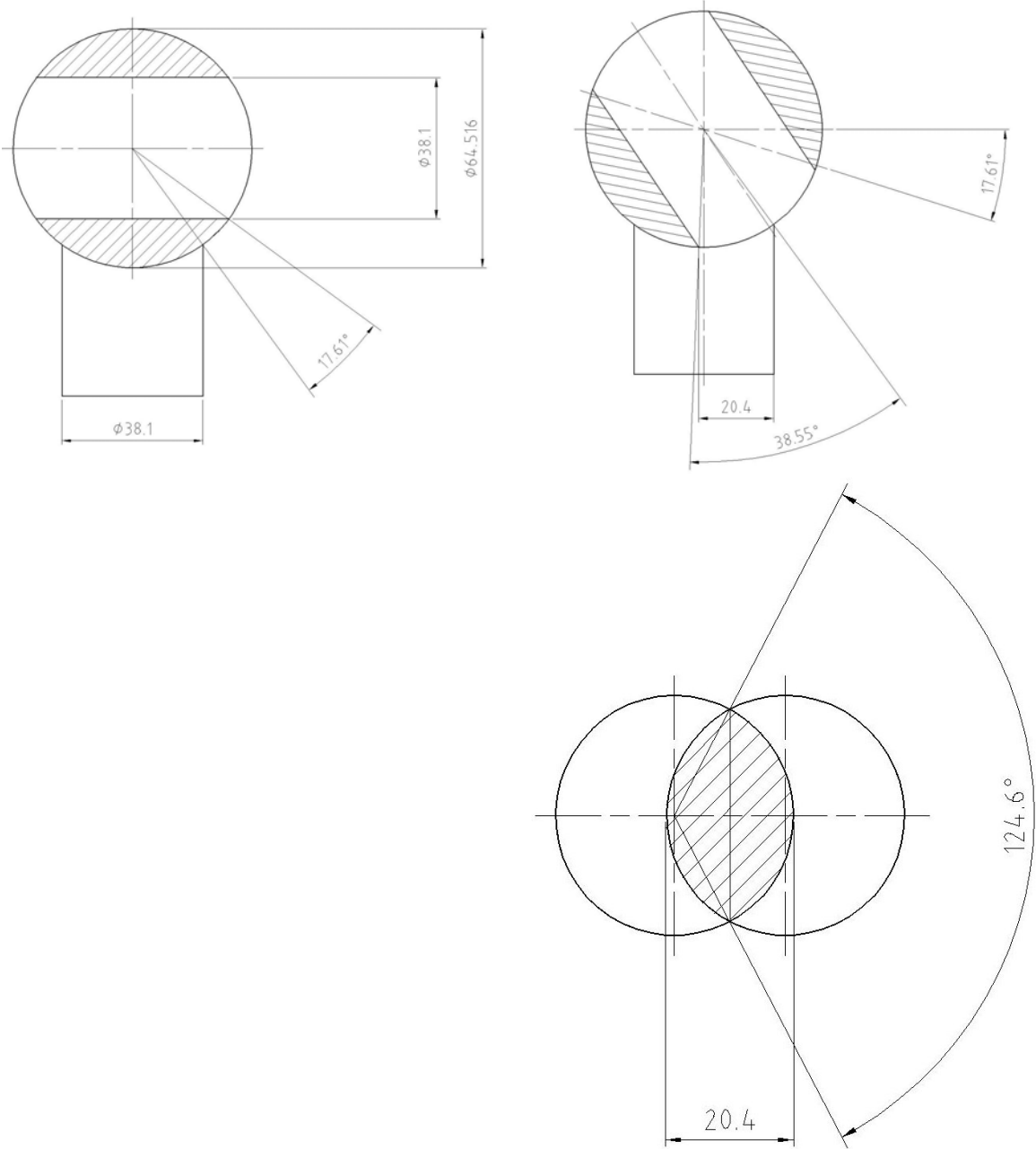


Fig. 11. Data of the ball valve



Fig. 12. View into containment vessel and cavity during assembly, G01-G06



Fig. 13. View into containment vessel, actual test configuration, G01-G06

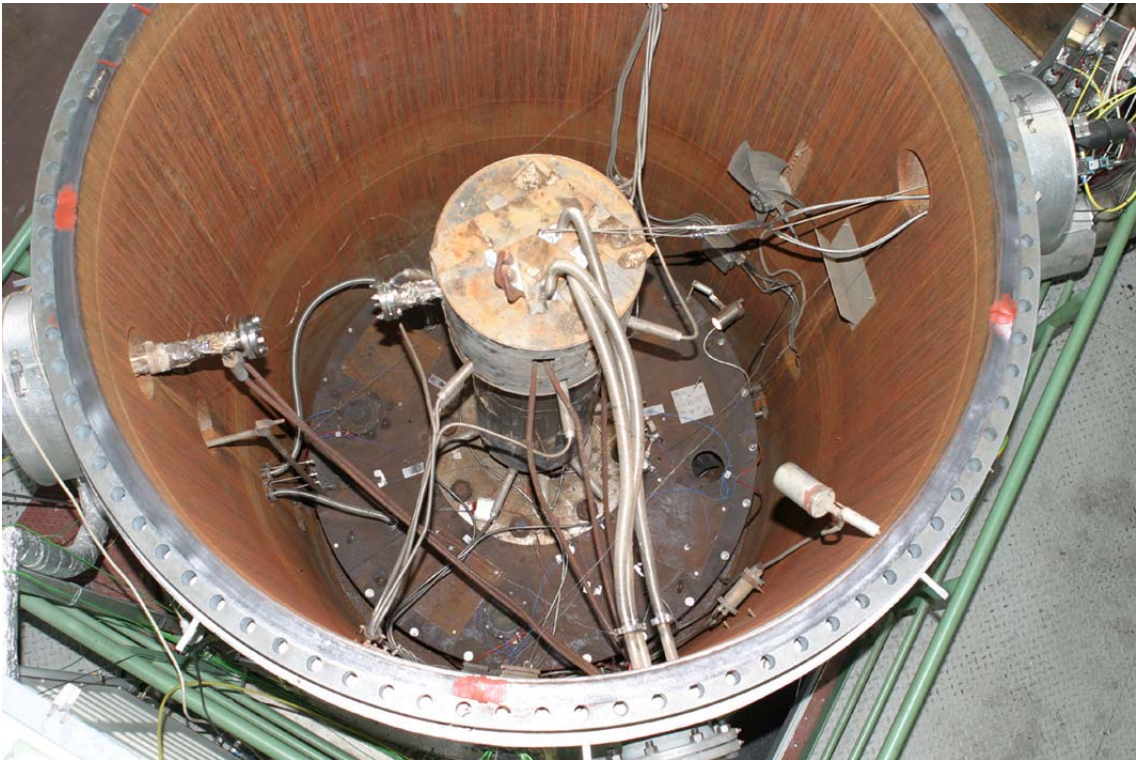


Fig. 14. View into containment vessel, actual test configuration, G07-G08

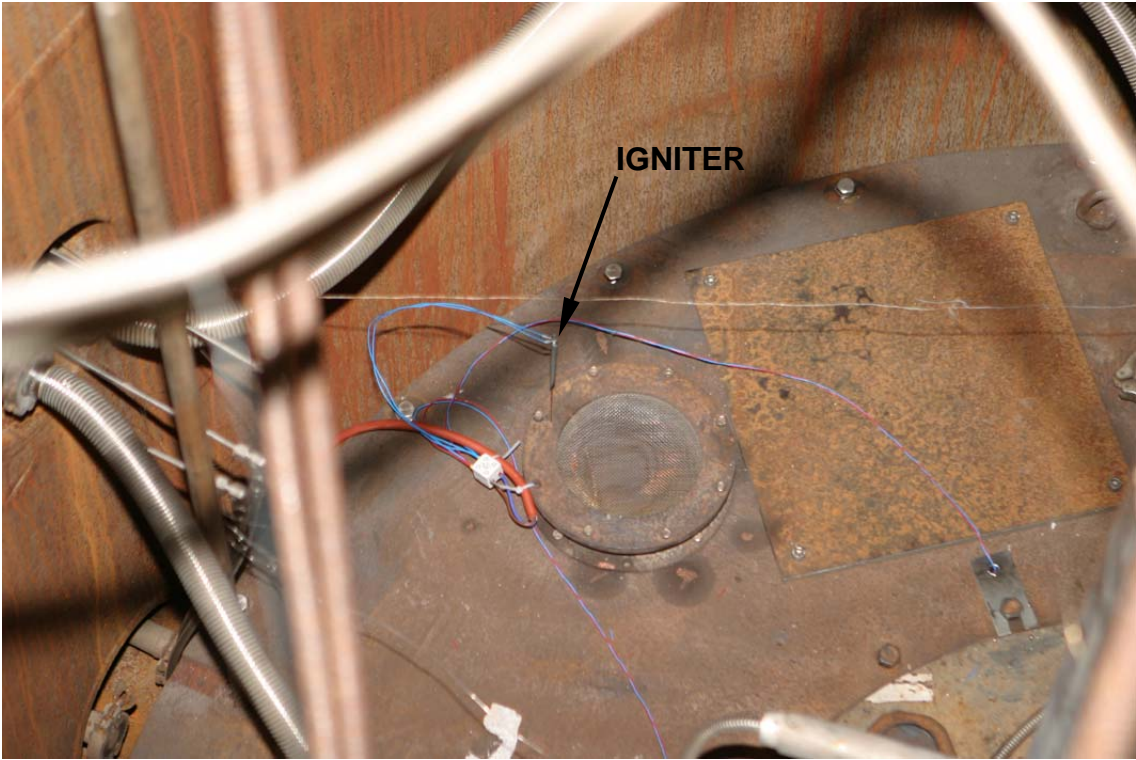


Fig. 15. Flow path from subcompartment with igniter, G07 – G08

FIGURES: Results

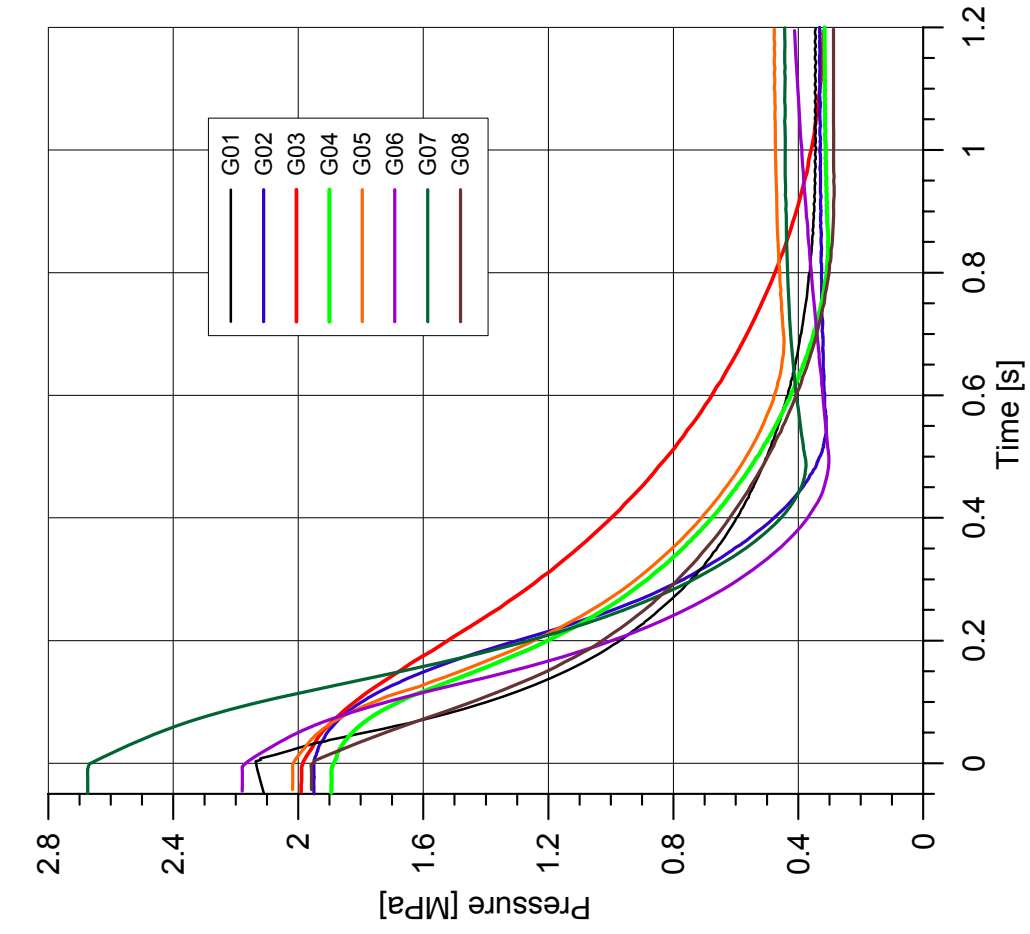


Fig. 16. Pressures in the RPV

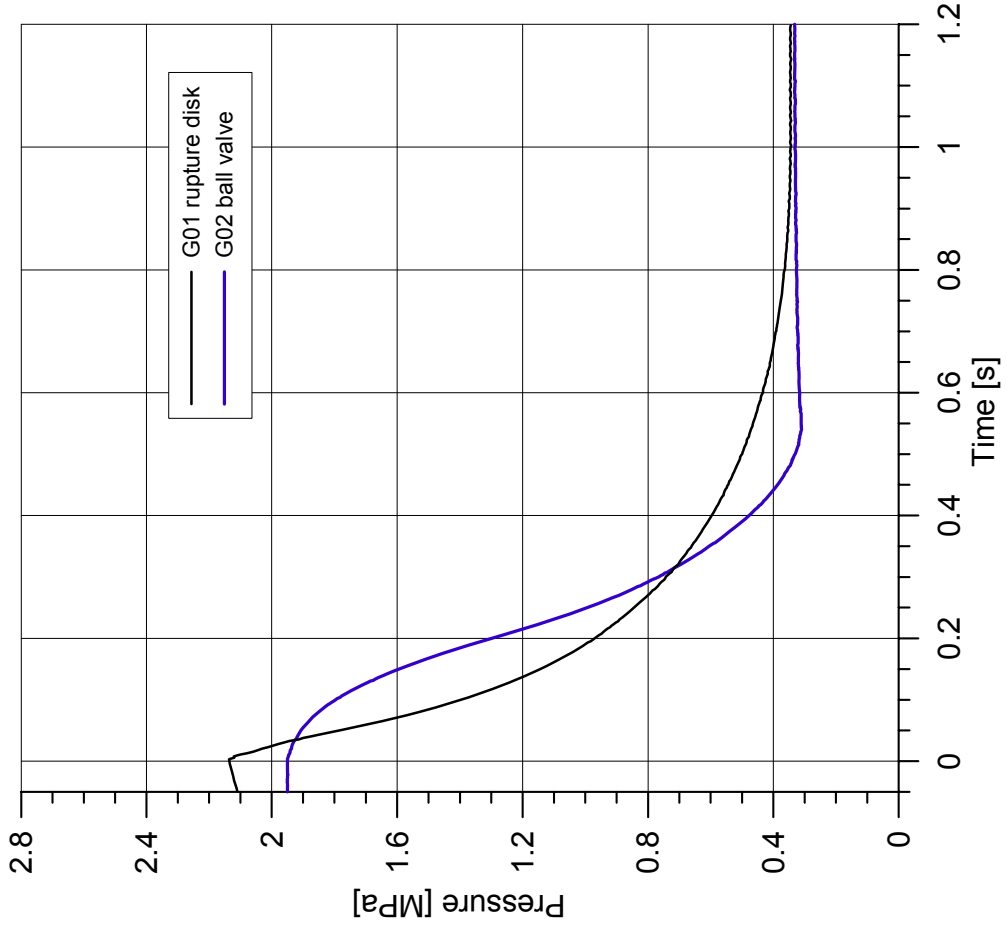


Fig. 17. Pressures in the RPV, rupture disk versus ball valve

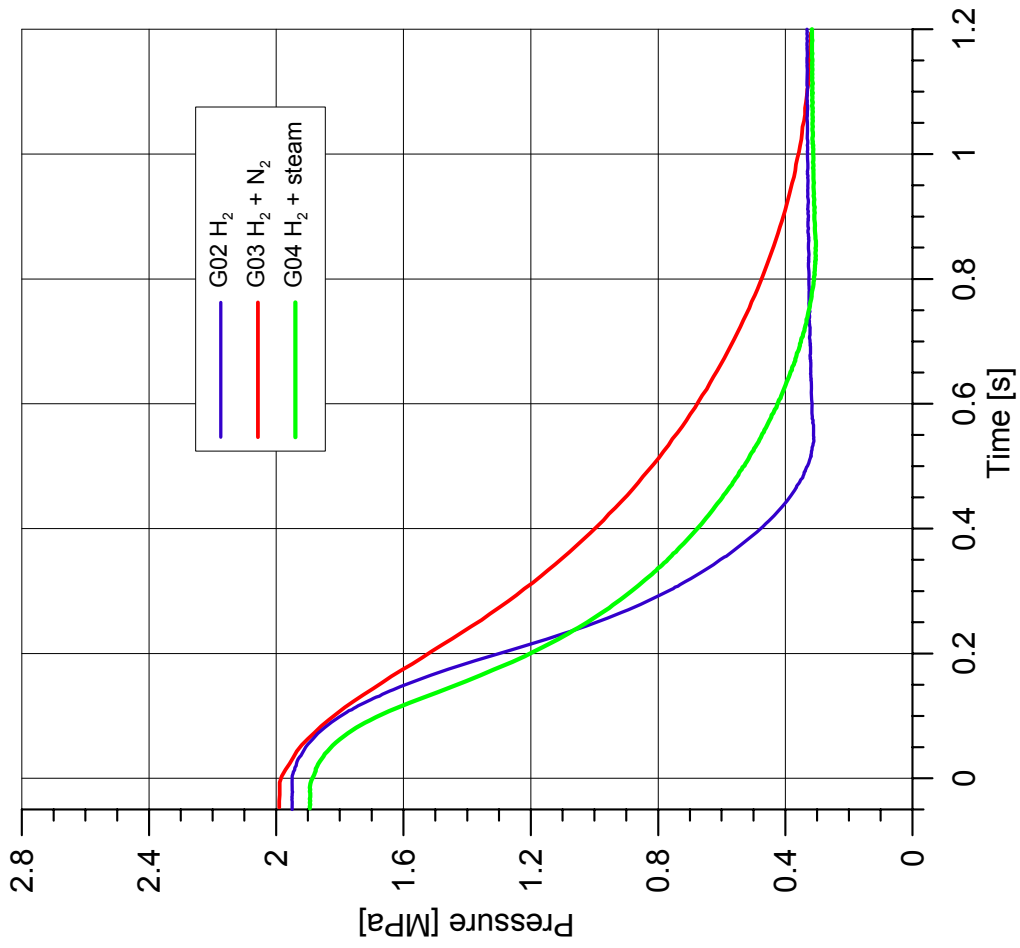


Fig. 18. Pressures in the RPV

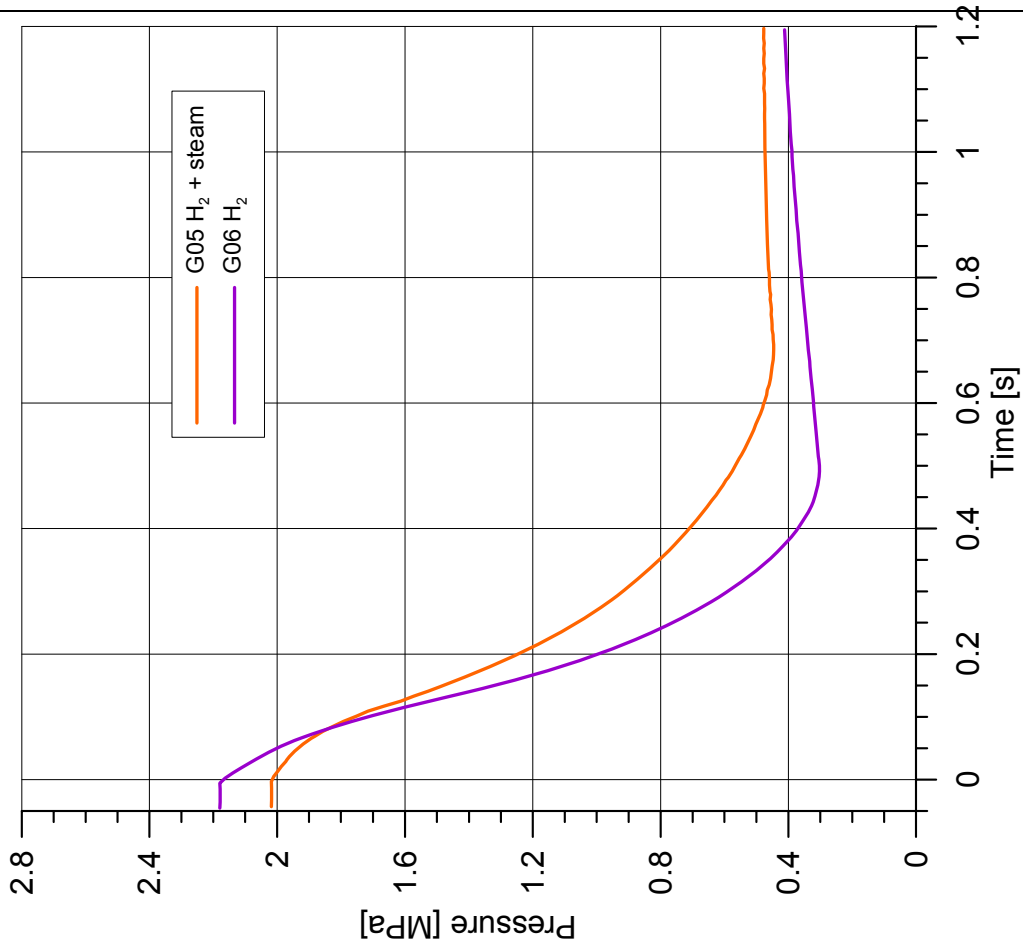


Fig. 19. Pressures in the RPV

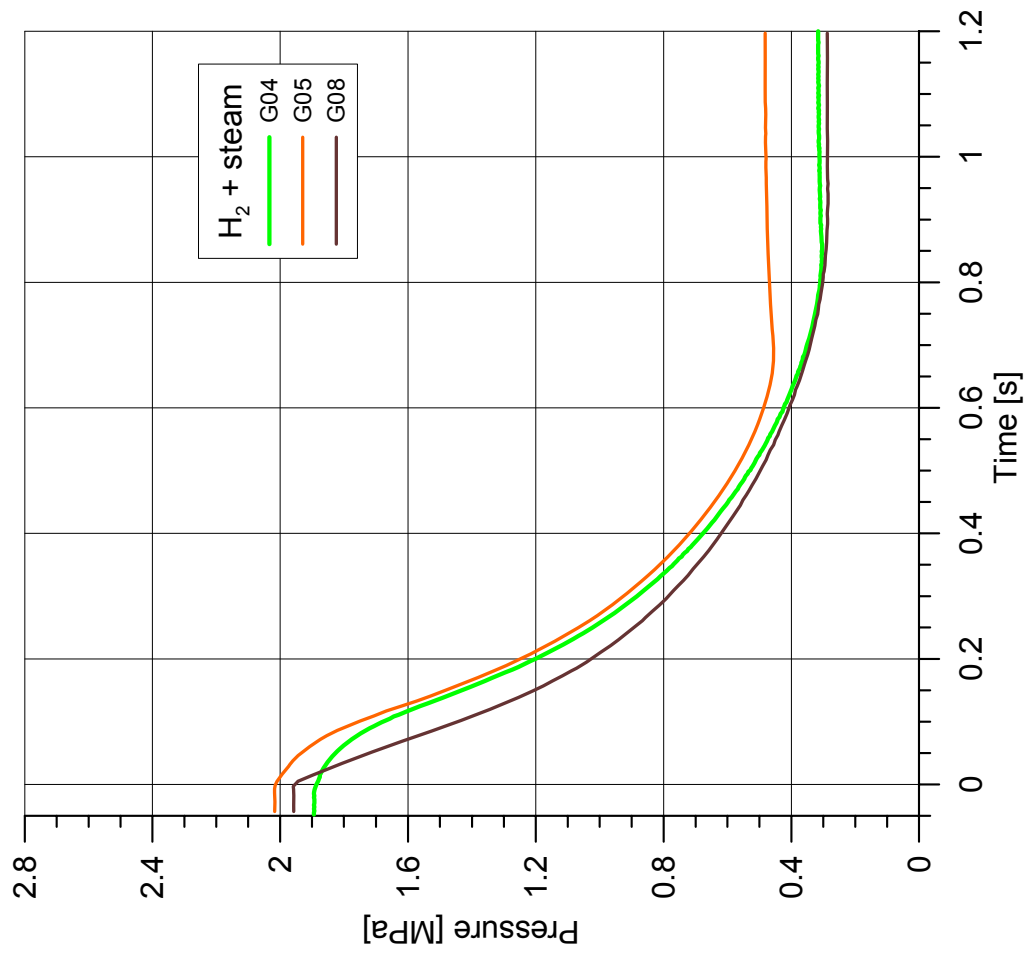


Fig. 20. Pressures in the RPV

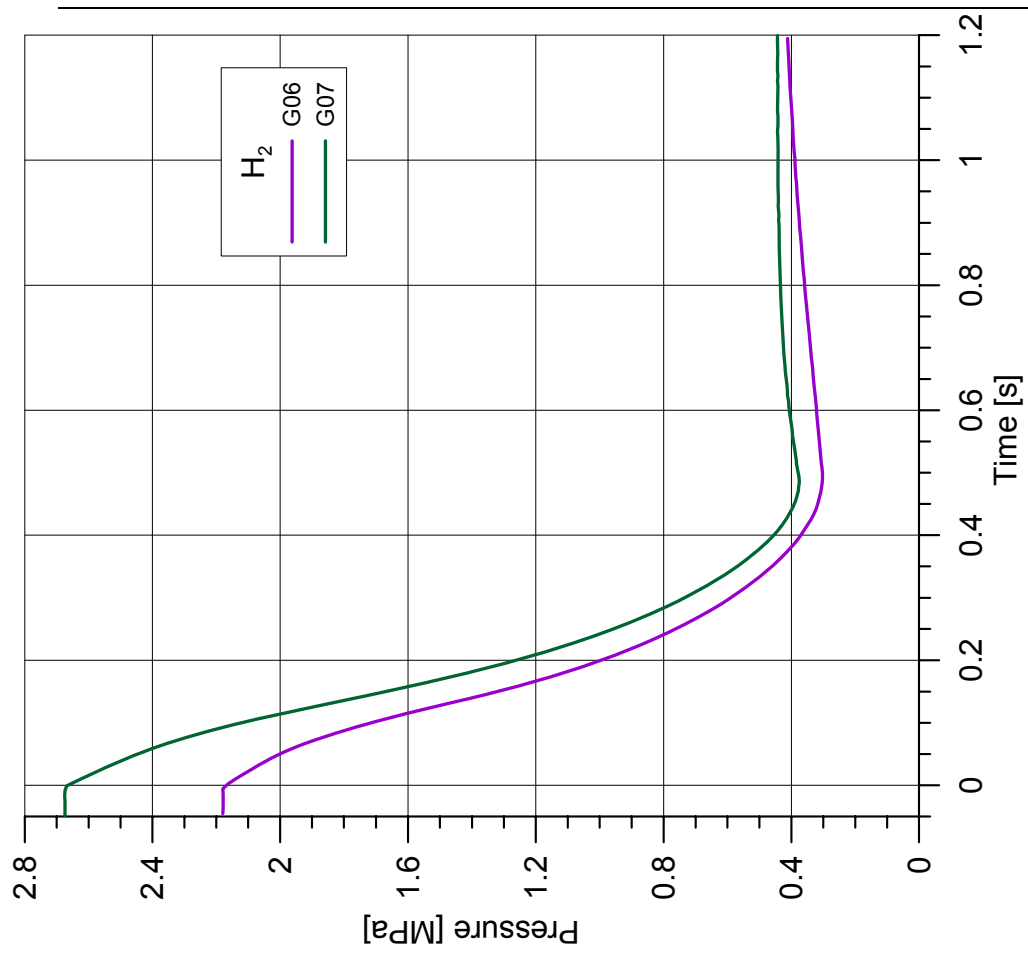
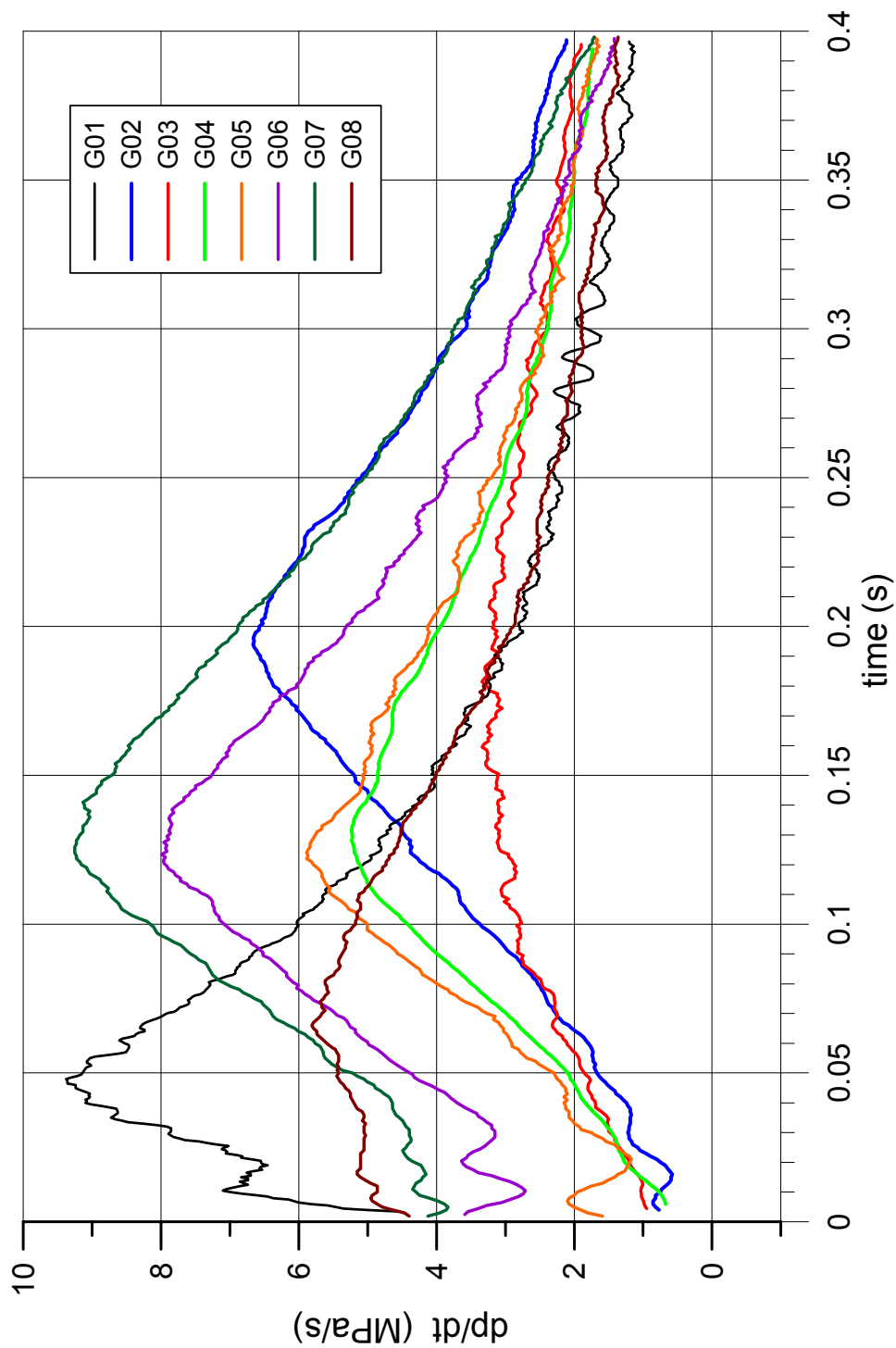


Fig. 21. Pressures in the RPV



No.	Gas	dp-max (ms)
G01	H ₂ + N ₂	49
G02	H ₂ + N ₂	192
G03	H ₂ + N ₂	192
G04	H ₂ + steam	120
G05	H ₂ + steam	120
G06	H ₂	120
G07	H ₂	120
G08	H ₂ + steam	68

Fig. 22. Pressure gradient dp/dt in the RPV

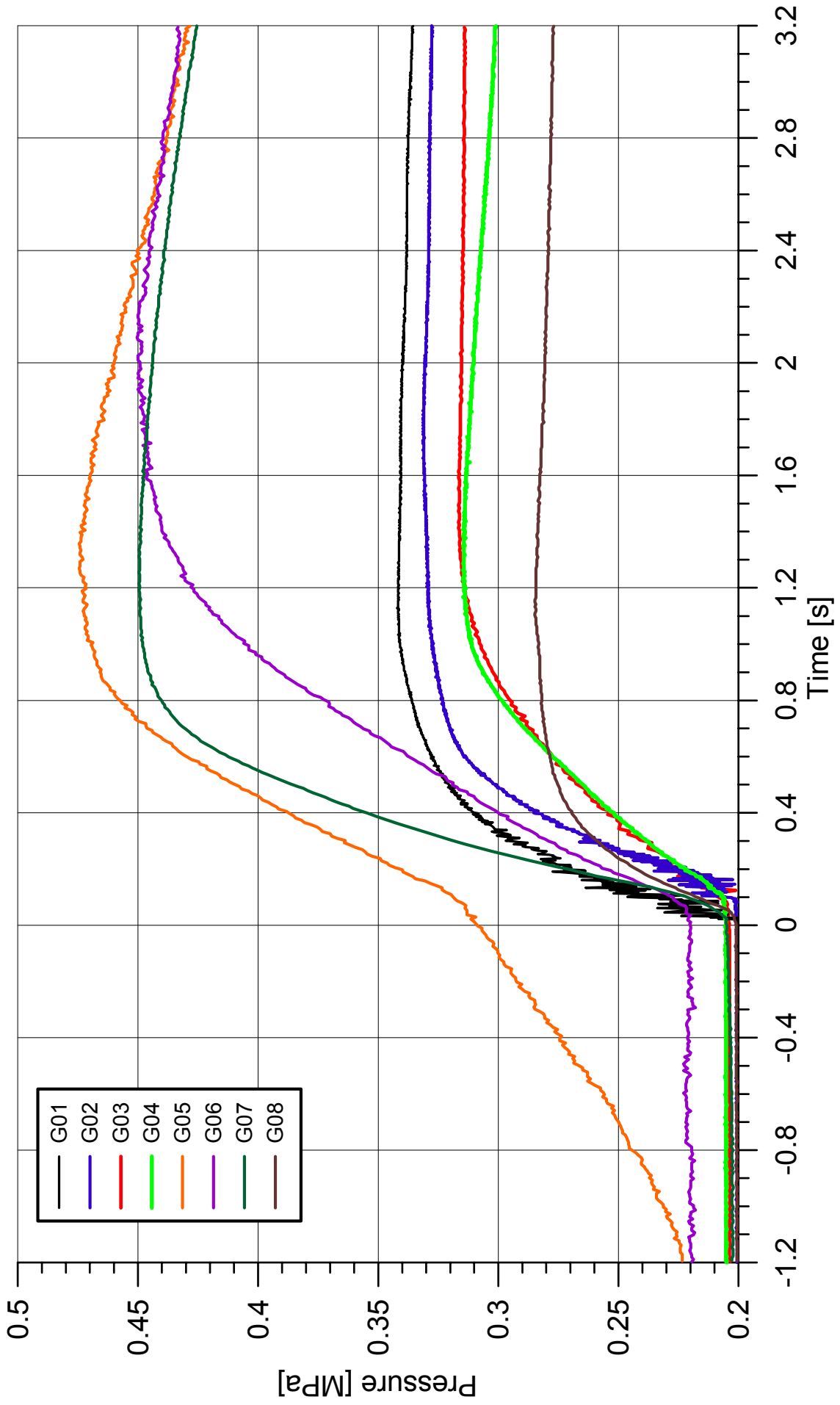


Fig. 23. Containment pressure

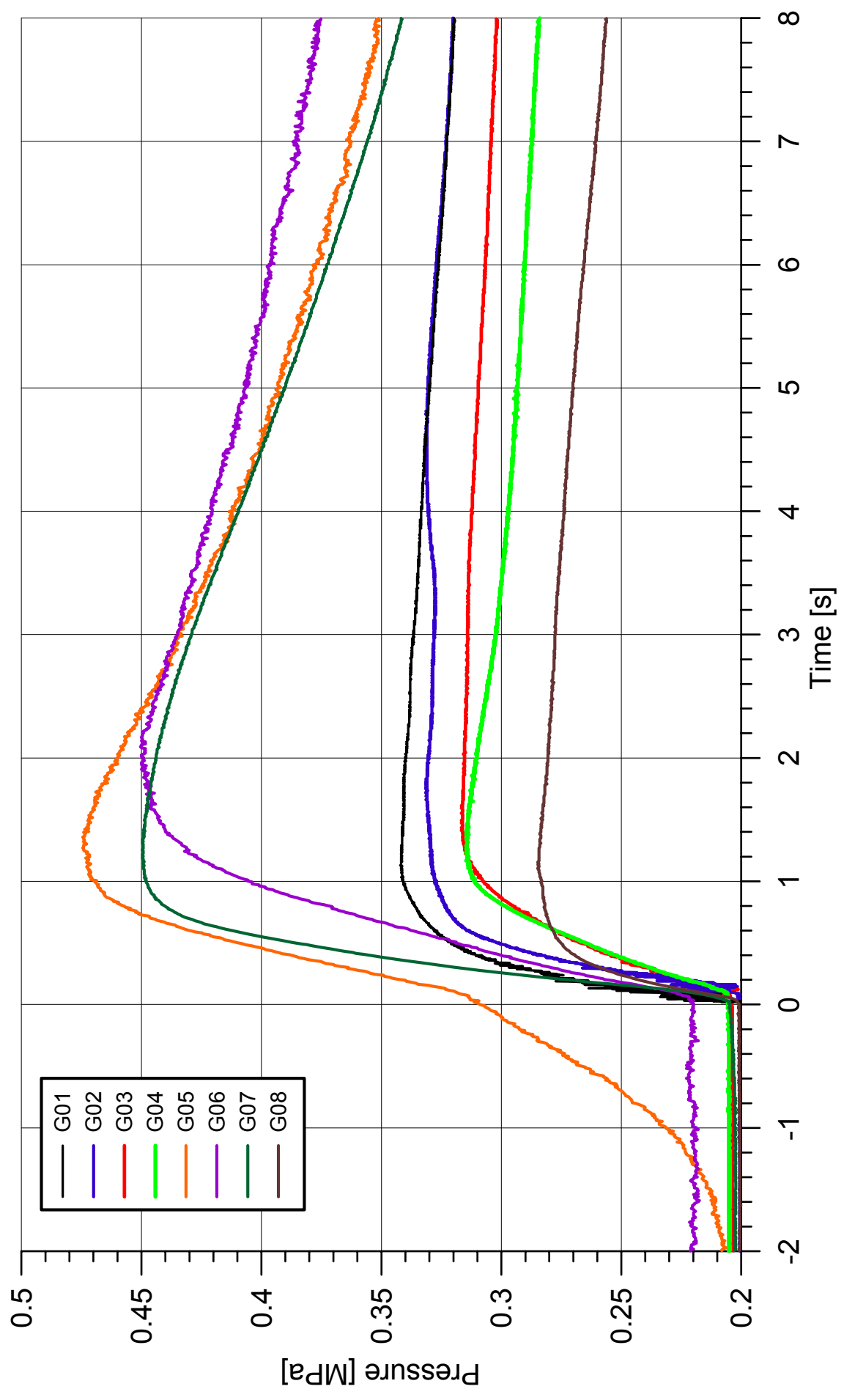


Fig. 24. Containment pressure

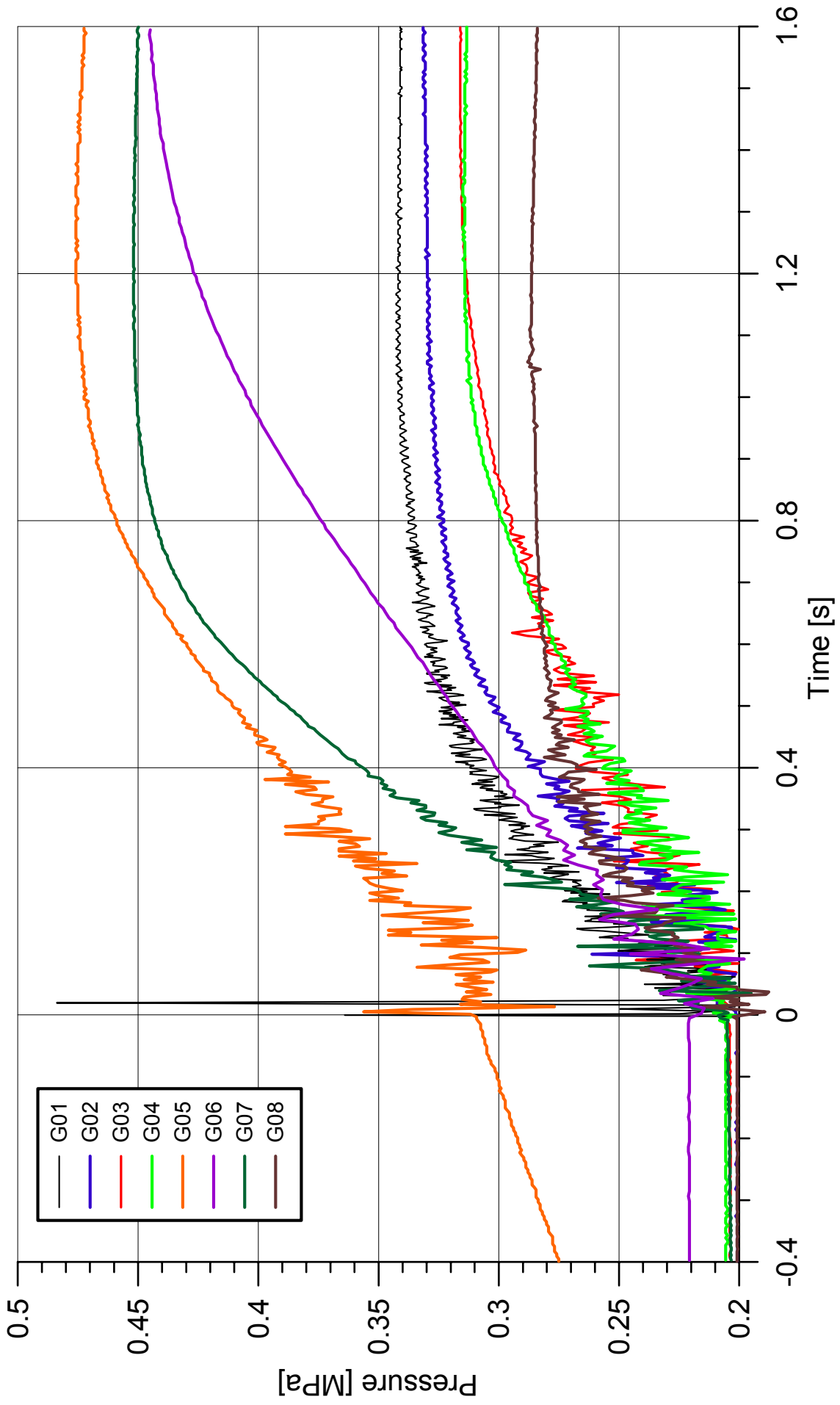


Fig. 25. Containment pressure (zoom)

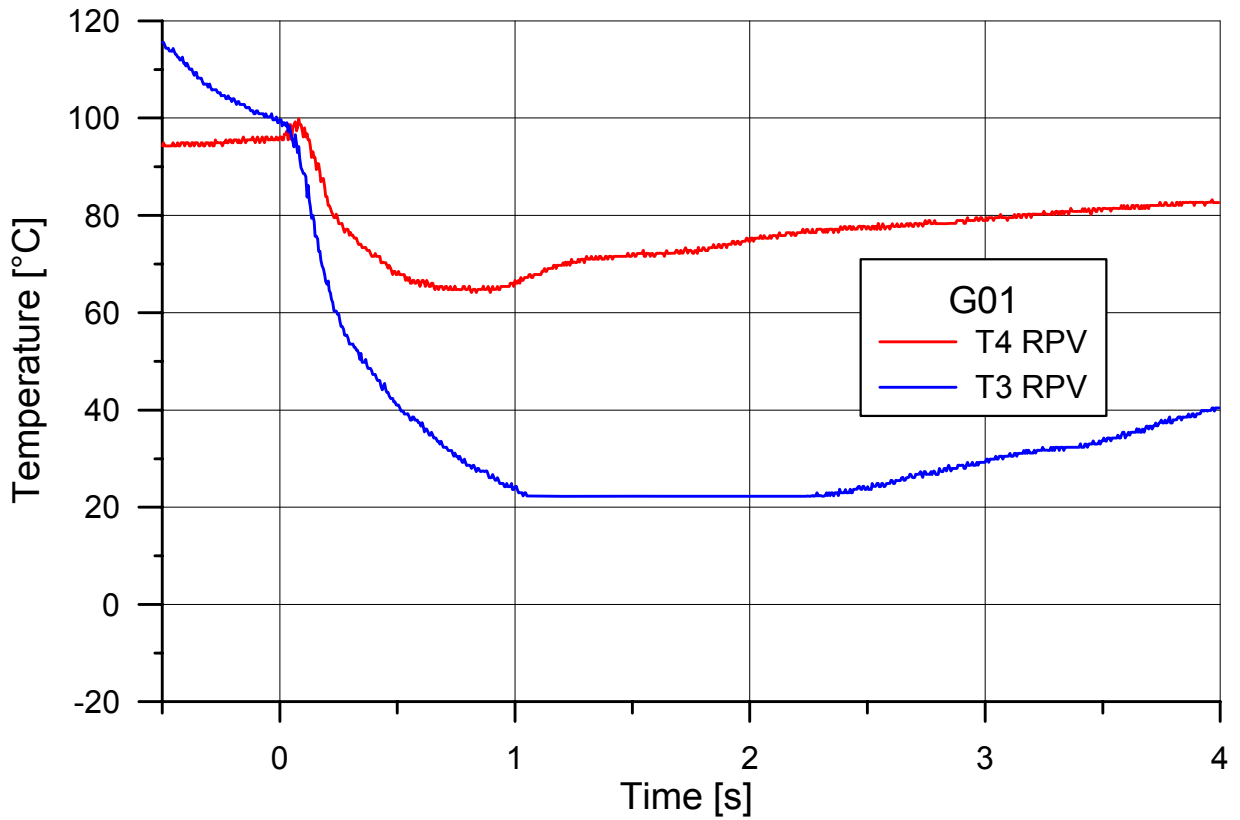


Fig. 26. Gas temperature in RPV vessel, G01

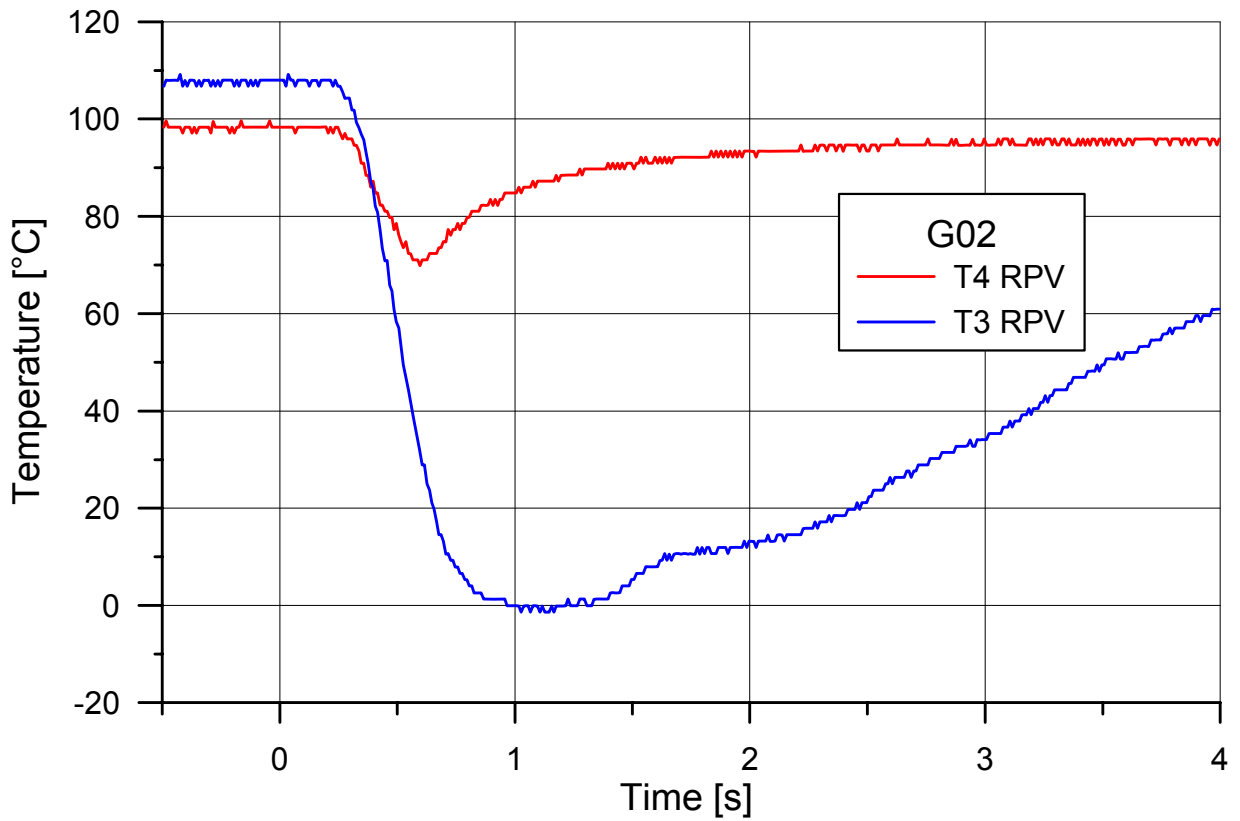


Fig. 27. Gas temperature in RPV vessel, G02

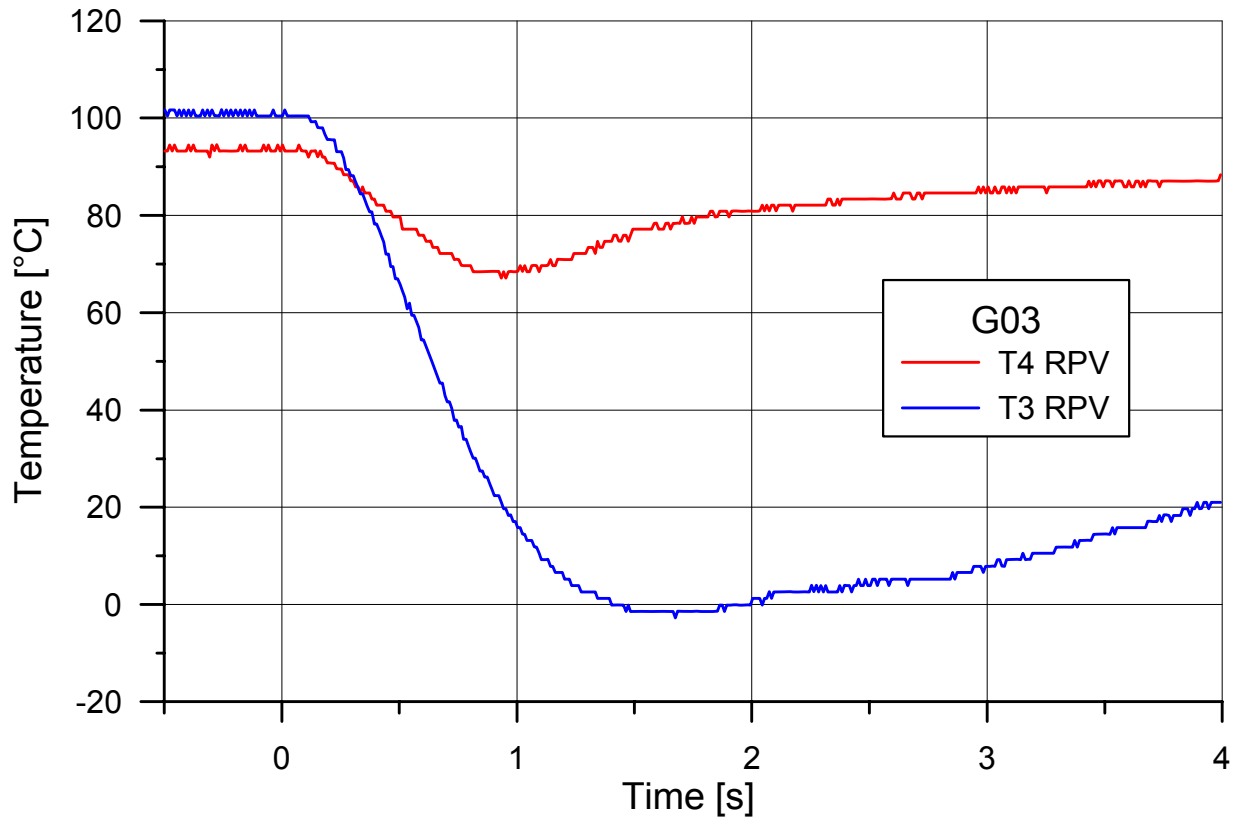


Fig. 28. Gas temperature in RPV vessel, G03

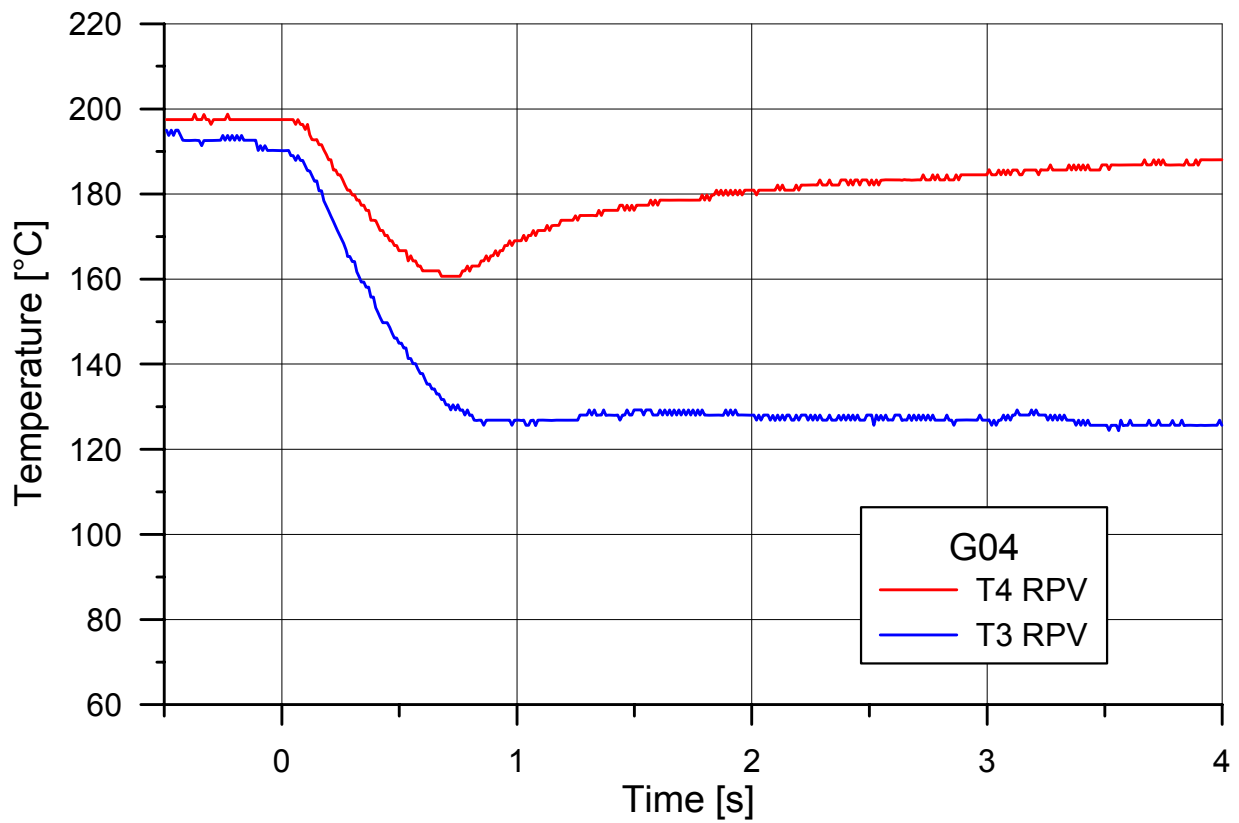


Fig. 29. Gas temperature in RPV vessel, G04

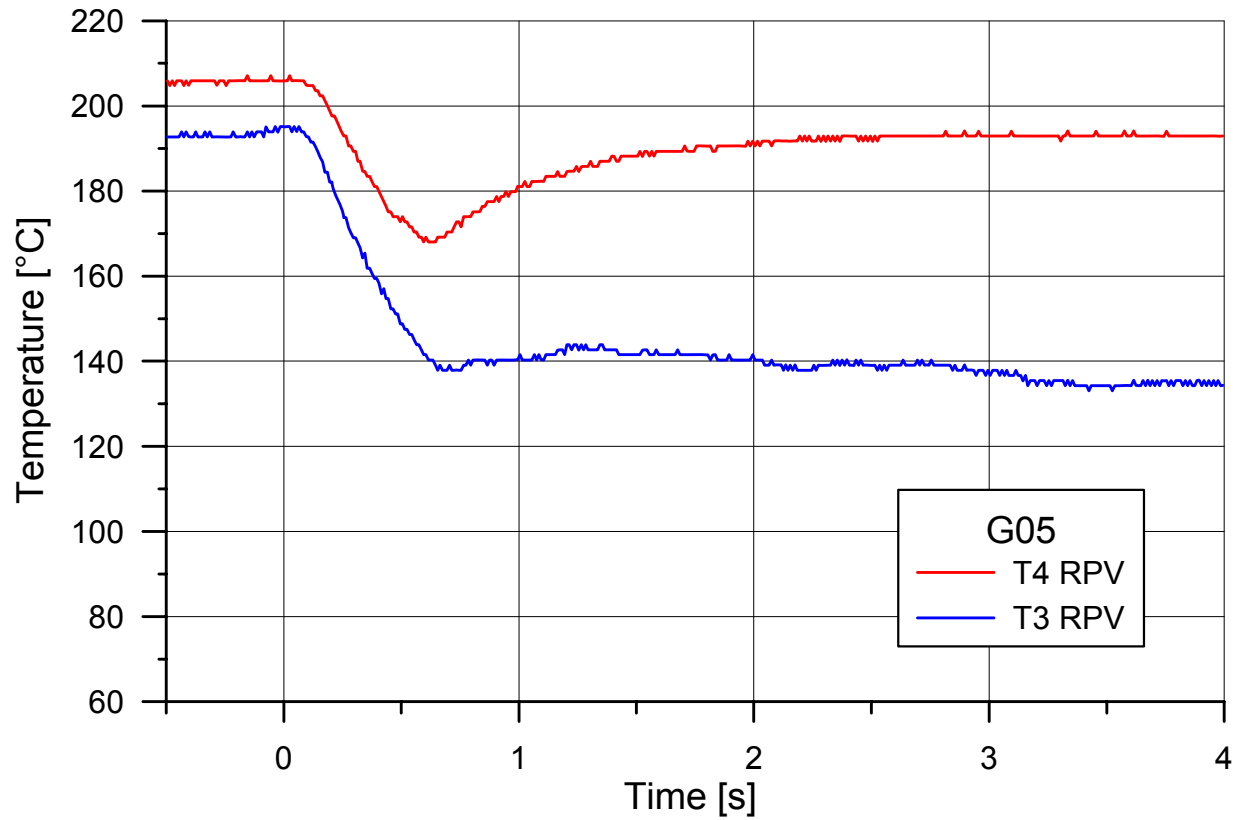


Fig. 30. Gas temperature in RPV vessel, G05

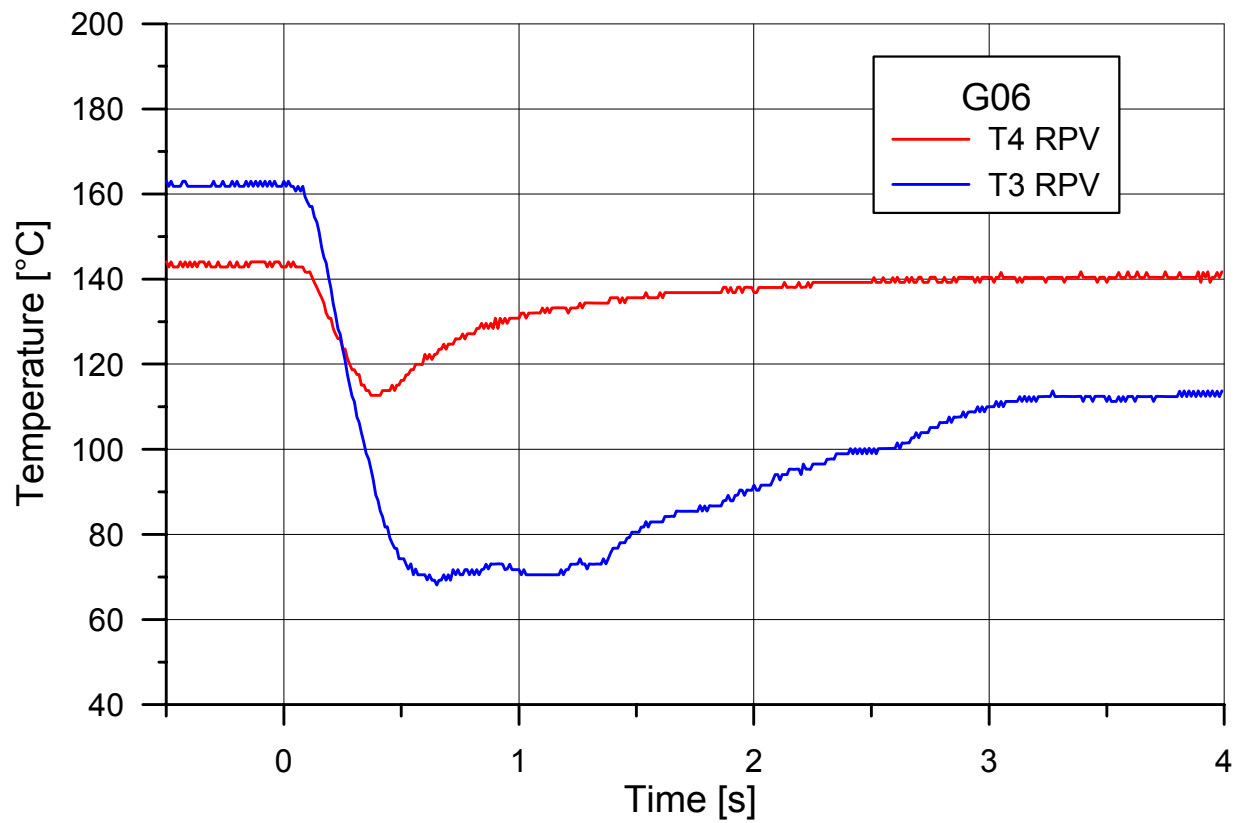


Fig. 31. Gas temperature in RPV vessel, G06

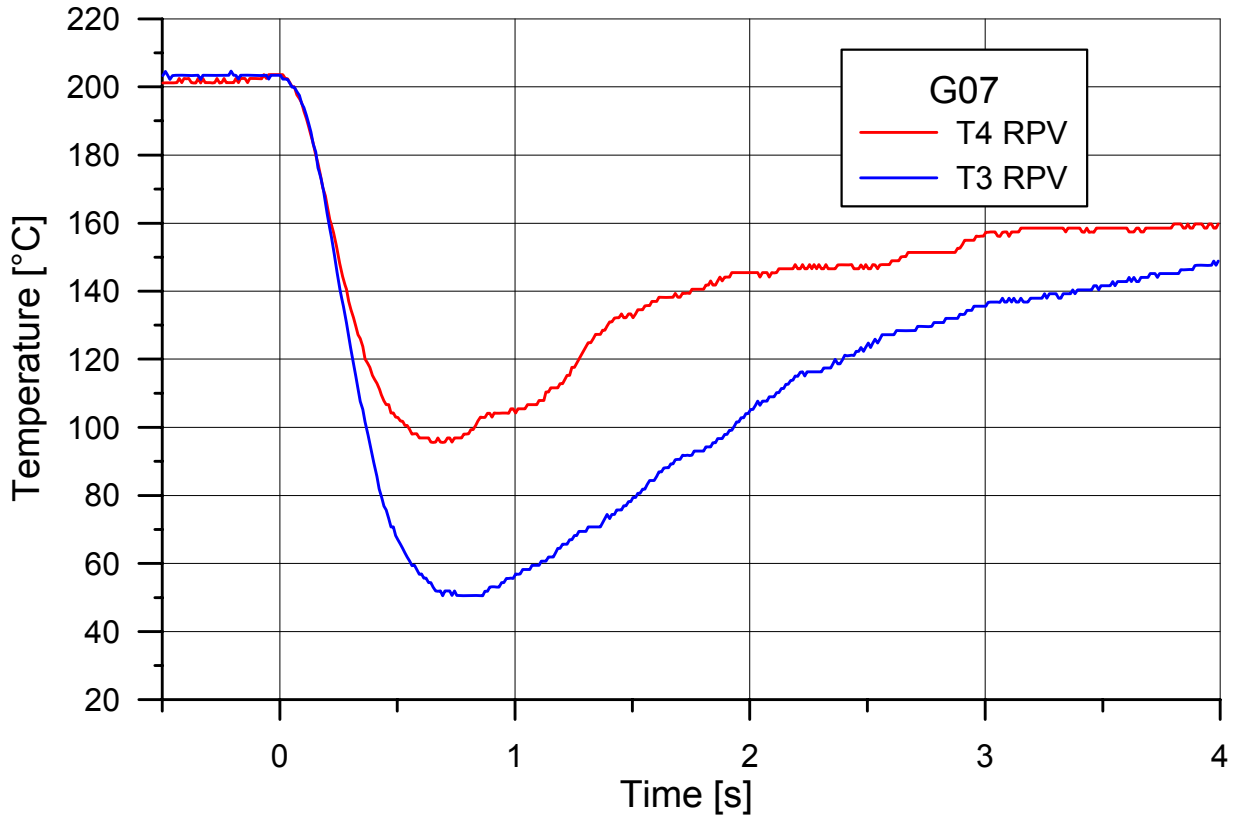


Fig. 32. Gas temperature in RPV vessel, G07

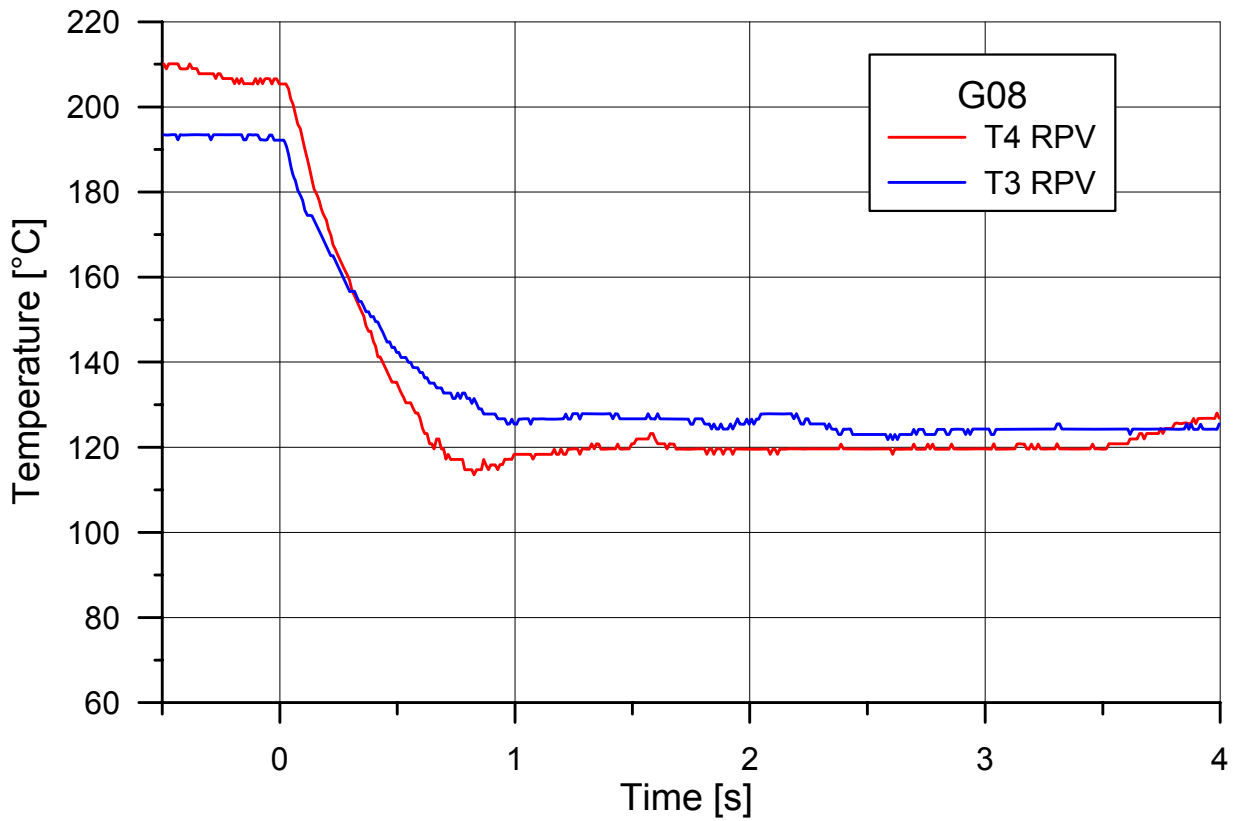


Fig. 33. Gas temperature in RPV vessel, G08

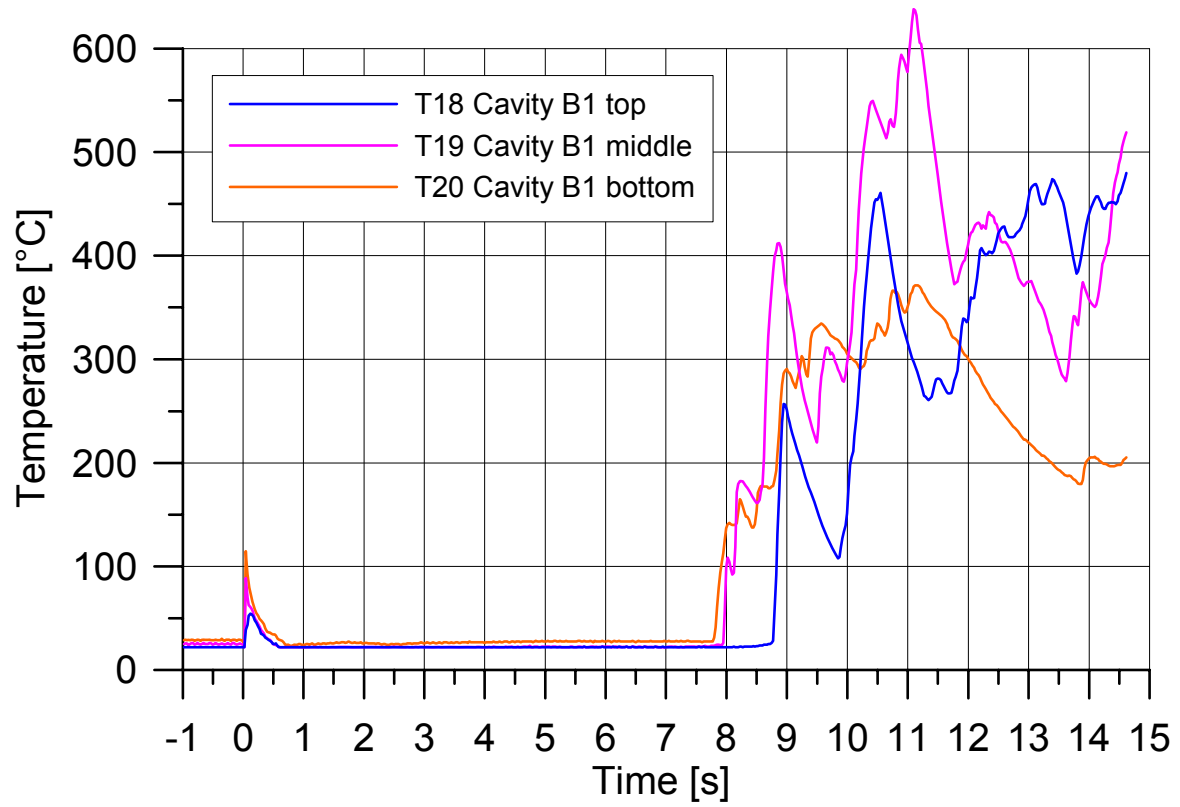


Fig. 34. G01: Temperatures in the reactor pit

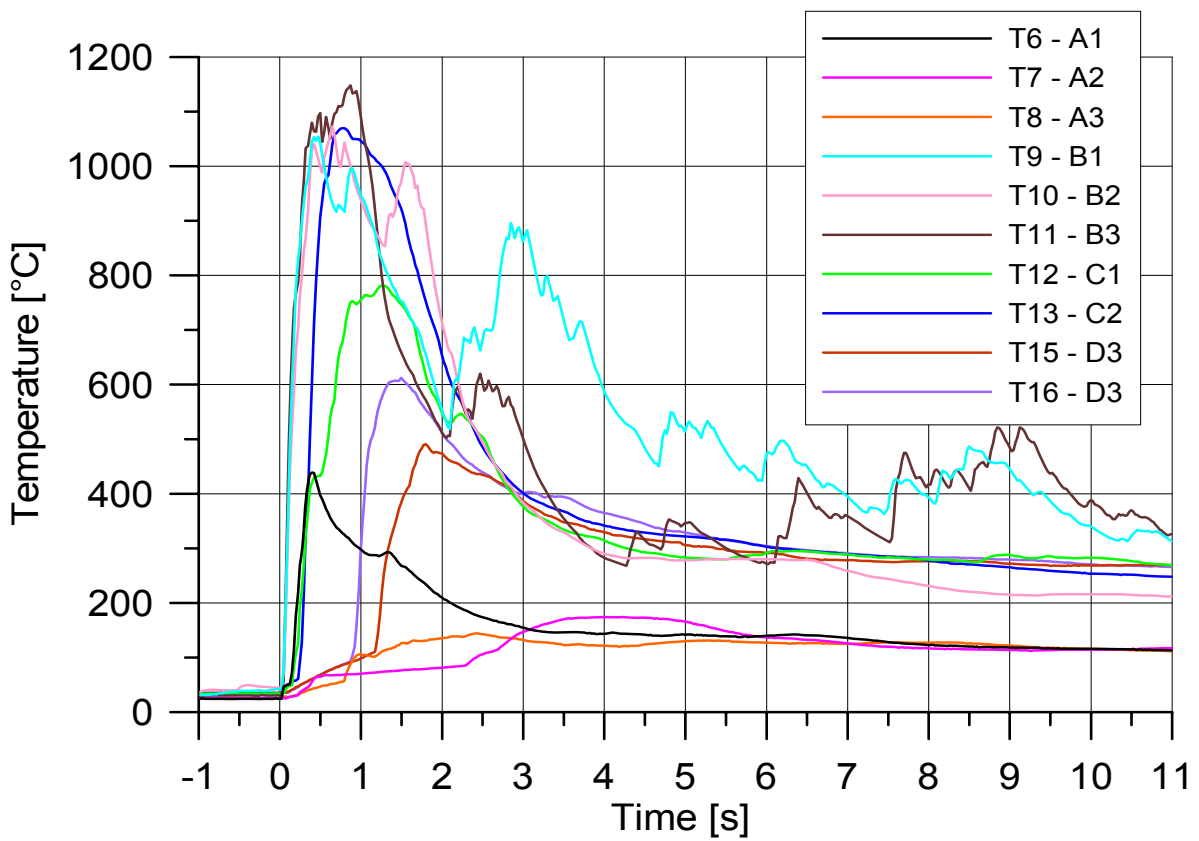


Fig. 35. G01: Temperatures in the containment vessel and subcompartment

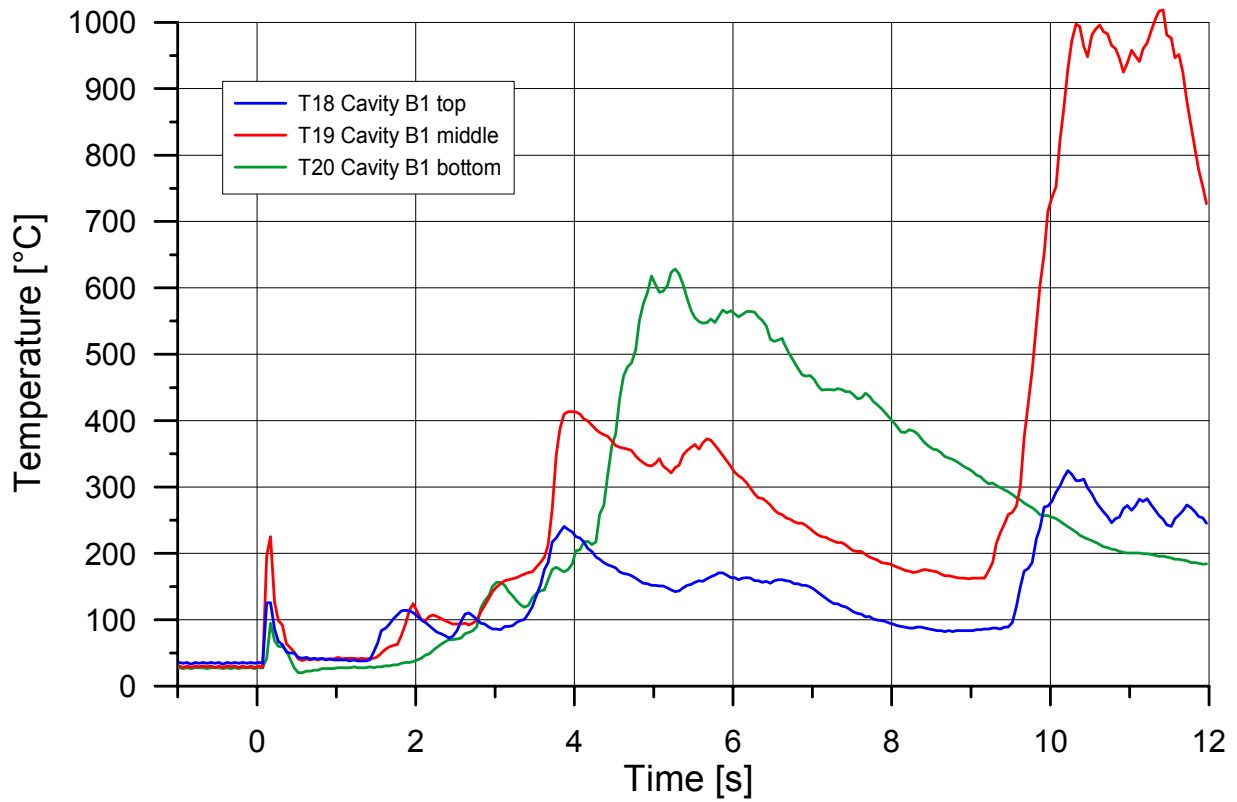


Fig. 36. G02: Temperatures in the reactor pit

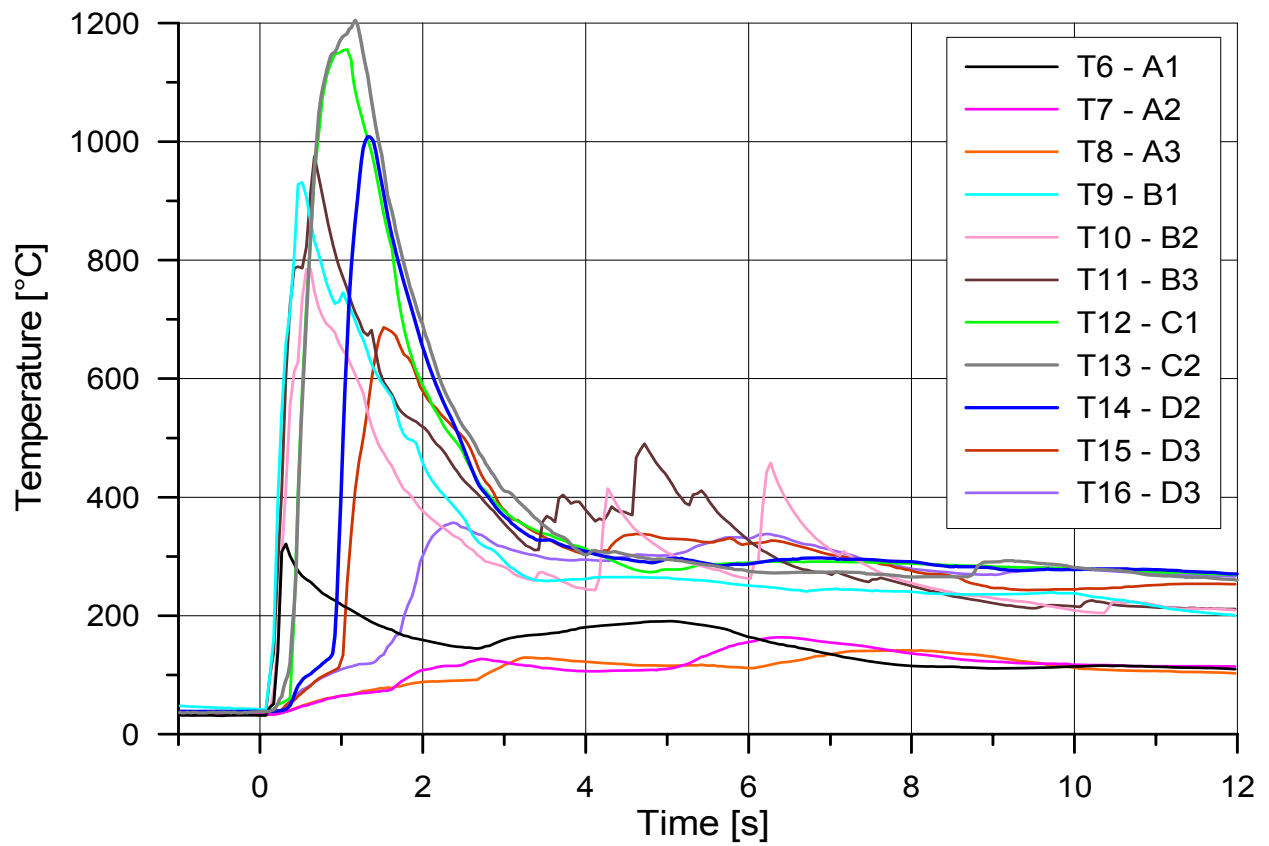


Fig. 37. G02: Temperatures in the containment vessel and subcompartment

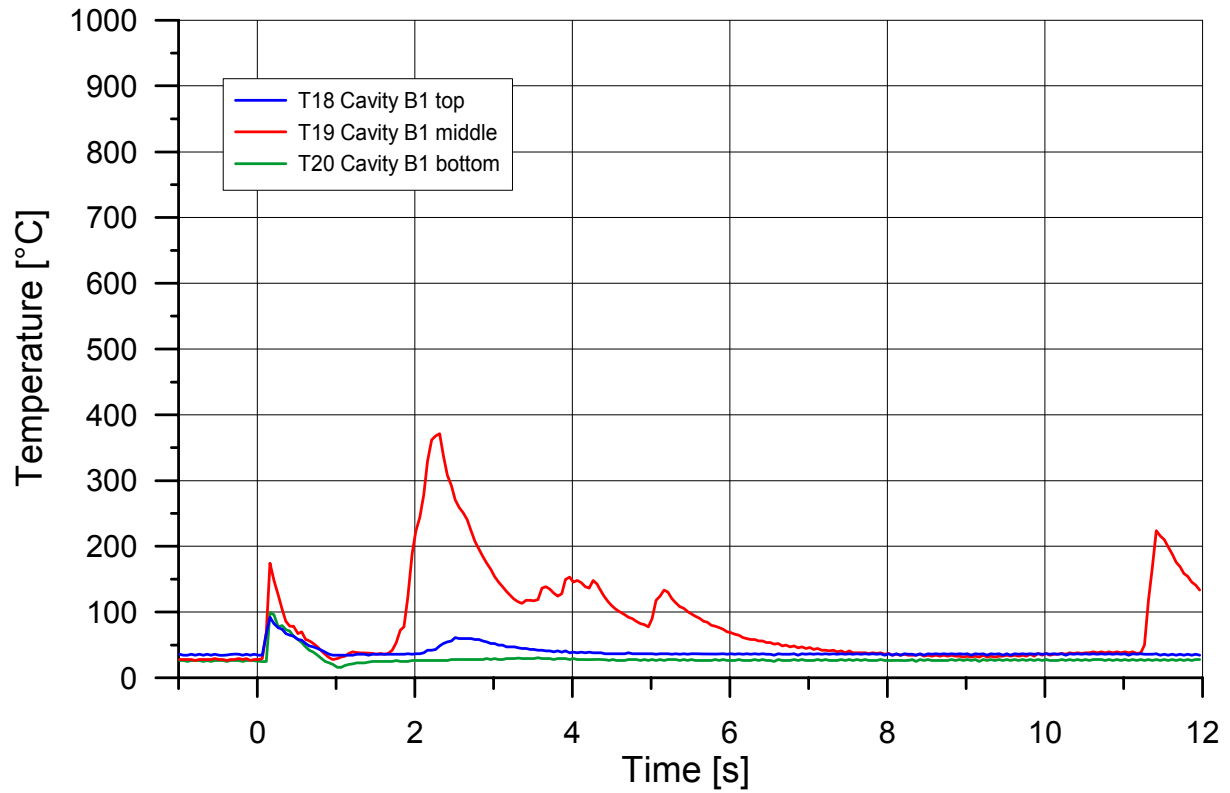


Fig. 38. G03: Temperatures in the reactor pit

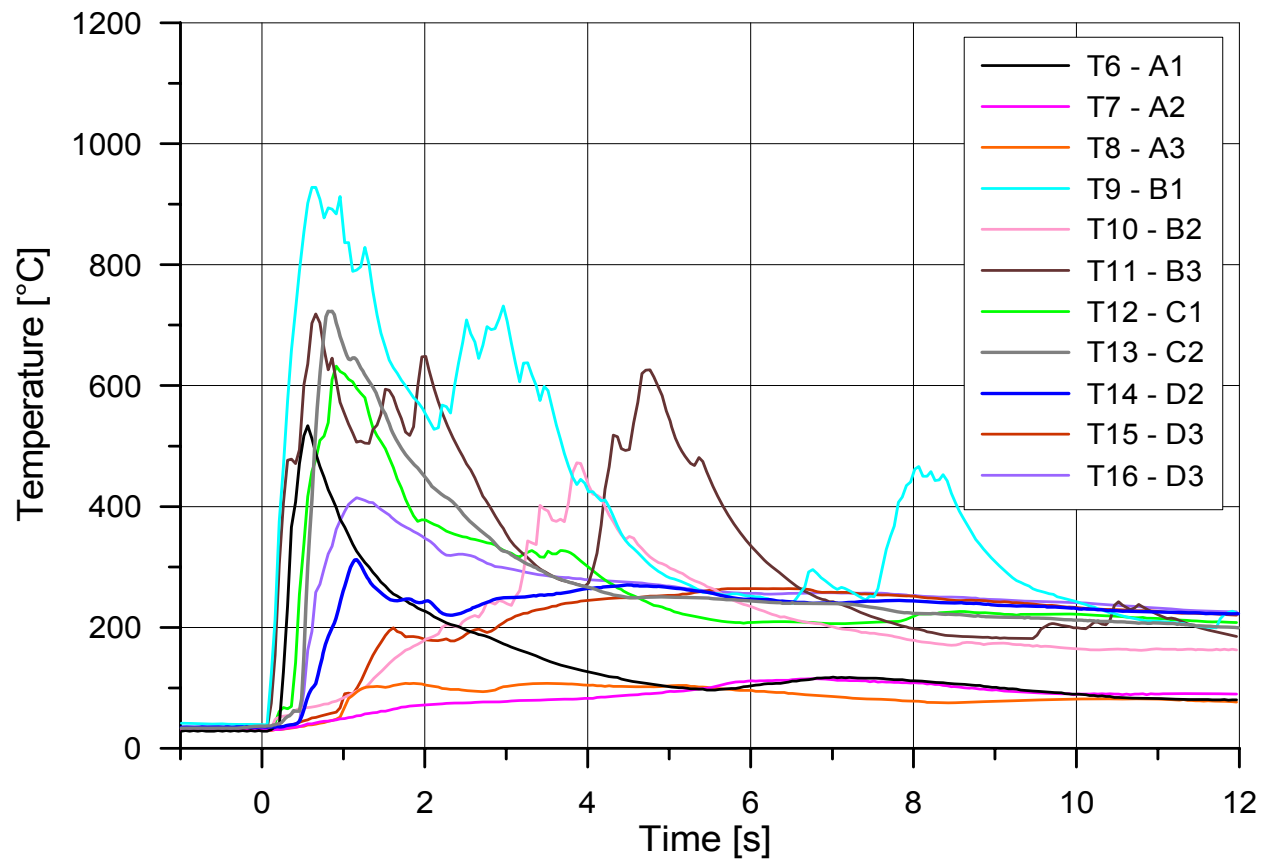


Fig. 39. G03: Temperatures in the containment vessel and subcompartment

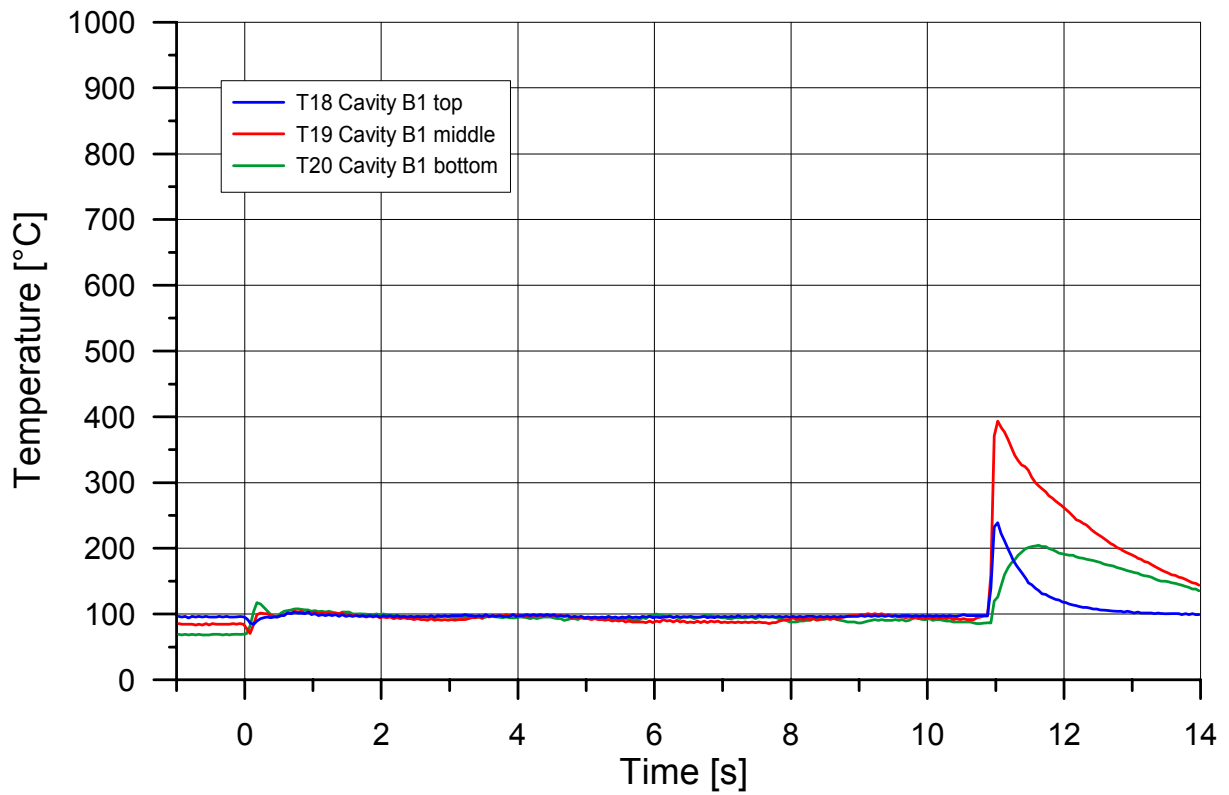


Fig. 40. G04: Temperatures in the reactor pit

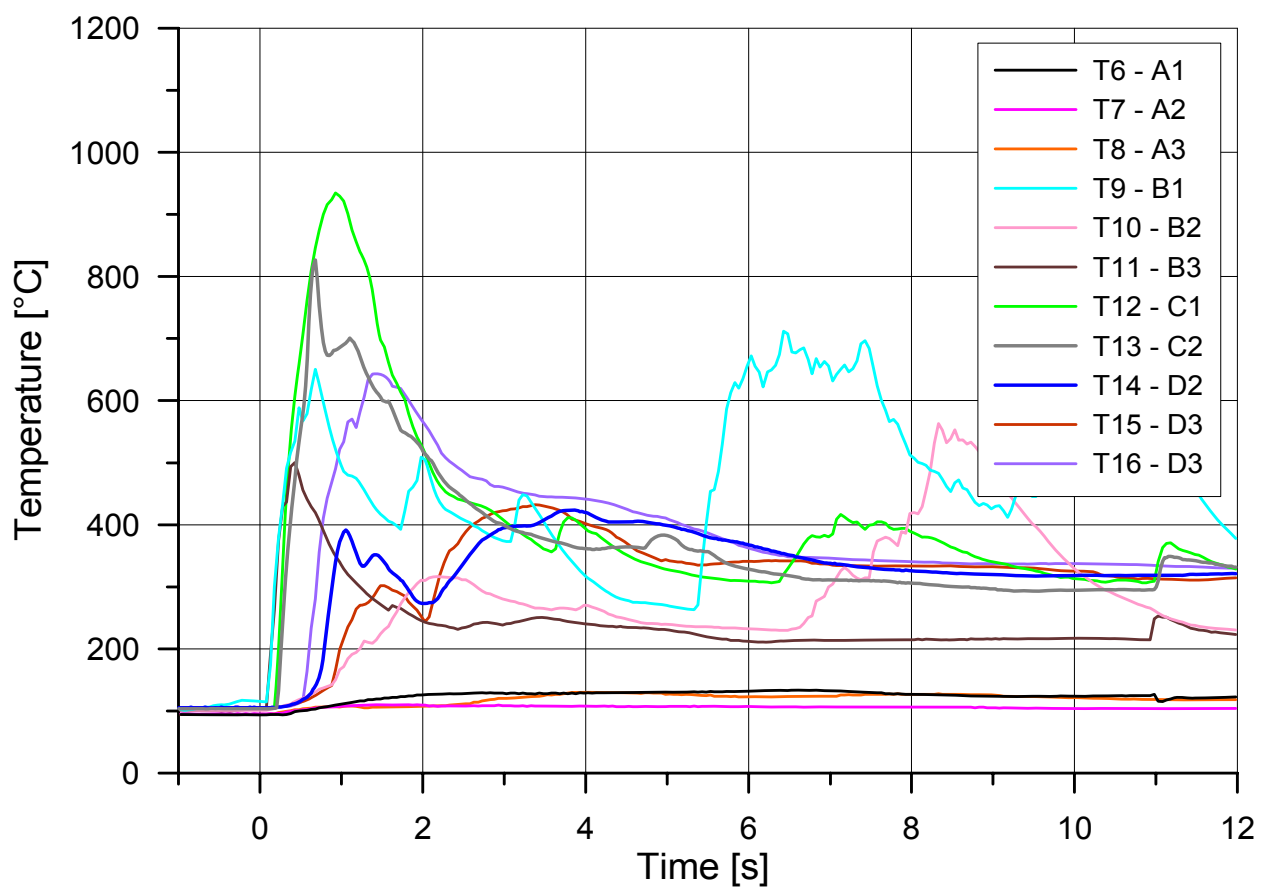


Fig. 41. G04: Temperatures in the containment vessel and subcompartment

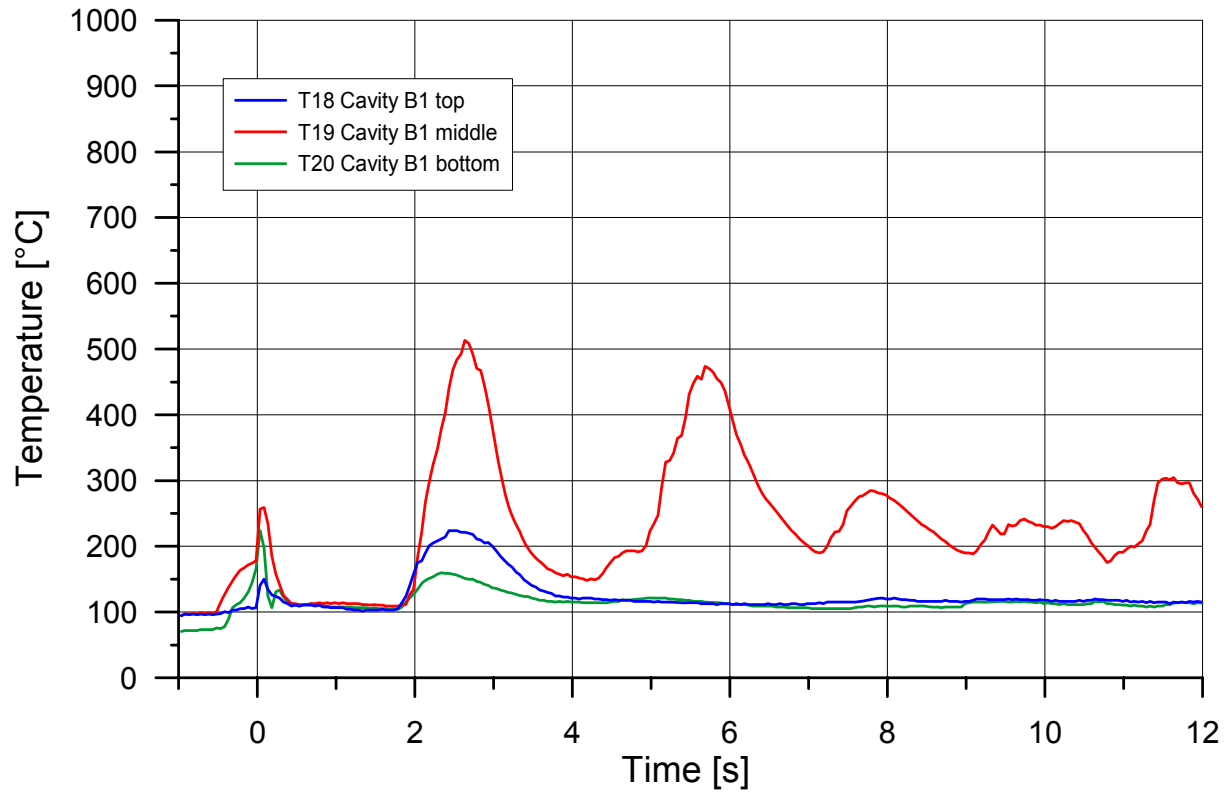


Fig. 42. G05: Temperatures in the reactor pit

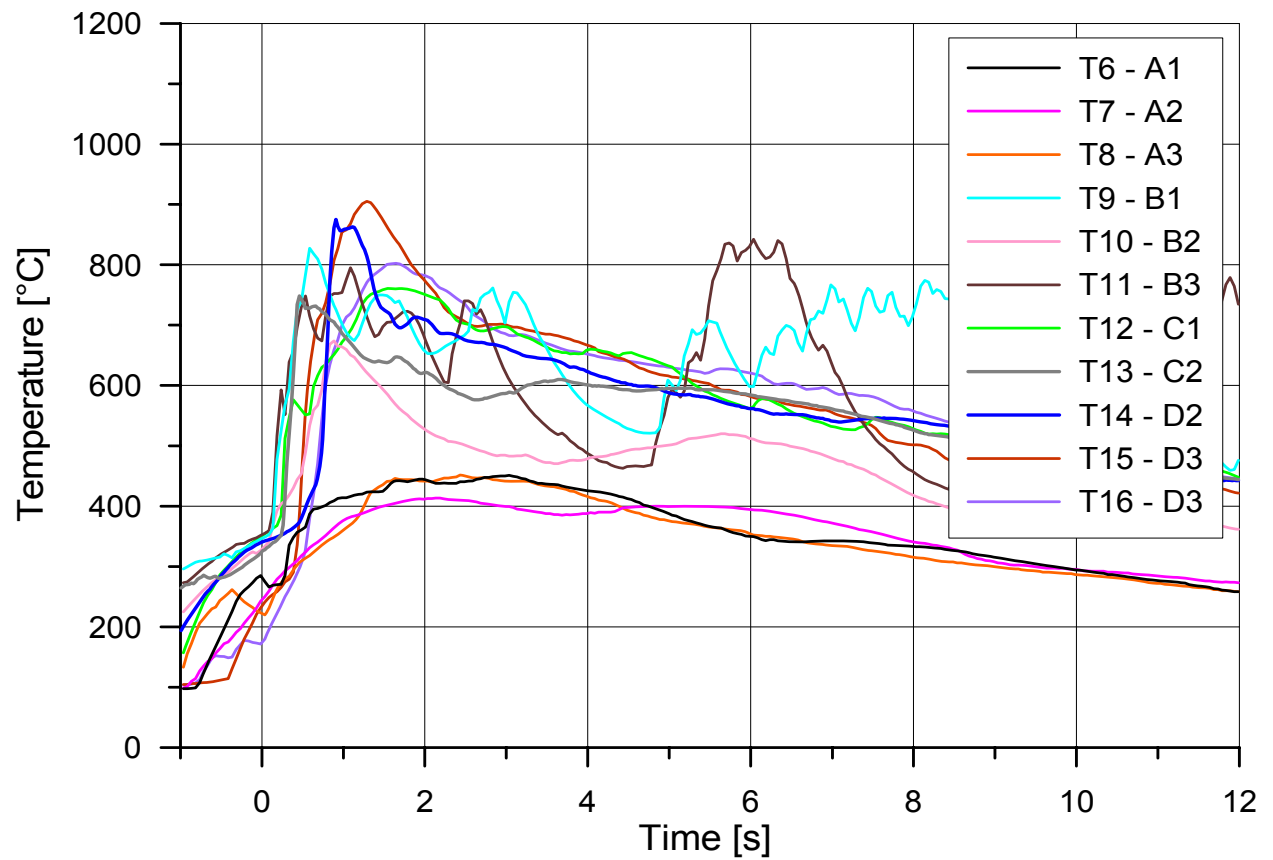


Fig. 43. G05: Temperatures in the containment vessel and subcompartment

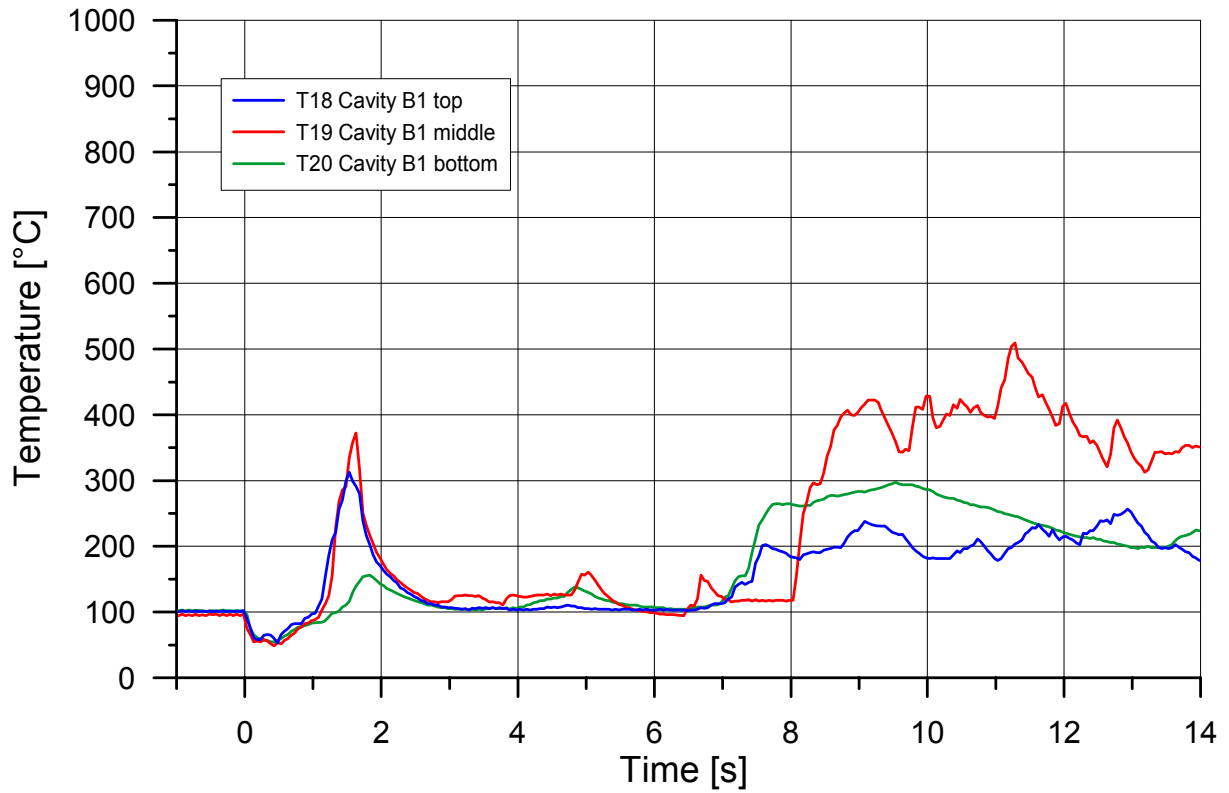


Fig. 44. G06: Temperatures in the reactor pit

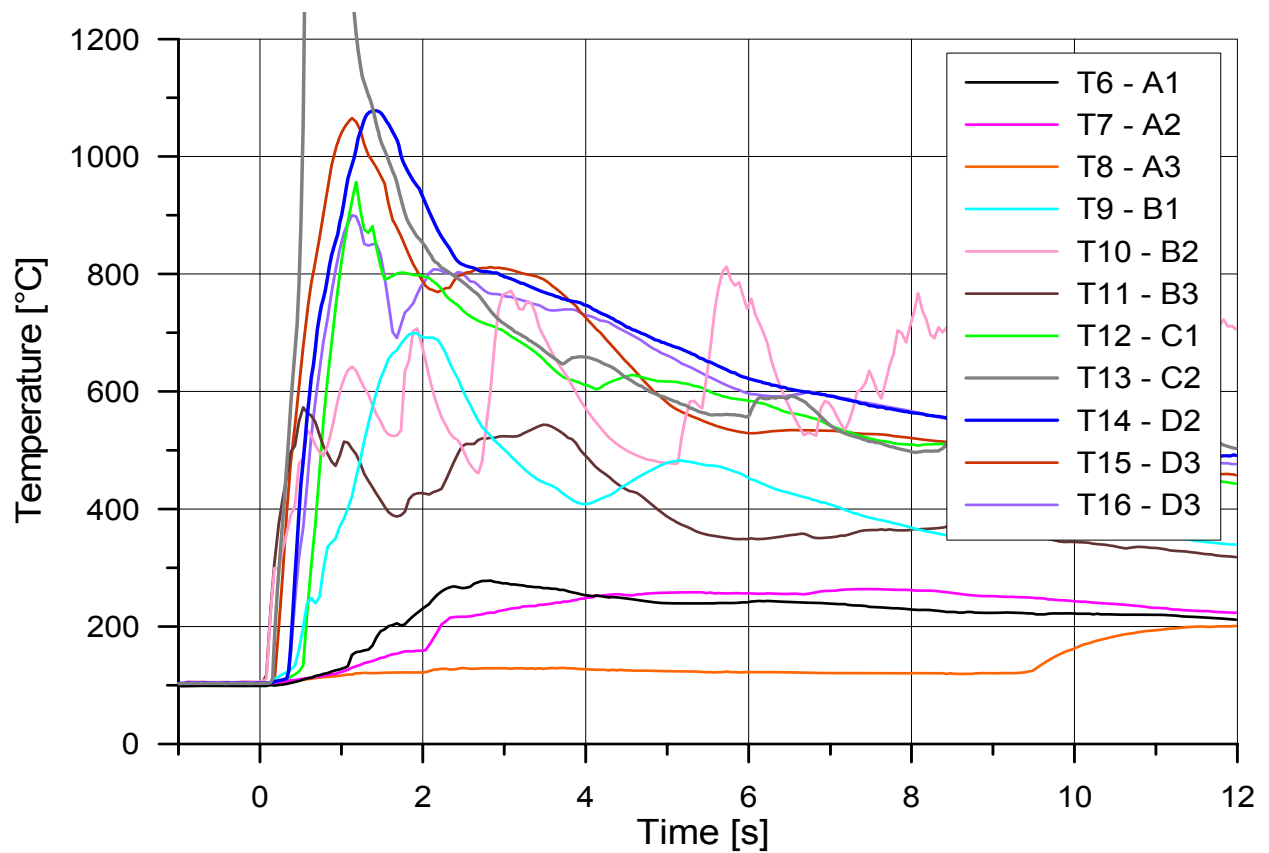


Fig. 45. G06: Temperatures in the containment vessel and subcompartment

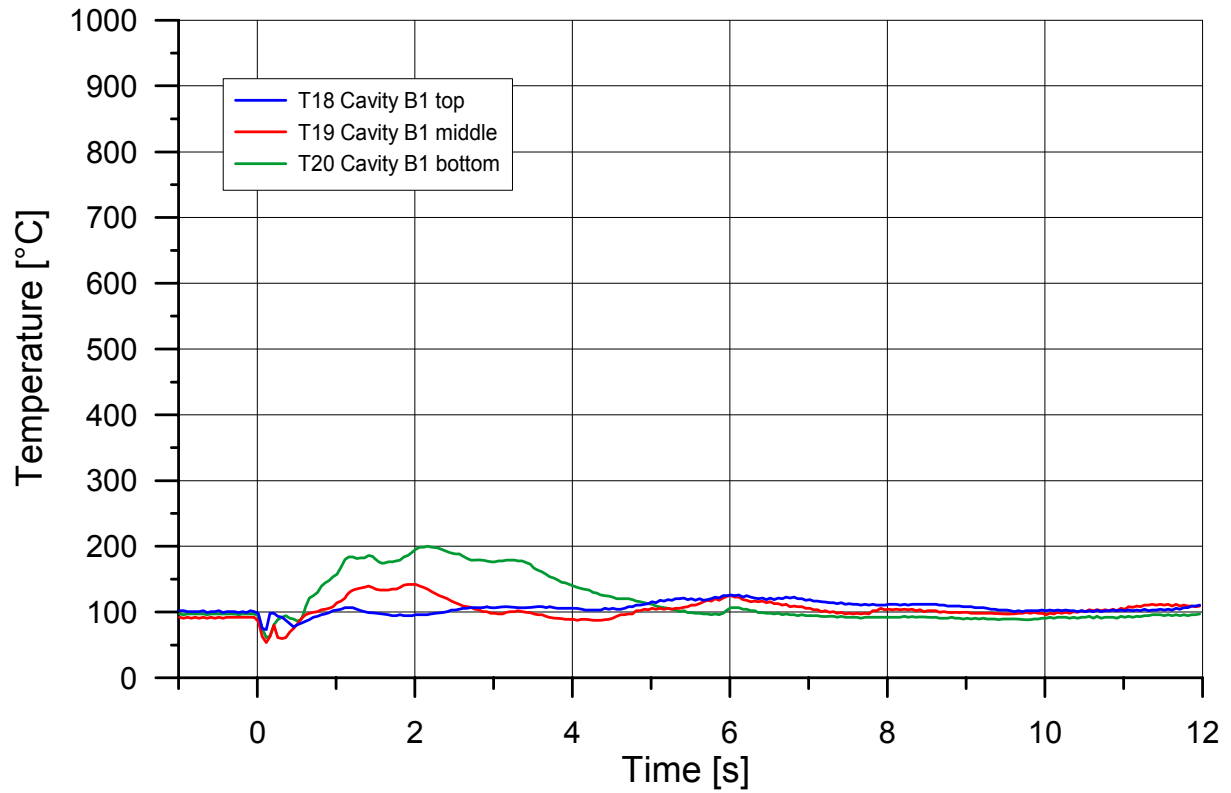


Fig. 46. G07: Temperatures in the reactor pit

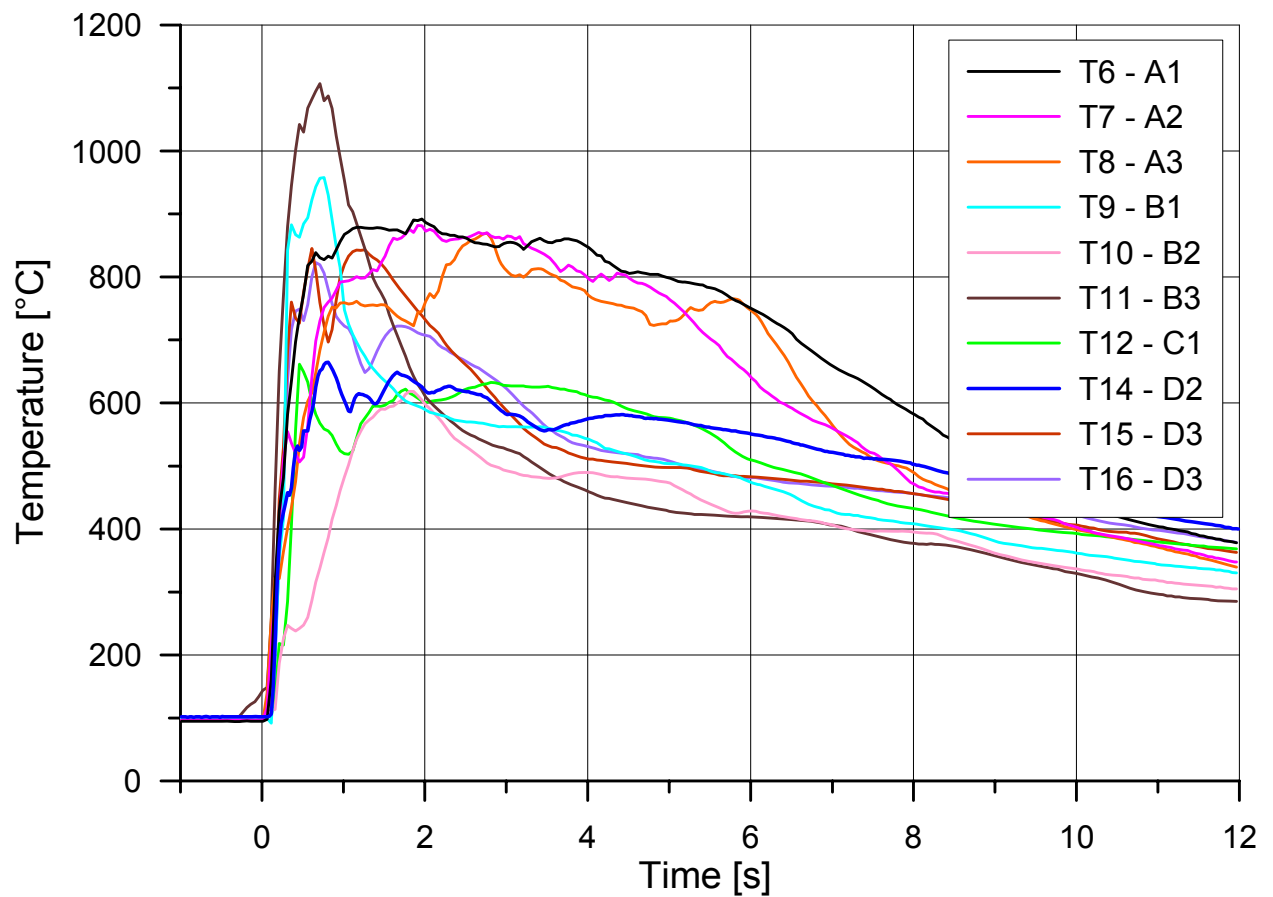


Fig. 47. G07: Temperatures in the containment vessel and subcompartment

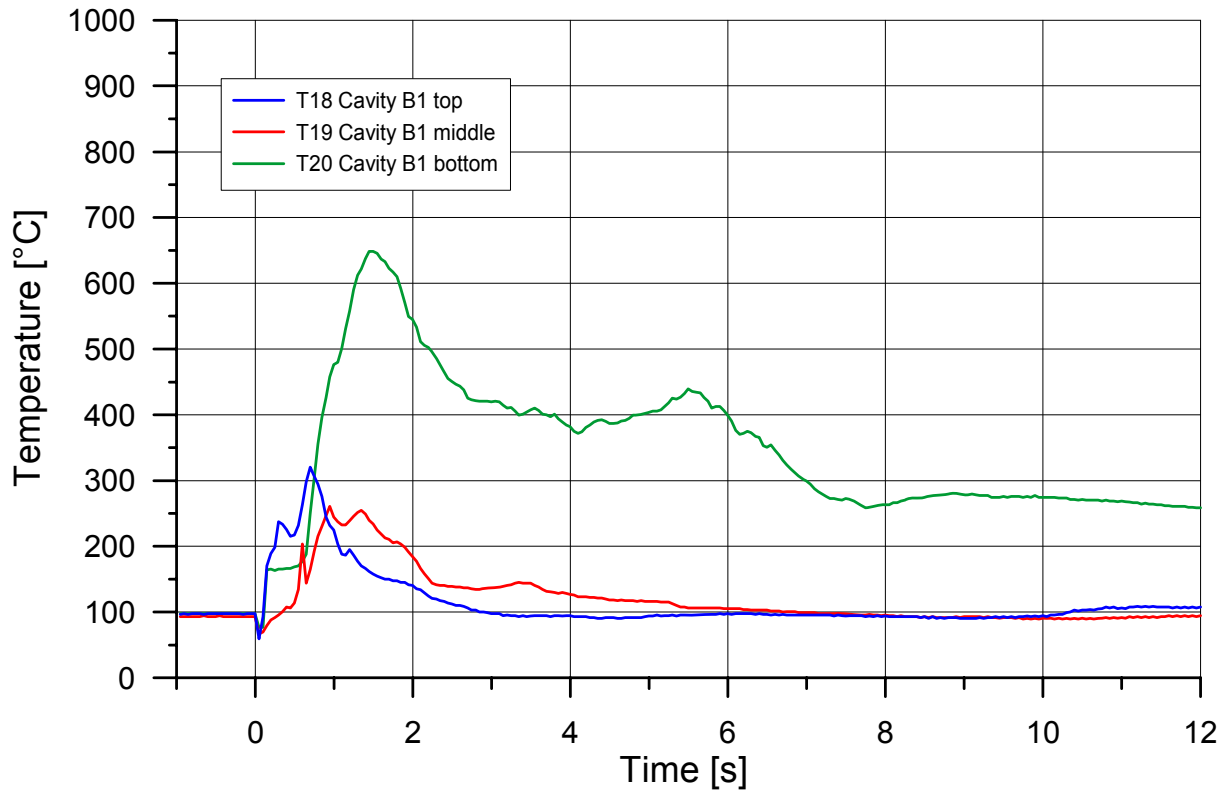


Fig. 48. G08: Temperatures in the reactor pit

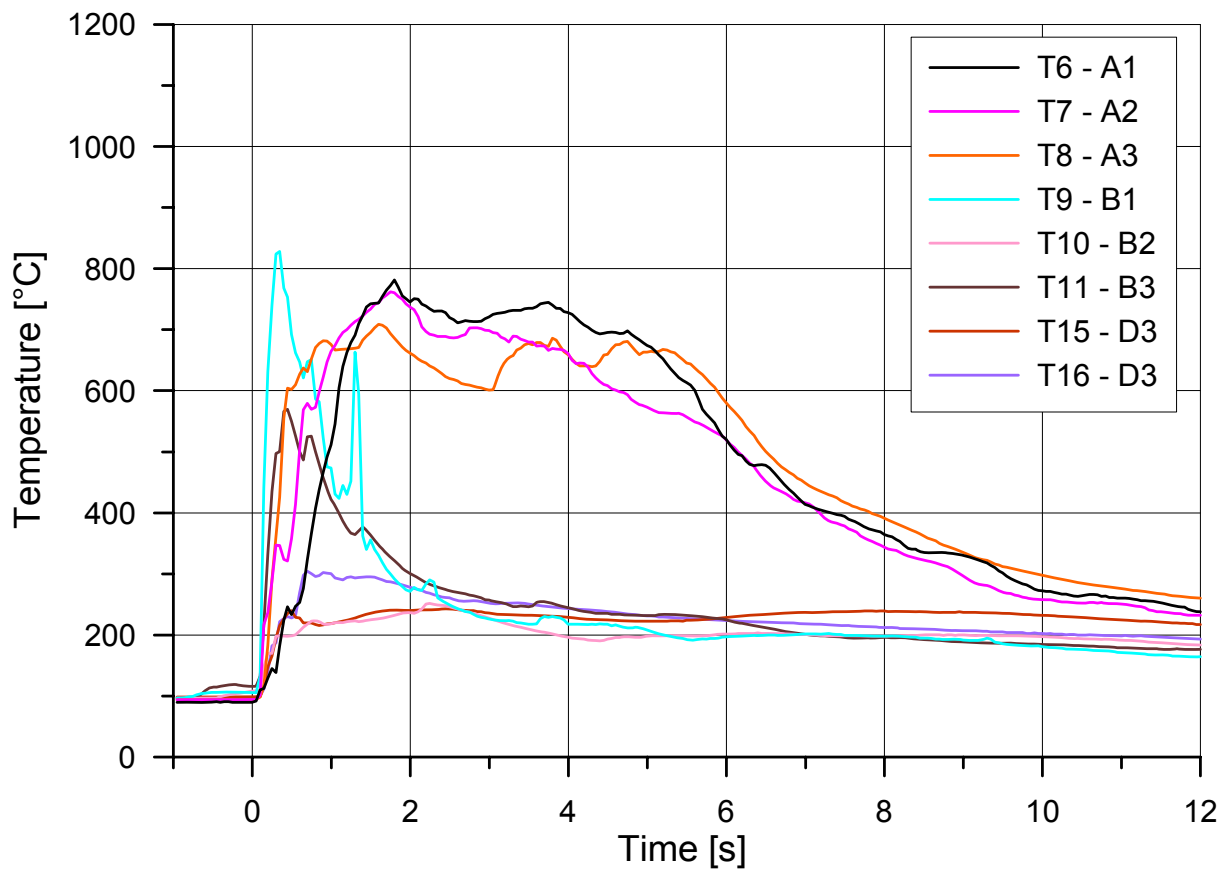


Fig. 49. G08: Temperatures in the containment vessel and subcompartment

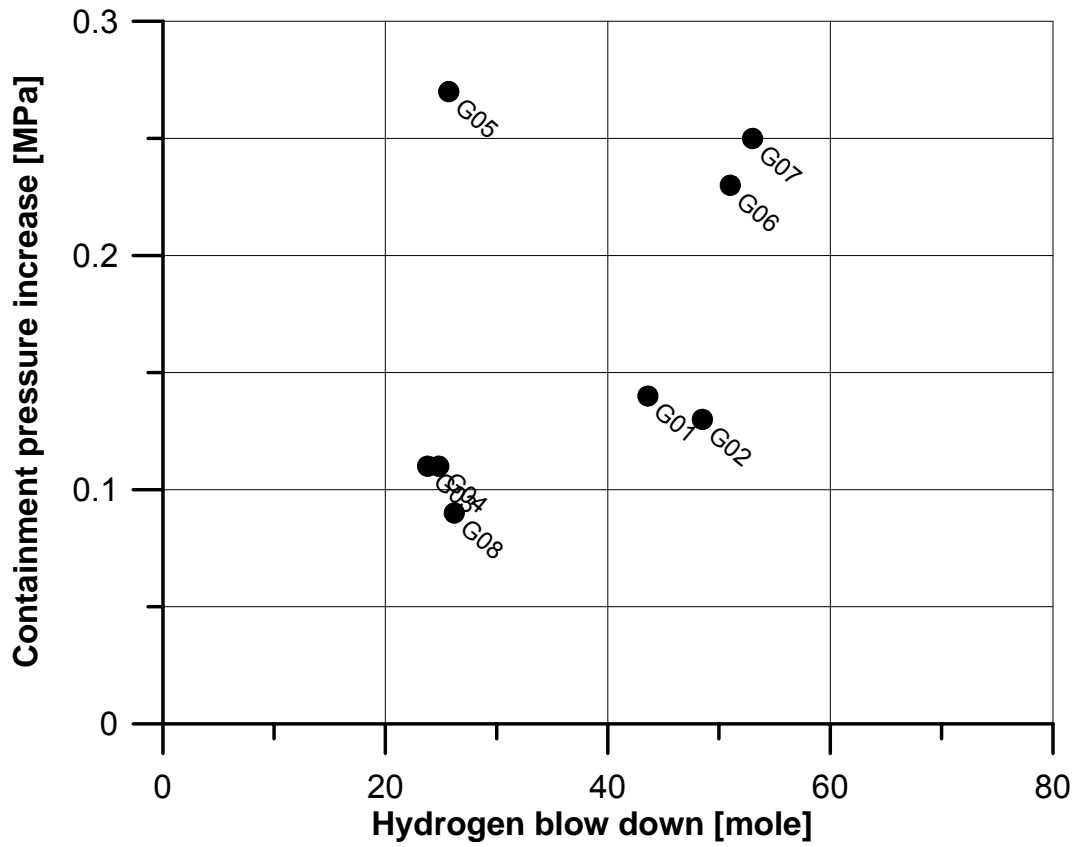


Fig. 50. Pressure increase versus blow down hydrogen

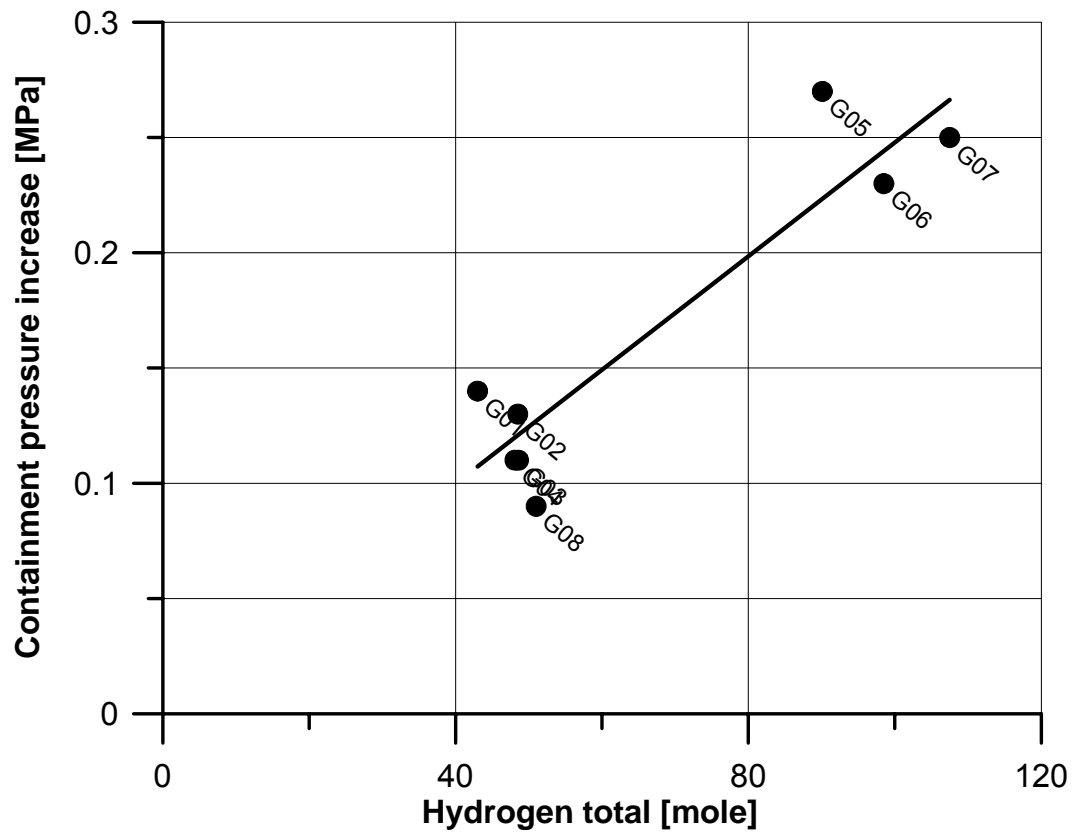


Fig. 51. Pressure increase versus total available hydrogen

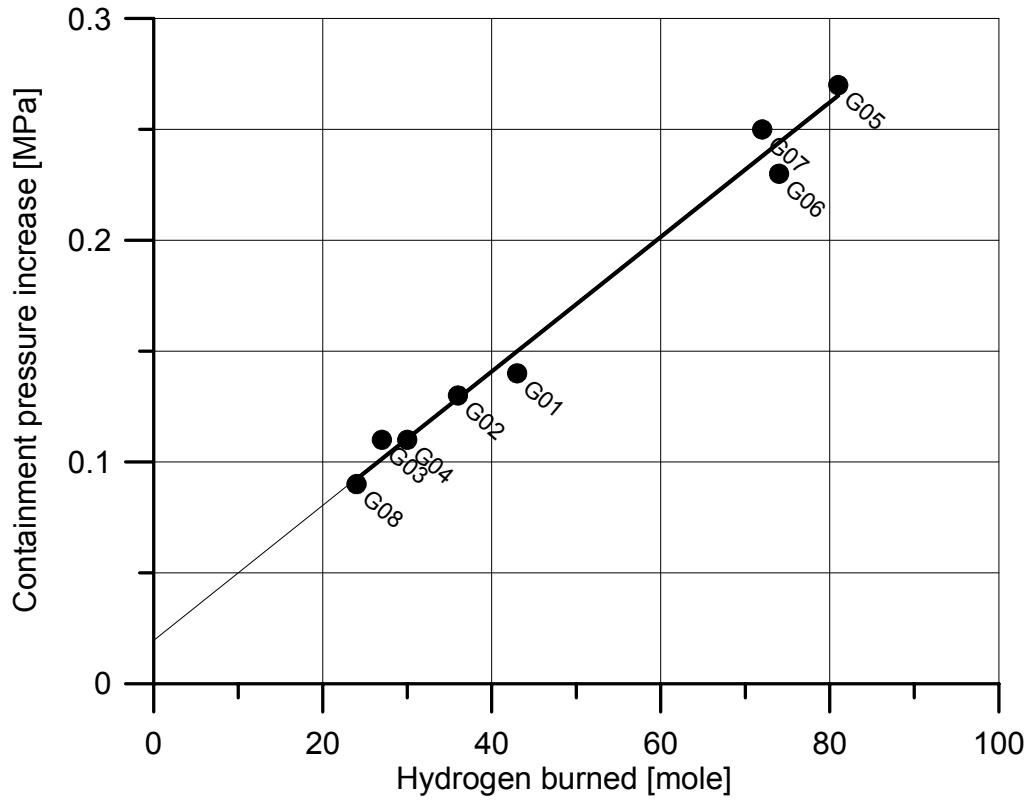


Fig. 52. Pressure increase versus burned hydrogen

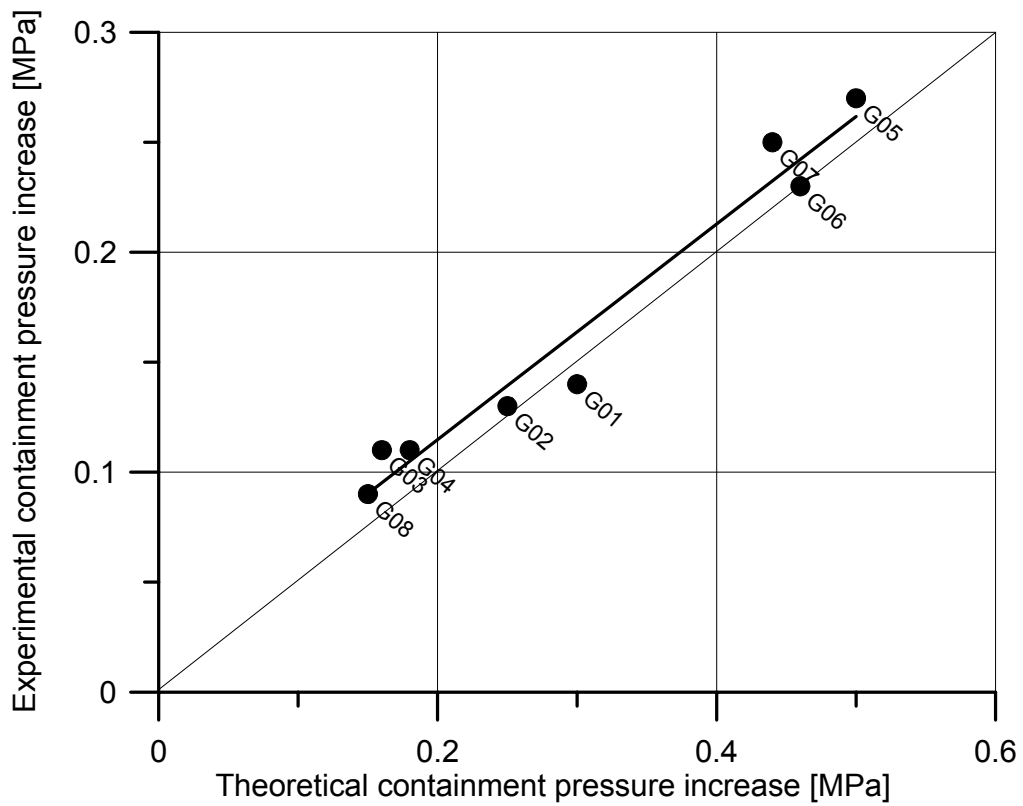


Fig. 53. Comparison of possible maximum pressure increase with measured data

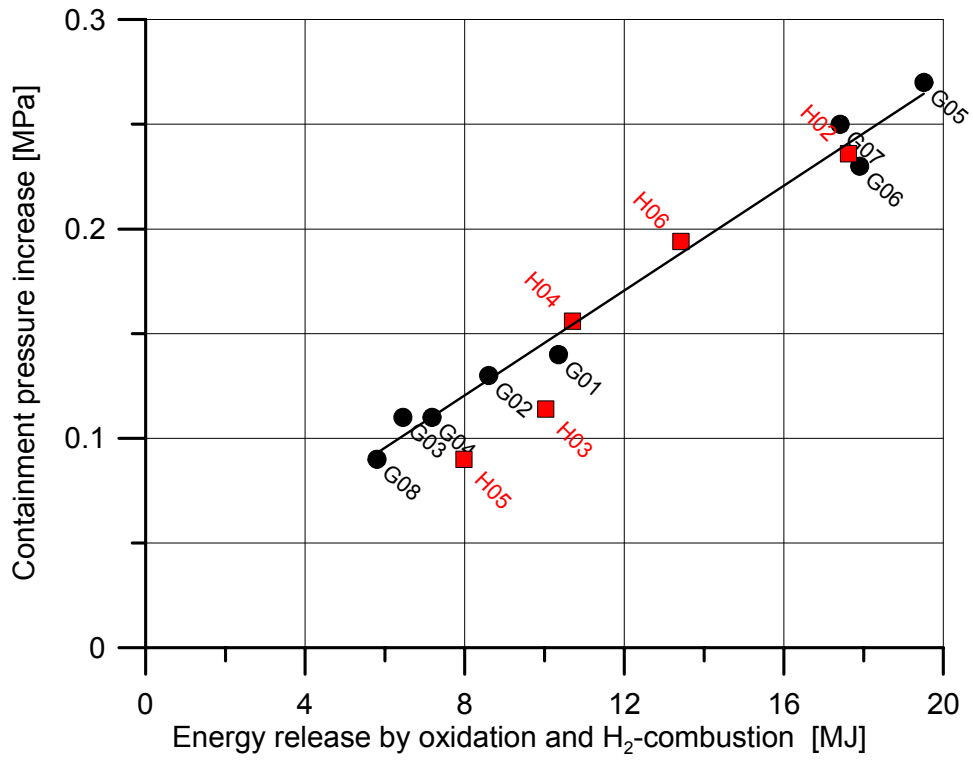


Fig. 54. Experimental pressure increase vs. energy release by oxidation and hydrogen combustion

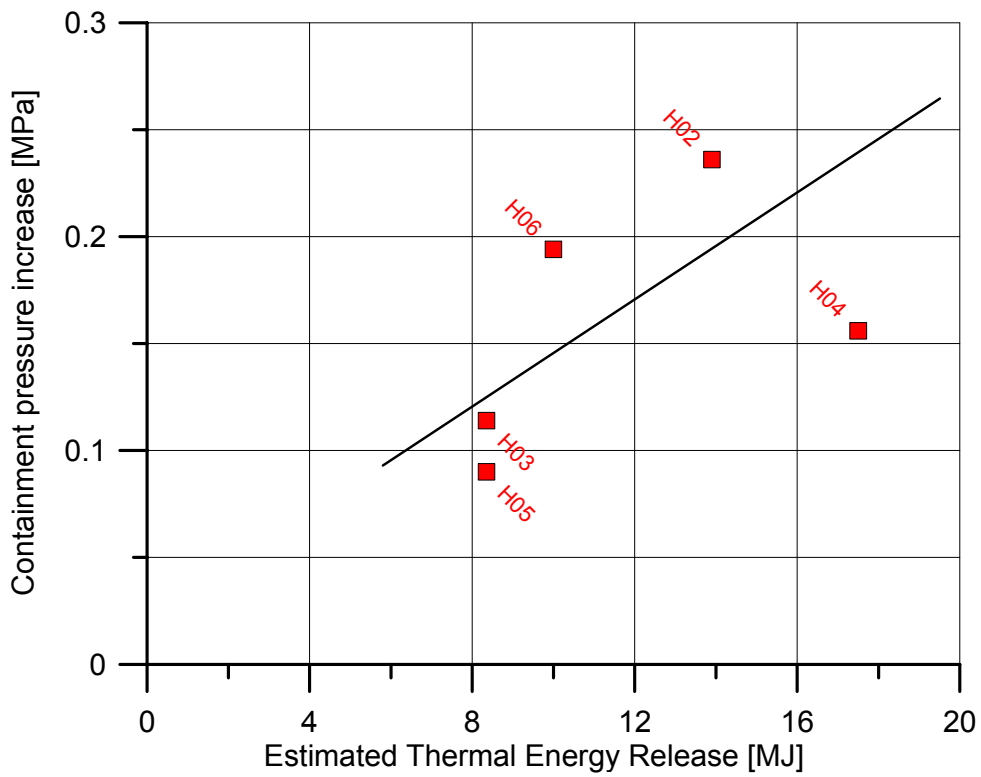


Fig. 55. Experimental pressure increase versus thermal energy release

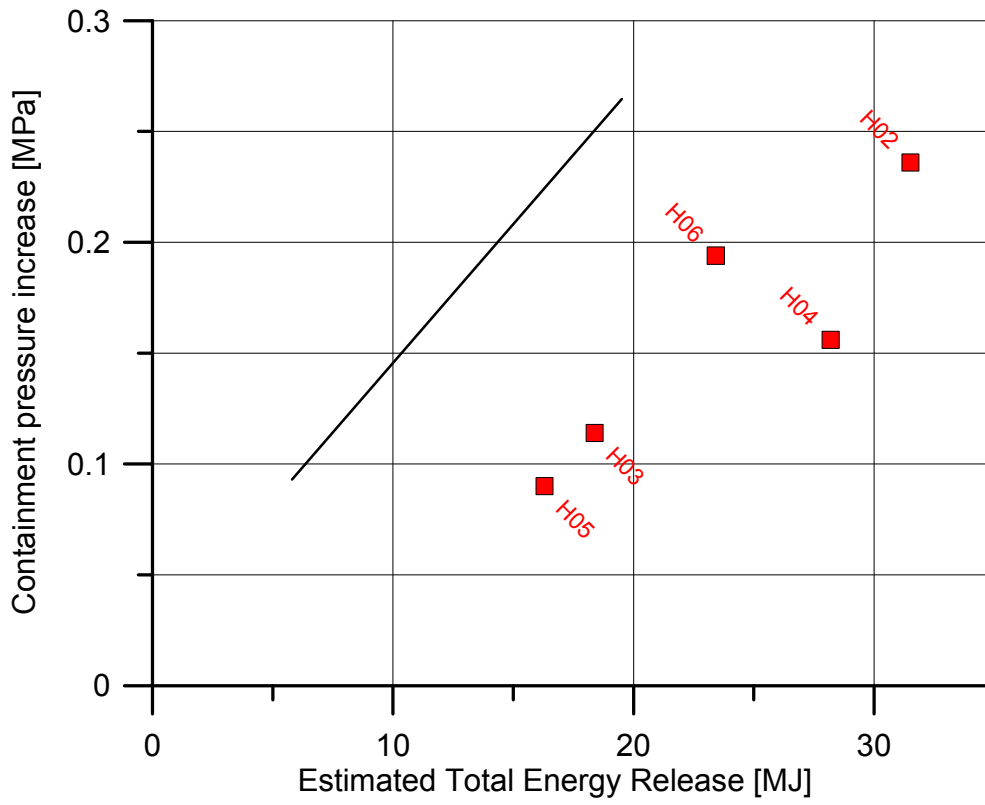


Fig. 56. Experimental pressure increase versus estimated total energy release

Video Pictures

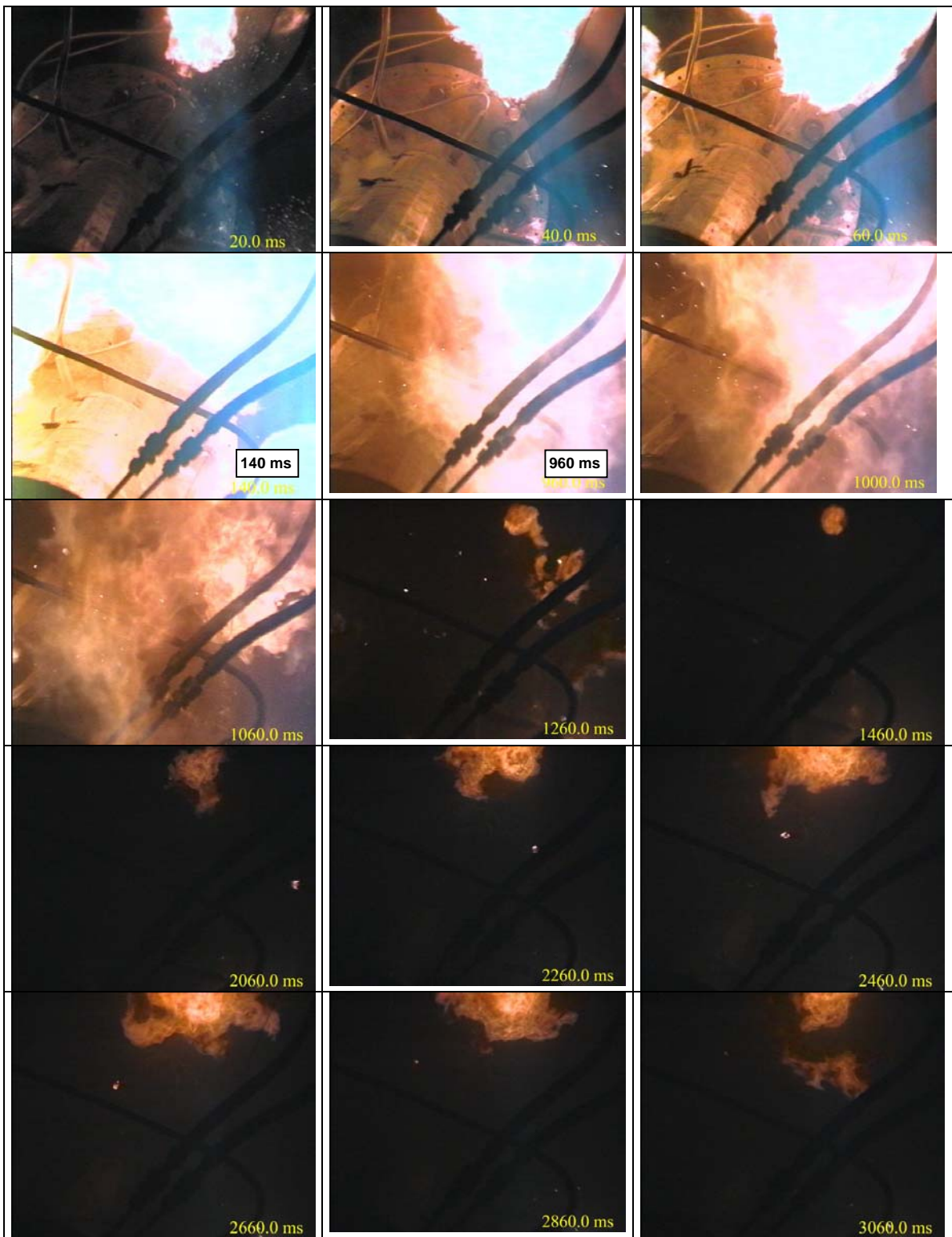


Fig. 57. G01: Video frames from top view into the containment

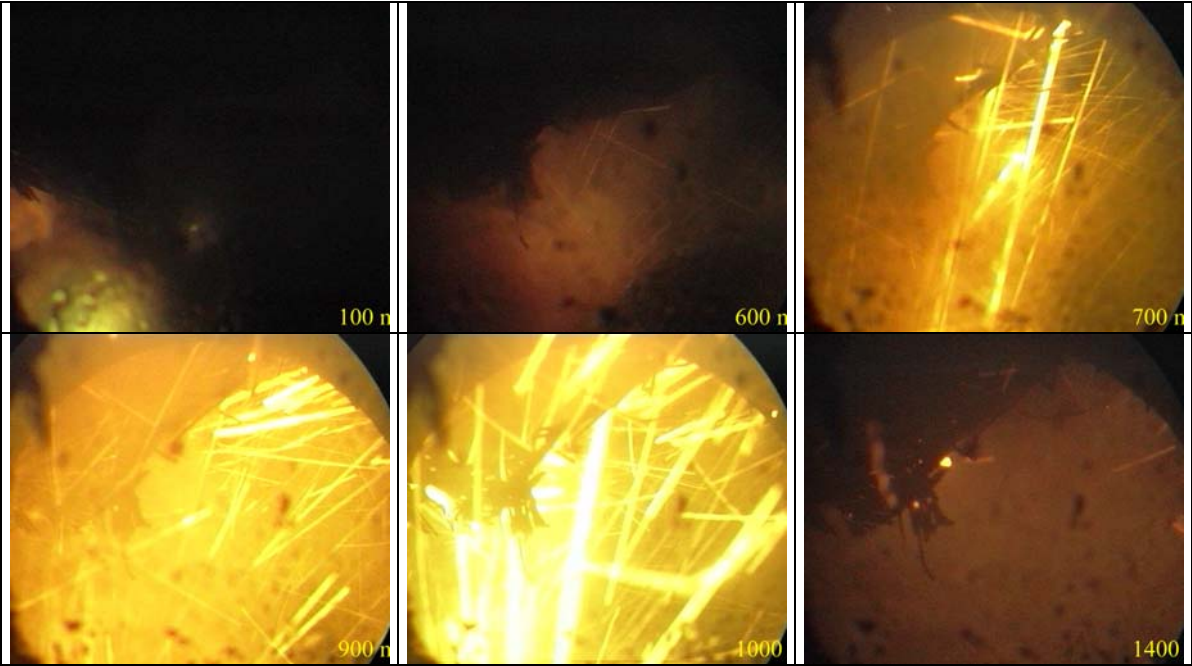


Fig. 58. G01: Video frames from the endoscope inside the subcompartment

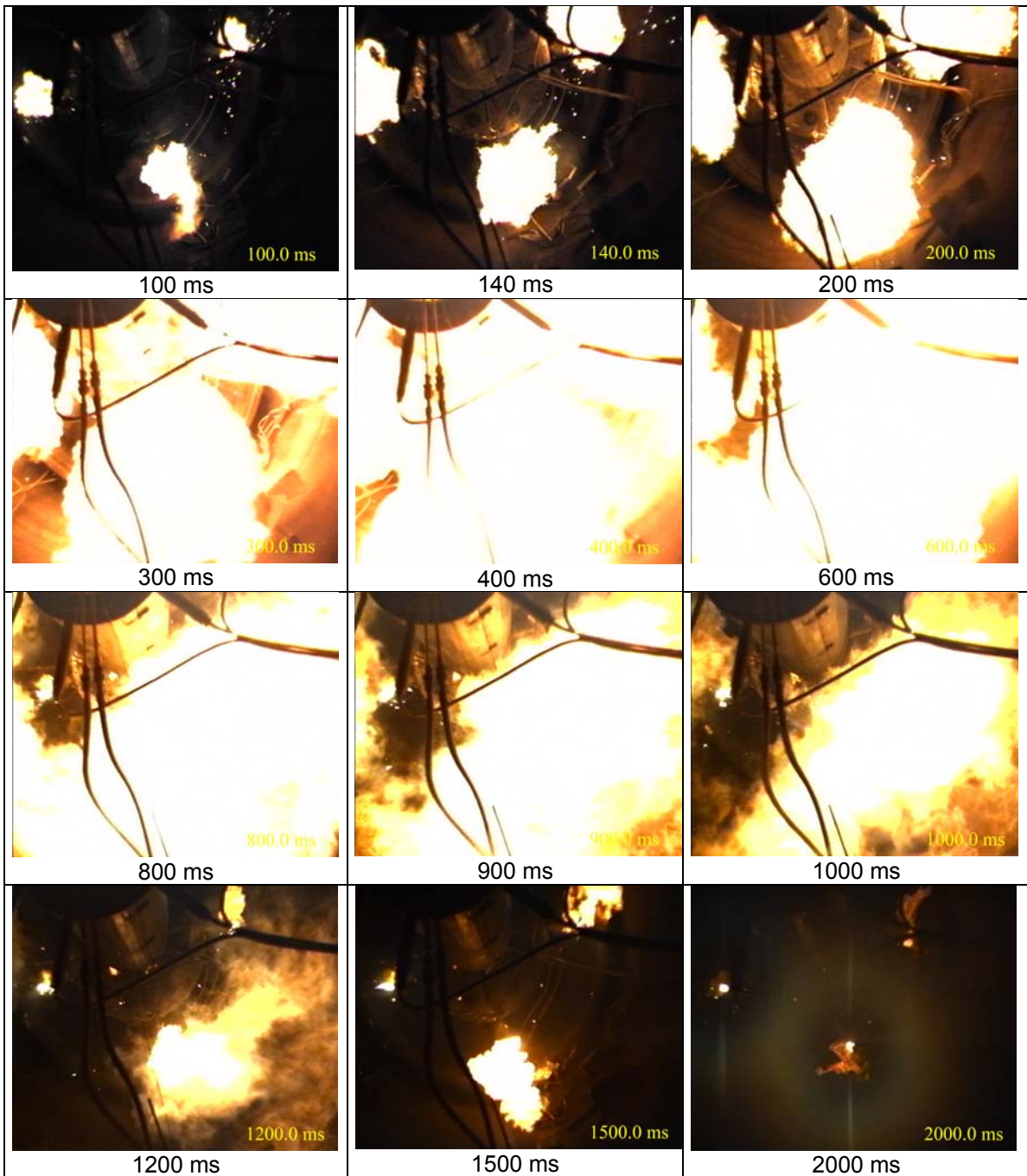


Fig. 59. G02: Video frames, top view into the containment

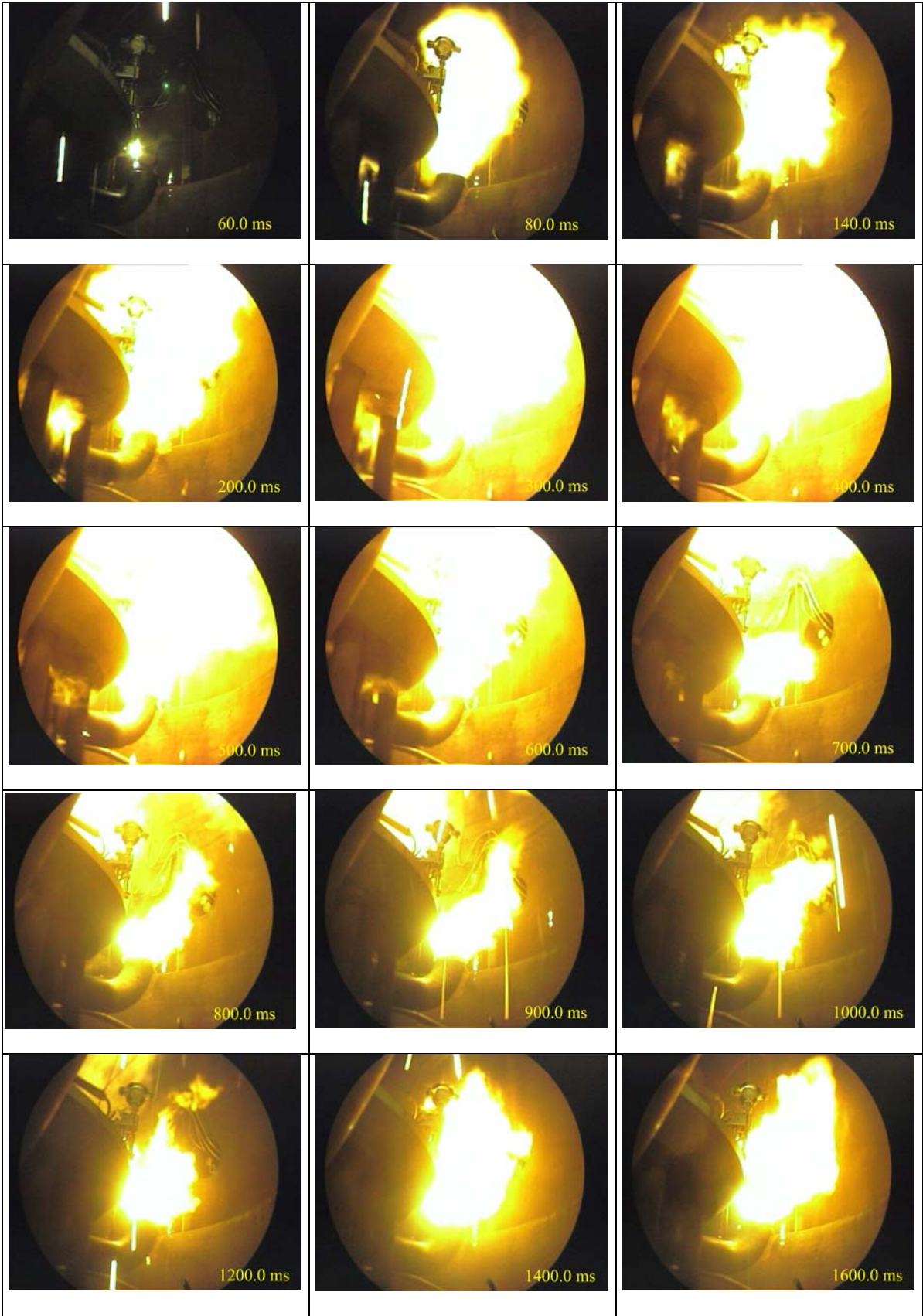


Fig. 60. G02: Video frames from the endoscope inside the subcompartment

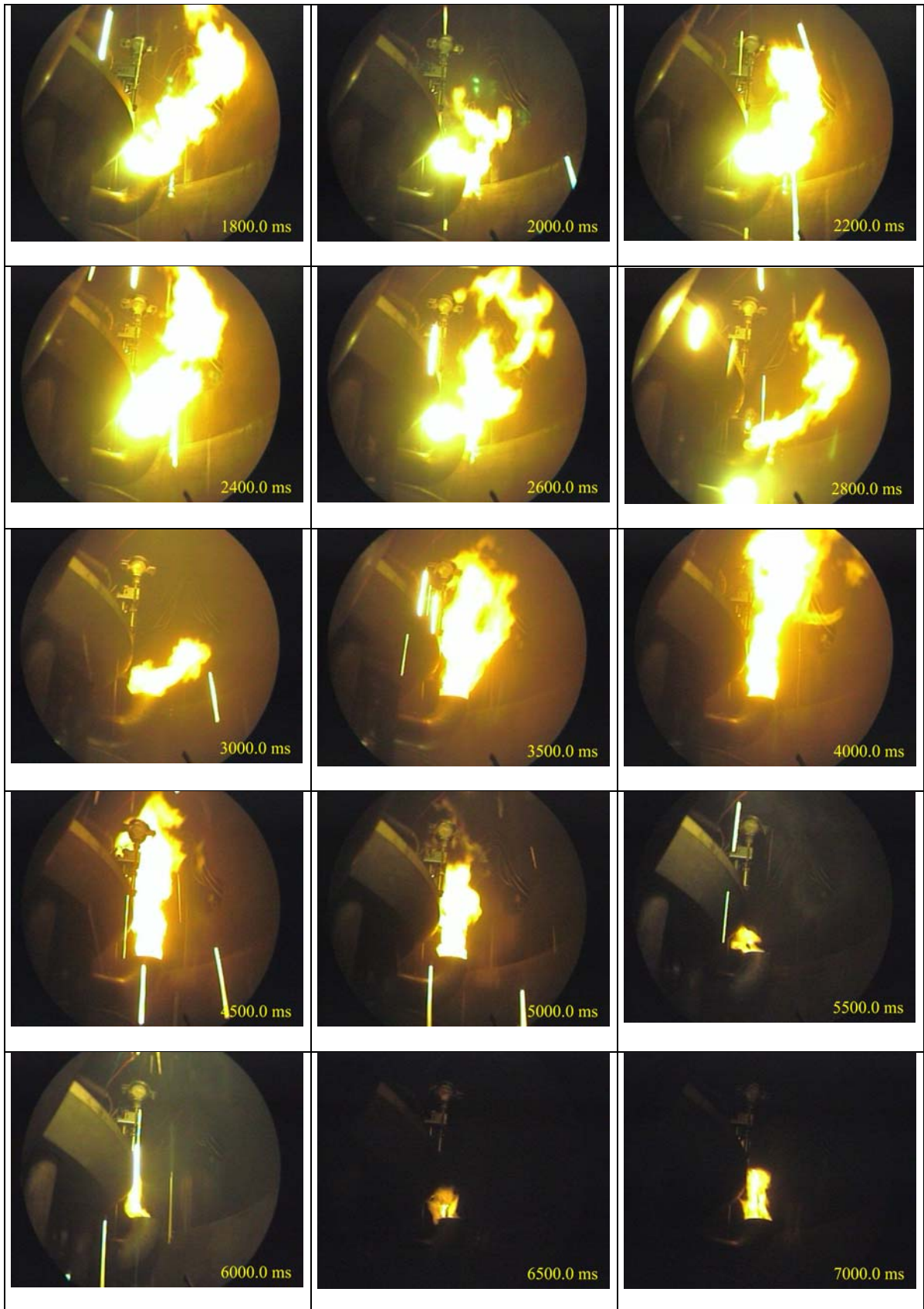


Fig.60. Continued

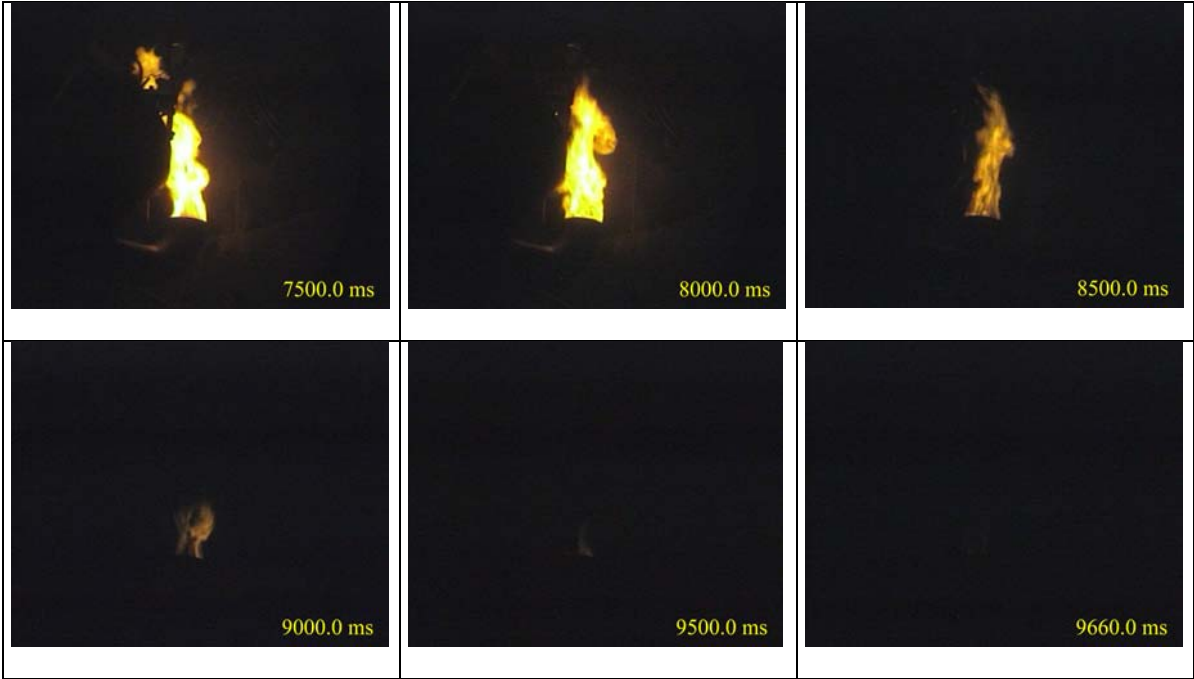


Fig.60. Continued



Fig. 61 G03: Video frames, top view into the containment

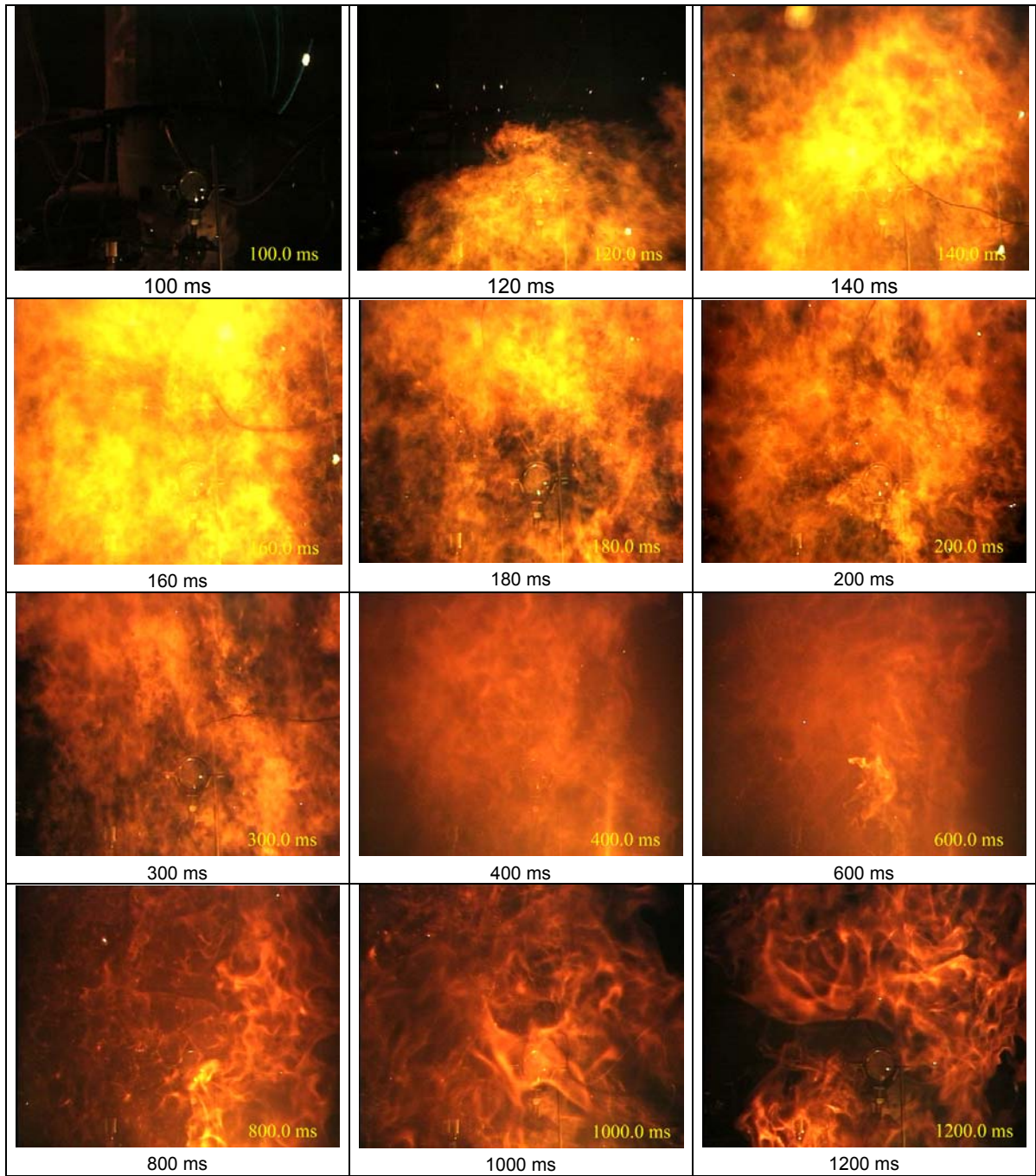


Fig. 62. G03: Video frames, view from the side, inside containment

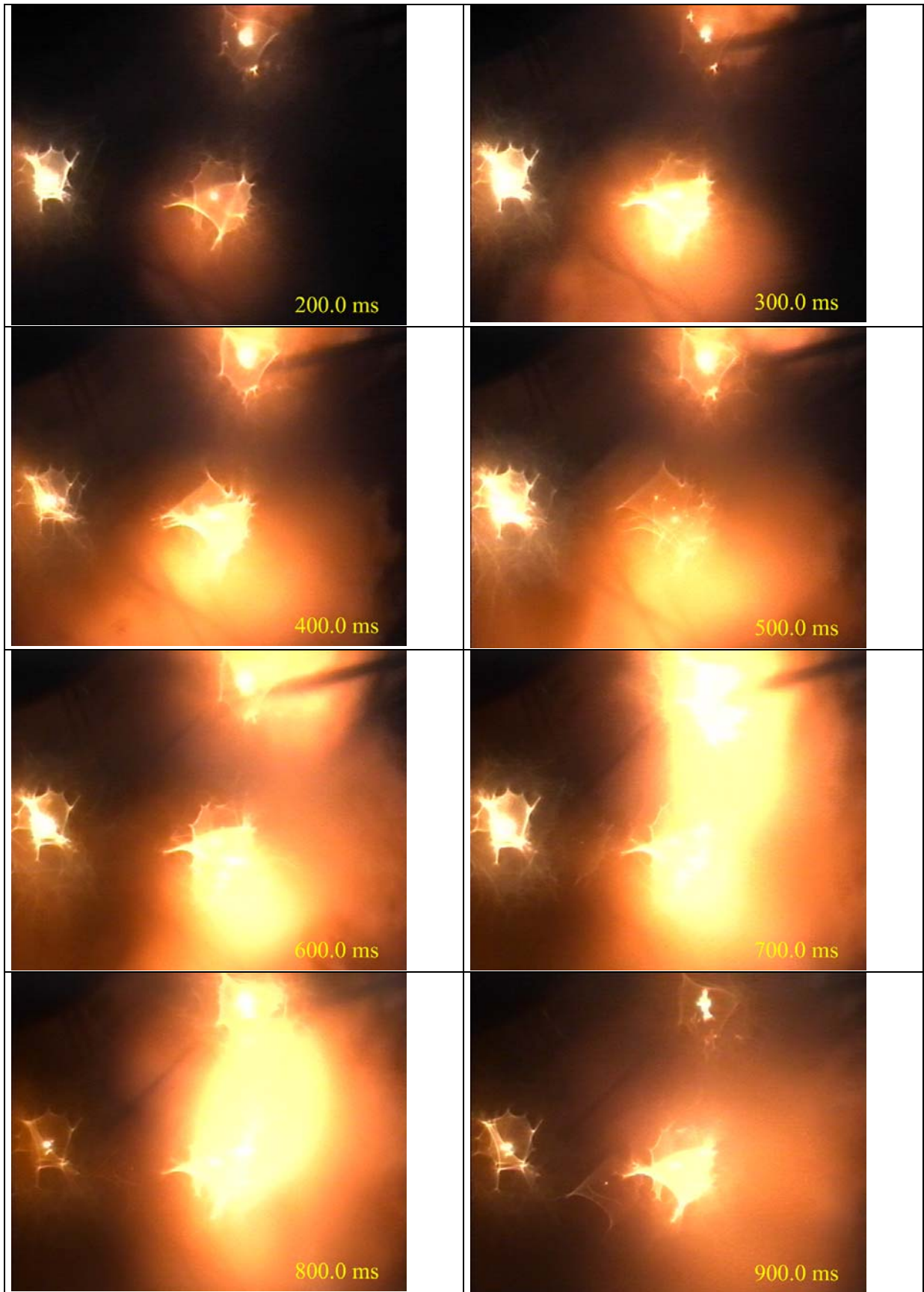


Fig. 63. G05: Video frames, top view into the containment

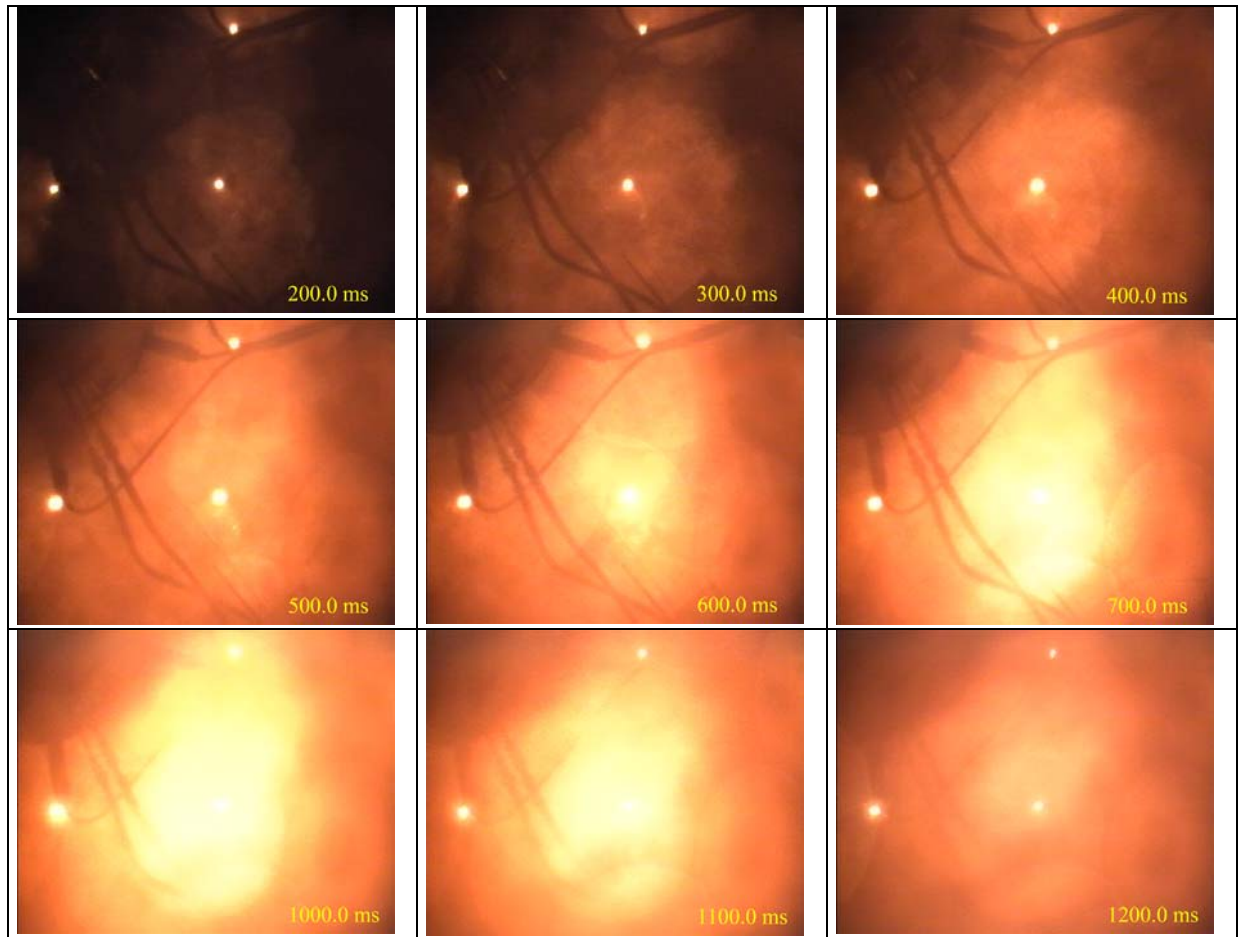


Fig. 64. G06: Video frames, top view into the containment

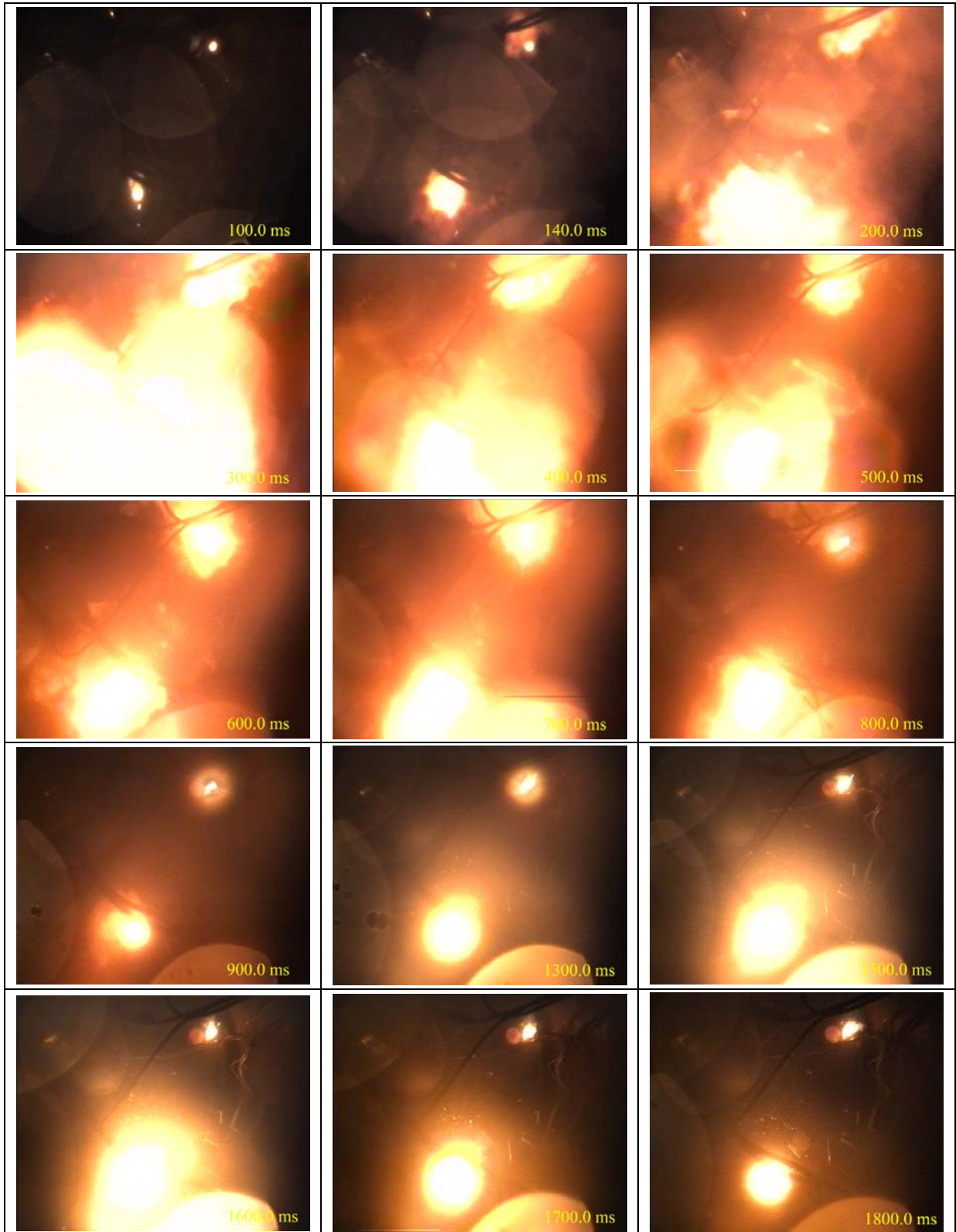


Fig. 65. G07: Video frames, top view into the containment

Annex A Gas analysis

The objective of the gas composition measurements and gas analysis is to obtain data on the chemical reactions taking place during the blow-down, that is, the production of hydrogen by the metal/steam reaction and the hydrogen combustion. We cannot distinguish these processes from direct metal/oxygen reactions, but in terms of total energy release, it makes little difference that direct metal/oxygen reaction initially deposits more energy in the debris and less in the gas, because, for small particles that react efficiently, heat transfer is also efficient.

The composition of the gas in the vessel is measured by taking gas samples. The gas samples are taken from an atmosphere containing a mixture of steam and noncondensable gases. Since the steam condenses the measured mole % of nitrogen, oxygen and hydrogen are given relative to the noncondensable part of the mixture. The uncertainty in the evaluation of the gas samples has been improved lately, and is 0.1 vol% for H₂, 0.3 for O₂ and 0.4 for N₂.

The pretest composition of the vessel atmosphere is known and the amount of each gas in moles can be calculated with the volume of the vessel V , the atmosphere pressure p_0 and temperature T_0 , and the measured amount of added hydrogen:

$$\text{Initial number of moles of hydrogen} \quad [\text{kmol}] \quad N_{H_2}^0 = m_{H_2} / M_{H_2} \quad (1)$$

$$\text{Initial number of moles of air} \quad [\text{kmol}] \quad N_{air}^0 = p_0 V / (R T_0) \quad (2)$$

$$\text{Initial mass of air} \quad [\text{kg}] \quad m_{air} = N_{air}^0 \cdot M_{air} \quad (3)$$

$$\text{Pre-test partial pressure of air} \quad [\text{MPa}] \quad p_{1\ air} = p_0 T_1 / T_0 \quad (4)$$

$$\text{Pre-test partial pressure of hydrogen} \quad [\text{MPa}] \quad p_{1\ H_2} = m_{H_2} R_{H_2} T_1 / V \quad (5)$$

$$\text{Pre-test partial pressure of steam} \quad [\text{MPa}] \quad p_{1\ steam} = p_1 - p_{1\ air} - p_{1\ H_2} \quad (6)$$

$$\text{Number of steam moles} \quad [\text{kmol}] \quad N_{steam}^0 = p_{1\ steam} V / (R T_1) \quad (7)$$

$$\text{Mass of steam} \quad [\text{kg}] \quad m_{steam} = N_{steam}^0 M_{H_2O} \quad (8)$$

$$\text{Total number of gas moles} \quad [\text{kmol}] \quad N_{total} = N_{air} + N_{H_2} + N_{steam} \quad (9)$$

$$\text{Number of nitrogen moles} \quad [\text{kmol}] \quad N_{N_2} = 0.7803 N_{air} \quad (10)$$

$$\text{Number of oxygen moles} \quad [\text{kmol}] \quad N_{O_2} = 0.2099 N_{air} \quad (11)$$

$$\text{Number of argon moles} \quad [\text{kmol}] \quad N_{Ar} = 0.0093 N_{air} \quad (12)$$

The constants are the molecular weights, $M_{H_2} = 2.02$ kg/kmol, $M_{air} = 28.96$ kg/kmol, $M_{H_2O} = 18.02$ kg/kmol, and the gas constants, $R = 8314$ J/kmol/K and $R_{H_2} = 4116$ J/kg/K.

The amount of hydrogen, that is produced and burned during the test, can be determined by the nitrogen ratio method [A1]. The data and assumptions required for this method are listed below:

1. The total pretest moles of noncondensable gases must be known.
2. The measured ratios of the pretest and posttest noncondensable gases must be known.
3. It must be assumed that nitrogen is neither produced nor consumed by chemical reactions.

With the measured data of the pretest mole fractions of species i , X_i^0 , the initial number of gas moles N_i^0 is:

$$N_i^0 = X_i^0 (N_{air}^0 + N_{H_2}^0 + N_{N_2\ RPV/RCS}) \quad (13)$$

The calculation is usually performed separately for the subcompartment and the rest of the containment volume. The sum of moles per species determined by gas sampling may deviate from the values determined by the theoretical determination of pretest composition, due to incomplete mixing of the components and the uncertainty in the acquisition and analysis of the gas samples. With the assumption that the number of nitrogen moles has not changed, the post test number of moles of oxygen and hydrogen can be determined from the measured post test mole fractions X_i^2 :

$$N_{O_2}^2 = N_{N_2}^0 X_{O_2}^2 / X_{N_2}^2 \quad (14)$$

$$N_{H_2}^2 = N_{N_2}^0 X_{H_2}^2 / X_{N_2}^2 \quad (15)$$

The number of moles of burned hydrogen is linked to the decrease of oxygen moles,

$$N_{H_2\ burned}^2 = 2 (N_{O_2}^0 - N_{O_2}^2) \quad (16)$$

and the balance of hydrogen gives the moles of produced hydrogen:

$$N_{H_2\ produced}^2 = N_{H_2}^2 - N_{H_2}^0 + N_{H_2\ burned}^2. \quad (17)$$

The fraction burned is $F_{H_2} = N_{H_2\ burned}^2 / (N_{H_2}^0 + N_{H_2\ produced}^2)$. (18)

The ratio of hydrogen moles produced to iron moles oxidized depends on the kind of iron oxide formed. Based on the experience at the Sandia National Laboratories, Blanchat [A2] gives a ratio of 1:1, which implies that in a first step only FeO is formed. For aluminum it is 1.5:1, 3 moles of hydrogen are produced by the oxidation of 2 moles of aluminum with water.

References

- [A1] T.K. Blanchat, M.D. Allen, M.M. Pilch, R.T. Nichols, "Experiments to Investigate Direct Containment Heating Phenomena with Scaled Models of the Surry Nuclear Power Plant", *NUREG/CR-6152, SAND93-2519*, Sandia Laboratories, Albuquerque, N.M., (1994)
- [A2] T.K. Blanchat, M.M. Pilch, R.Y. Lee, L. Meyer, and M. Petit, "Direct Containment Heating Experiments at Low Reactor Coolant System Pressure in the Surtsey Test Facility," *NUREG/CR-5746, SAND99-1634*, Sandia National Laboratories, Albuquerque, N.M., (1999).